Università degli Studi di Cagliari

PhD Degree

Industrial Engineering

Cycle: XXXII

MODELLING, THERMOECONOMIC ANALYSIS AND OPTIMIZATION OF HYBRID SOLAR-BIOMASS ORGANIC RANKINE CYCLE POWER PLANTS

Scientific Disciplinary Sector(s):

ING-IND/09 - Systems for Energy and the Environment

PhD Student: Joseph Oyetola OYEKALE

Coordinator of the PhD Programme: Prof. Ing. Francesco AYMERICH

Supervisor: Prof. Ing. Giorgio CAU

Co-Supervisors: Prof. Dr –Ing. Dieter BRÜGGEMANN
Chair of Technical Thermodynamics and Transport Processes (LTTT), Center of Energy Technology (ZET), University of Bayreuth, Germany.

Dr Ing. Mario PETROLLESE

Final Exam. Academic Year 2018 – 2019

Thesis defence: January-February 2020 Session

Page left blank intentionally

“That which we persist in doing becomes easier,
not that the nature of the task has changed,
but our ability to do has increased.”
- Ralph Waldo Emerson

If little advancements are consistent enough,
the big and desired results will surely emerge.
The idea is, no matter how small,
one should strive to make specific progress each day.

- Joseph Oyekale

Dedication

To everyone around the world who, due to disadvantaged social and economic background, should ordinarily not have access to university education; but who, as a result of strong will, doggedness, perseverance and hard work, would not only be able to acquire quality university education, but could even proceed all the way to bagging the highest academic degree possible. I identify with you!

Acknowledgements

First of all, I would like to place on record here, my profound gratitude to Jesus Christ, the Lord Almighty, who has given me the strength and ability to attain this lofty height. A thousand pages of acknowledgements would not be enough to describe how much He helped and led me all the way. I am indeed grateful to Him! To Him alone be all the glory, honour and majesty! “How can I repay the Lord for all His goodness to me?”

Next, I would like to heartily appreciate my chief supervisor, Prof. Giorgio Cau, for the innumerable scientific and personal supports he rendered to me during the course of this project. He was always available for discussions whenever I needed him, without denying me the autonomy to chart the course of my research. I am very grateful to him for the patience and kindness he exhibited in all our dealings. I appreciate him for his approvals that facilitated my attendance in a good number of academic conferences and PhD school, amongst several other acts of generosity. I am indeed grateful to Prof. Cau! In addition, I would like to appreciate my German supervisor, Prof. Dieter Brüggemann, for the very many fruitful discussions we had at the University of Bayreuth, and for all his scientific contributions. Prof. Brüggemann tactically taught me how to balance academic work with social life and, truly, the very many social gatherings we had in Bayreuth were somewhat magical as to how productive I was at work after each of them. More so, I would like to appreciate the scientific supports of other senior colleagues I had worked with during this project: Prof. Daniele Cocco, Prof. Vittorio Tola, Dr Mario Petrollese and Dr Florian Heberle. I owe a lot of thanks to them all for their encouragement and substantial scientific supports, both in Cagliari and Bayreuth.

Furthermore, I would like to acknowledge the very many supports of UNICA, without which this project would not have been as fun. Mere written words won’t be sufficient to express my sincere gratitude to UNICA. I deeply appreciate the opportunities given me! I am also grateful to Prof.

Francesco Aymerich, for all his friendly gestures towards me, right before I ever set my eyes on him, and even much more after I had met him in person. Thanks to him for always seeking the best for me, as for other PhD candidates under his co-ordination. Also, I am deeply grateful to Prof. Matthias Finkenrath of Kempten University of Applied Sciences, Germany, and Prof. Javier Uche of Zaragoza University, Spain, for consenting to serve as external reviewers/assessors for my PhD thesis. I also appreciate Francesco Lonis and Daniele Carta, for their very many assistance and help in the course of this journey. Francesco Lonis would sometimes go out of his way just to ensure that all was well with my affairs. I am deeply grateful to him. I am also grateful to Irene Virdis for being a good friend. I appreciate Simone Arena, Mario Cascetta and Effisio Casti for their good neighbourliness along the way. In addition, I would like to acknowledge the friendliness and supports of some colleagues in Germany: Davide Toselli (my office mate), Sebastian Kuboth, Michael Kaeser, Osama Aljolani, Thomas Hillenbrand, Christian Zollner, Andrea Obermeier, Tim Eller, Claudia Trautmann, Gabriele Braese and Andreas Konig-Haagen, amongst others. The Monday-evening soccer sessions with Sebastian, Florian and other friends outside LTTT were always stimulating for research productivity, to say the least. Thanks to these guys for showing me another (somewhat better) approach to life! Also, I deeply appreciate Tetfund for its academic training and development scheme at the University of Bayreuth. This facilitated the huge success recorded with my research, in no small measure.

In continuation, I owe a lot of sincere appreciation to my parents for the substantial roles they played in my life, without which I would probably never have come this far. My mother made a lot of sacrifices to ascertain my well being, especially at the beginning of my university education back in Nigeria. Mother fought tooth and nail to see us forge ahead and live our dreams. The little space here won't be sufficient to acknowledge my beloved mother, actually. I thank her so much for believing especially in me, and for supporting my dogged aspirations and decisions all the way. As for my late father, if he were to be here with us on the surface of the earth, I am sure he would be

very proud of the level of academic success I have attained today by the mercies of God. He was going to give us the very best things of life, but life itself would not allow him. Continue to rest in the bossom of the Lord, beloved father! Also, I would like to deeply appreciate the diverse supports and love of my siblings: Opeyemi (nee Oyekale), Grace (nee Oyekale), and Bukola Oyekale. Their affectionate belief in my dreams was enough reason for me not to succumb to failure in the face of challenges. I am grateful to them all! I equally appreciate my brother-in-law, Shola Okeyode, for giving me the avenue to 'hustle' in Abuja after my undergraduate studies in Nigeria, and for all his assistance along the way. I also appreciate my darling niece, OluwaSemilore Okeyode, for her priceless and innocent love towards me while she was growing up. More so, I appreciate my uncle, Oyetunji Oyekale, for his numerous supports and assistance.

Finally, I would like to acknowledge and appreciate the love, supports and understanding of Omolola Florence through this obviously challenging journey. I really appreciate her sacrifices and companionship. I am very grateful!

A lot of other people deserve to be mentioned and acknowledged specifically, to be honest, but the space here is really limited that I cannot list all their names and contributions one after the other. I am really grateful to them all. Yes, I mean you!

Page left blank intentionally

Abstract

The need for modern energy systems to embrace the requirements of energy security, sustainability and affordability in their designs has placed emphatic importance on exploitation of renewable resources, such as solar and wind energy, etc. However, these resources often lead to reduced reliability and dispatchability of energy systems; less-efficient conversion processes; high cost of power production; etc. One promising way to ameliorate these challenges is through hybridization of renewable energy resources, and by using organic Rankine cycle (ORC) for power generation. Thus, this PhD research project is aimed at conceptual design and techno-economic optimization of hybrid solar-biomass ORC power plants.

The methodologies adopted are in four distinct phases:

- First, novel hybrid concentrated solar power (CSP)-biomass scheme was conceived that could function as retrofit to existing CSP-ORC plants as well as in new hybrid plant designs. Thermodynamic models were developed for each plant sub-unit, and yearly techno-economic performance was assessed for the entire system. Specifically, the ORC was modelled based on characteristics of an existing CSP-ORC plant, which currently operates at Ottana, Italy. Off-design models of ORC components were integrated, and their performance was validated using experimental data obtained from the aforementioned real plant.
- Second, detailed exergy and exergoeconomic analyses were performed on the proposed hybrid plant, in order to examine the system components with remarkable optimization potentials. The evaluation on optimization potentials considered intrinsic irreversibilities in the respective components, which are imposed by assumptions of systemic and economic

constraints. This has been termed enhanced exergy and enhanced exergoeconomic analyses here.

- Third, the techno-economic implications of using siloxane mixtures as ORC working fluid were investigated, with the aim of improving heat transfer processes in the ORC plant. The studied fluid pairs were actively selected to satisfy classical thermodynamic requirements, based on established criteria.
- Fourth, the biomass retrofit system was optimized multi-objectively, to minimize biomass consumption rate (maximize exergetic efficiency) and to minimize exergy cost rate. Non-dominated Sorting Genetic Algorithm (NSGA-II) was adopted for multi-objective optimization.

The conceptual scheme involves parallel hybridization of CSP and biomass systems, such that each is capable of feeding the ORC directly. Results showed that the proposed biomass hybridization concept would increase both thermodynamic efficiency and economic performance of CSP-ORC plants, thereby improving their market competitiveness. Total exergy destroyed and exergy efficiency were quantified for each component, and for the whole system. Overall system exergetic efficiency of about 7 % was obtained. Similarly, exergoeconomic factor was obtained for each system component, and their implications were analysed to identify system components with high potentials for optimization. Furthermore, it was observed that thermodynamic performance of the hybrid plant would be optimized by using siloxane mixtures as ORC working fluid. However, this would result in larger heat exchange surface area, with its attendant cost implications. Lastly, biomass combustion and furnace parameters were obtained, which would simultaneously optimize exergetic efficiency and exergy cost rate for the hybrid plant.

In sum, a novel scheme has been developed for hybridizing solar and biomass energy for ORC plants, with huge potentials to improve techno-economic competitiveness of solar-ORC systems.

Page left blank intentionally

Table of Contents

List of Figures

List of Tables

Nomenclature

Symbols

A	area (m^2)
AC	annual operating expenditure (€/year)
B	experimentally fitted constant
b	biomass fraction
$\dot{C}$	exergy cost rate (€/h)
c	specific costs
$\dot{E}$	rate of exergy (kW)
e	exergy
ex	excess air
$\dot{E}_s$	exergy of the sun (kW)
F	cost coefficient
f	exergoeconomic factor
f^e	enhanced exergoeconomic factor
FL	collector focal length (m)
H	annual plant operation (hours)
h	specific enthalpy (kJ/kg)
$\dot{I}$	rate of destroyed exergy/irreversibility (kW)
i	interest rate
IAM	incidence angle modifier
IC	initial expenditure (€)
K	cost coefficient

L	collector length (m)
LHV	lower heating value
$\dot{m}$	mass flow rate (kg/s)
MF	maintenance factor
N	plant lifetime (years)
Q	thermal energy (kWh)
$\dot{Q}$	thermal power (kW)
$\dot{q}$	specific thermal power (W/m^2)
R_{cr}	relative avoidable cost rates
RI	relative irreversibility
S	component size factor
s	entropy (kJ/kgK)
T	temperature (°C)
U	overall heat transfer coefficient (W/m^2K)
$\dot{V}$	volumetric flow rate (m^3/s)
$\dot{W}$	electrical power (kW)
x	vapour quality
Z	investment cost (€)
$\dot{Z}$	investment and operation cost rate (€/h)

Greek letters

ε	exergetic efficiency
Δt	time step (h)
ΔT	change in temperature
α	convective heat transfer coefficient (W/m^2K)

η	efficiency
θ	incident angle (deg)

Subscripts

A	annual
amb	ambient
Bio	biomass
c	component boundary
cond	condenser
DIR	direct
eff	effective
f	fuel
F	biomass furnace
G	glide
g	vapour
HTF_B	heat transfer fluid circulating in biomass section
HTF_S	heat transfer fluid circulating in solar section
HTF_T	heat transfer fluid circulating in ORC unit
i	inlet side
id	ideal
IND	indirect
l	liquid
M	marginal
o	outlet side
OF	organic fluid
pm	pump motor

RF	retrofit
SF	solar field
sk	sink

Superscripts

D	design conditions
off	off-design conditions

Abbreviations

ASW	Aspen Simulation Workbook
CAMD	computer aided molecular design
CSP	concentrating solar power
DNI	direct normal irradiance
FIT	feed-in tariff
HTF	heat transfer fluid
IOP	imaginary optimal point
LCOE	levelized cost of electricity
LFC	linear Fresnel collector
NPV	net present value (€)
NEE	annualized net electrical efficiency
ORC	organic Rankine cycle
SIC	specific investment cost
SPB	simple payback period (years)
SQP	sequential quadratic programming
TES	thermal energy storage

Page left blank intentionally

Chapter 1

Introduction

1.1Background

Energy, in all its forms, constitutes basic necessities of life. Not only is it needed for sustained existence of man; its degree of availability has direct impact on economic and social prosperity of nations around the world. This assertion is somewhat justified by the predicted and experienced increase in the world energy demands as population increases. In quantitative terms, the New Policies Scenario (NPS) of the International Energy Agency (IEA) reported in the World Energy Outlook (WEO) for the year 2018 stated that world total demand of primary energy had increased from 10,027 MToe in the year 2000 to 13,972 MToe in the year 2017, and it is projected to rise to 17,715 MToe by the year 2040 [1]. This translates to about 27 % projected increase in world energy need in the next 20 years, and it places high premium on the need for continued research and developmental efforts that would facilitate continuous satisfaction of human energy needs.

Also, the NPS of IEA-WOE 2018 has it that 80.8 % of total world energy demand is currently satisfied by non-renewable fossil fuels such as coal, oil, and gas [1]. This is due majorly to advancement in technologies for exploiting these fuels, as well as their relative advantages for low-cost investments and operations. However, emissions from combustion of fossil fuels are healthily unpropitious to the sustained existence of living species and the environment. The repugnant consequences of acid rain and global warming ravaging our society today is a case in point to justify the hazard of fossil fuel exploitations and usage. Also, fossil fuels are considered unsecure, since their sources will get depleted one day, no matter how long.

In the light of these unfavourable consequences of continued dependent on fossil fuels, consensus seems to have been reached globally on the quest to develop renewable energy sources and their

accompanying conversion technologies, which would satisfy the three-phase requirements of sustainability, security and affordability of modern energy supply. In fact, number 7 of the United Nations Sustainable Development Goals (SDGs) 2030 succinctly captured these essential features for consideration in the design of modern energy systems [2]. In this regard, increased efforts have been witnessed in recent times on the exploitations of renewable energy sources. National and international organizations are committing huge funds to their advancement, and research and technical experts are expending a great deal of time and efforts in developing adequate conversion technologies and process integration mechanisms for the renewables.

However, renewable energy sources are equally characterised by a number of challenges. First, their technologies are quite low in reliability and dispatchability, due to diurnal and seasonal fluctuations of most renewable energy resources. Next, systems based on these resources often record less efficient conversion processes for power generation, basically due to their low enthalpy contents. Consequently, thermo-economic performance of renewable energy technologies is badly impacted, which has also led to their low commercialization potentials. This is especially true for distributed systems rated at small and medium power scales, which can mostly not survive at present without some sorts of economic incentives or subsidies from governments.

Thus, substantial research and developmental efforts are yet required to optimize design and operation of renewable-based energy technologies, for improved techno-economic performance, in order to facilitate their growth in the world energy mix. This understanding is the basis for the outlook of the academic research study being reported in this thesis.

1.2 Justification for the Study Focus and Theme

This study focuses specifically on conceptual design and operation of solar-based organic Rankine cycle (ORC) plants. Solar energy is one of the renewable sources attracting keen attention around the world today, perhaps due to its free accessibility [3]. Photovoltaic (PV) and Concentrated Solar Power (CSP) systems are currently being mostly used for exploitation of solar energy [4,5].

However, for generation of thermal power for use in different applications, CSP technology is considered more suitable than PV, as it is easily amenable to application in plants where heat sources and power cycles run on two distinct working media (binary cycles) [6]. In this respect, CSP plants should play a key role in increasing renewable energy penetration into the future energy mix, as evidenced by the increase in number of projects on solar thermal plants globally [4,6]. More so, in pursuit of increased degenerated energy systems that could be applied in rural and isolated regions, CSP plants at low and medium scales are gaining wider attention nowadays, relative to large-scale systems.

Furthermore, ORC technology has been adjudged to be quite promising for the conversion of solar and other low-temperature heat sources into useful electrical and thermal power [7]. It bothers on using organic fluid as working media in Rankine cycle plants, for vaporization at low pressure, by low-temperature heat sources. At such instances, performance of conventional steam Rankine cycle is quite limited. Thus, substantial economic investments have been made towards advancing ORC technology, and research and practical applications are being hugely deployed around the world today [8].

However, just like for most other renewable energy technologies as aforementioned, solar-based ORC plants are mostly associated with low reliability/dispatchability, low capacity factor, frequent system shutdown/start-up, high operational losses and costs, amongst others. This is because solar irradiation is transient in nature, which mostly results in high fluctuation of solar energy available for exploitation, and it badly impacts practical implementation of solar-ORC plants. For instance, Petrollese *et al.* reported that only eleven real CSP-ORC plants in the range of 50 kW-5 MW exist around the world [9]. Amongst these is a linear Fresnel collector (LFC)-based ORC plant, rated at about 630 kWe, which currently runs at Ottana (NU), Italy. The Department of Mechanical, Chemical and Materials Engineering of the University of Cagliari collaborates with other stakeholders for the conceptual design, installation and commissioning of this plant, up till the present moment for real operation and continuous development of this plant. Suffice it to report that

the real experience with this solar-only ORC plant is quite in agreement with the aforementioned challenges generally associated with all plants of such kind. In essence, potential ways should be sought to upgrade the operation of not only the Ottana Solar Facility, but also of the similar ones in existence, and also to promote increase in practical implementation of this type of energy system, without compromising the fully-renewable feature.

Consequently, a number of solution strategies are currently being reported as potential measures to ameliorate the highlighted challenges in real CSP-ORC plants. These include integration of thermal energy storage (TES) systems, which has attracted huge scientific and economic efforts in recent times [10]. In addition, hybridizing solar systems with other more dispatchable renewable energy resources is another solution strategy being vigorously investigated in literature [11]. And since geothermal and biomass are among the most dispatchable of all renewable energy resources, their suitability for hybridization with solar systems in ORC plants is widely studied. However, in a situation where a solar ORC plant is the base system in existence, as it is the case with the aforementioned Ottana Solar Facility, hybridizing a geothermal system would be capital intensive. The location of such plant might also not be favourable for exploiting geothermal resources. In this case, biomass hybridization would be a better alternative. Moreover, biomass and solar ORC plants share a lot of equipment in common, and technical and cost implications make their hybridization favourable for practical implementation. Also, biomass energy sources are suitable for retrofit to existing solar-ORC plants and vice versa, and this has necessitated the specific focus on conceptual design and analysis of hybrid solar-biomass ORC plants in this study. Although a couple of schemes have been presented to hybridize solar and biomass energy for power production, most of them have hitherto focused on series hybridization scheme either for upgrading thermodynamic processes of existing plants, or for heat recovery processes. To the best of author's knowledge, dedicated biomass hybridization scheme that aims to improve dispatchability of existing CSP-ORC plants is lacking in the state of the art, which is one of the main novelties of this study.

1.3 Aim and Objectives

The aim of this study concerns conceptual design and analysis of biomass hybridization scheme that could improve dispatchability and thermo-economic performance of CSP-ORC power plants. The pursued tangential objectives are:

- Conceptual design and techno-economic assessment of a novel biomass hybridization scheme, which could be applied both as retrofit to upgrade existing CSP-ORC plants as well as in newly-designed hybrid CSP-biomass ORC plants;
- Investigation of sources of thermo-economic losses in the proposed hybrid CSP-biomass ORC plant through second-law analysis;
- Assessment of thermo-economic effects of using siloxane mixtures as working fluid in the ORC unit of the proposed hybrid CSP-biomass plant;
- Determination of selected design parameters of the biomass system that would simultaneously optimize thermodynamic and economic performance of the hybrid plant for a retrofit case study.

1.4 Scientific Publications and Thesis Structure

1.4.1 Scientific publications

Substantial parts of the methods and results reported in this thesis have been published in international journals and peer-reviewed international conference proceedings, as follows:

1. **J. Oyekale**, F. Heberle, M. Petrollese, D. Brüggemann, G. Cau, Biomass retrofit for existing solar organic Rankine cycle power plants: conceptual hybridization strategy and techno-economic assessment, Energy Convers. Manag. 196 (2019) 831–845.
2. **J. Oyekale**, F. Heberle, M. Petrollese, D. Brüggemann, G. Cau, Thermo-economic evaluation of actively selected siloxane mixtures in a hybrid solar-biomass organic Rankine cycle power plant, App. Therm. Eng, https://doi.org/10.1016/j.applthermaleng.2019.114607.

3. **J. Oyekale**, M. Petrollese, G. Cau, Multi-objective thermo-economic optimization of biomass retrofit for an existing solar organic Rankine cycle power plant based on NSGA-II. Energy Reports (2019), https://doi.org/10.1016/j.egyr.2019.10.032.
4. **J. Oyekale**, M. Petrollese, F. Heberle, D. Brüggemann, G. Cau, Exergetic and integrated exergoeconomic analyses of a hybrid solar-biomass organic Rankine cycle cogeneration plant, under review with Energy Conversion and Management Journal.
5. **J. Oyekale**, M. Petrollese, G. Cau, Modified auxiliary exergy costing in applied exergoeconomic analysis applied to a hybrid solar-biomass organic Rankine cycle cogeneration plant, under review with Applied Energy Journal.
6. **J. Oyekale**, M. Petrollese, F. Heberle, D. Brüggemann, G. Cau, Exergy and exergoeconomic analyses of a hybrid solar-biomass organic Rankine cycle cogeneration plant, in: 32nd International Conference on Efficiency, Cost, Optimization, Simulation and Environmental Impact of Energy Systems (ECOS) 2019, Wraclaw; Poland.
7. **J. Oyekale**, G. Cau, Enhanced exergoeconomic analysis of a hybrid solar-biomass organic Rankine cycle cogeneration plant, in: International Conference on Applied Energy (ICAE) 2019, Vasteras; Sweden. – **Selected for special issue publication in Applied Energy Journal.**
8. **J. Oyekale**, M. Petrollese, V. Tola, G. Cau, Conceptual design and preliminary analysis of a CSP-biomass organic Rankine cycle plant, in: 31st International Conference on Efficiency, Cost, Optimization, Simulation and Environmental Impact of Energy Systems (ECOS) 2018, Guimaraes; Portugal.
9. M. Petrollese, **J. Oyekale**, V. Tola, D. Cocco, Optimal ORC configuration for the combined production of heat and power utilizing solar energy and biomass, in: 31st International Conference on Efficiency, Cost, Optimization, Simulation and Environmental Impact of Energy Systems (ECOS) 2018, Guimaraes; Portugal.

1.4.2 Thesis structure

This thesis is structured in 6 more chapters, from 2 to 7, as summarized in the following.

Chapter 2 consists of literature review, subdivided into two parts. The first part consists of overview of different technologies present in the proposed hybrid plant: CSP, TES, biomass energy systems and ORC. In the second part, the need for each of the issues addressed in this thesis are underscored, based on available studies in literature. This has been structured to match each of the highlighted tangential thesis objectives, and new thesis contributions that depart from literature information are highlighted at the sections where they are present.

Chapter 3 contains the description of the newly proposed biomass hybridization scheme, as well as the methods and results of techno-economic assessments of the hybrid plant. This essentially addresses objective number 1 highlighted above, and it is the basis for the scientific papers numbered 1, 8 and 9 above. The issues contained in this chapter contributes to knowledge by the proposal of a scheme that is applicable to retrofit existing CSP-ORC plants, different from what had been studied in the state of the art.

Chapter 4 consists of the methods and results of detailed exergy, exergoeconomic, enhanced exergy and enhanced exergoeconomic analyses of the proposed hybrid plant, aimed at addressing objective number 2 of the thesis. It is the basis for the scientific papers numbered 4, 5, 6 and 7 above. Although the applied methodologies are classical, their application to new systems are usually considered necessary for system optimization, and are thus well regarded in the state of the art. Moreover, a new cost formulation concept is implemented for exergoeconomic methodology, by regarding energy quality level of thermodynamic states for allocating unit exergy costs. This is termed here as integrated exergoeconomic approach, and it departs from what is common in literature.

Chapter 5 consists of the methods and results of thermo-economic evaluation of siloxane mixtures in the ORC unit of the hybrid plant, aimed at addressing objective number 3. It is the basis for the scientific paper numbered 2 above. This chapter contributes to knowledge by being the first to

incorporate off-design analysis into investigation of potential thermo-economic benefits of mixtures in ORC applications, as well as the first to focus on hybrid solar-biomass thermal sources for the study of applications of fluid mixtures in ORC plants.

Chapter 6 consists of the methods and results of multi-objective thermo-economic optimization of biomass retrofit for the existing CSP-ORC plant, aimed at addressing objective number 4 of the thesis. It is the basis for the scientific paper numbered 3 above. Also, although NSGA-II optimization approach has been in existence for a while, its application to multi-objective optimization of systems is quite relevant both for academic study as well as for practical improvement of industrial systems.

Overall conclusions are summarized in Chapter 7. Also, main thesis contributions to knowledge as well as recommendations for further studies are highlighted in this chapter.

Page left blank intentionally

Chapter 2

Literature Review

2.1Preamble

The synthesized literature is in two broad categories. The first category contains overview of the different technologies involved in the hybrid plant under discussion: concentrated solar power (CSP) systems, thermal energy storage (TES) systems, biomass energy systems and organic Rankine cycle (ORC) plants. In the second category, available literature on CSP-biomass hybridization strategies is reviewed, as well as available studies on application of mixtures as working fluid in ORC. Also, state-of-the-art on applications of different exergy, exergoeconomic and optimization methodologies for energy plant design and analyses are highlighted. The latter category is in an attempt to give background information on, and further justify, the specific approach and methodologies applied in this study.

2.2Brief overview of major technologies contained in the studied hybrid CSP-biomass plant

2.2.1 Concentrated solar power systems

Concentrated solar power systems are solar-energy exploitation/conversion technologies, which mostly operate by concentrating energy content of the sun (direct solar irradiation) to collecting devices, for thermal power production [12]. Specifically, some forms of tracking mechanisms are used for positioning collectors such that solar rays impinge on their external surfaces. The collectors then focus the solar rays to the receiver, which comprises of absorber for conversion of solar to thermal energy, as well as piping, where heat transfer fluid (HTF) that carries produced thermal energy flows [13]. The thermal energy is either channelled to heat engine for conversion to

electrical power, or stored in thermal energy storage (TES) system for deferred usage [14]. Figure 2.1 illustrates the different components of a typical CSP system.

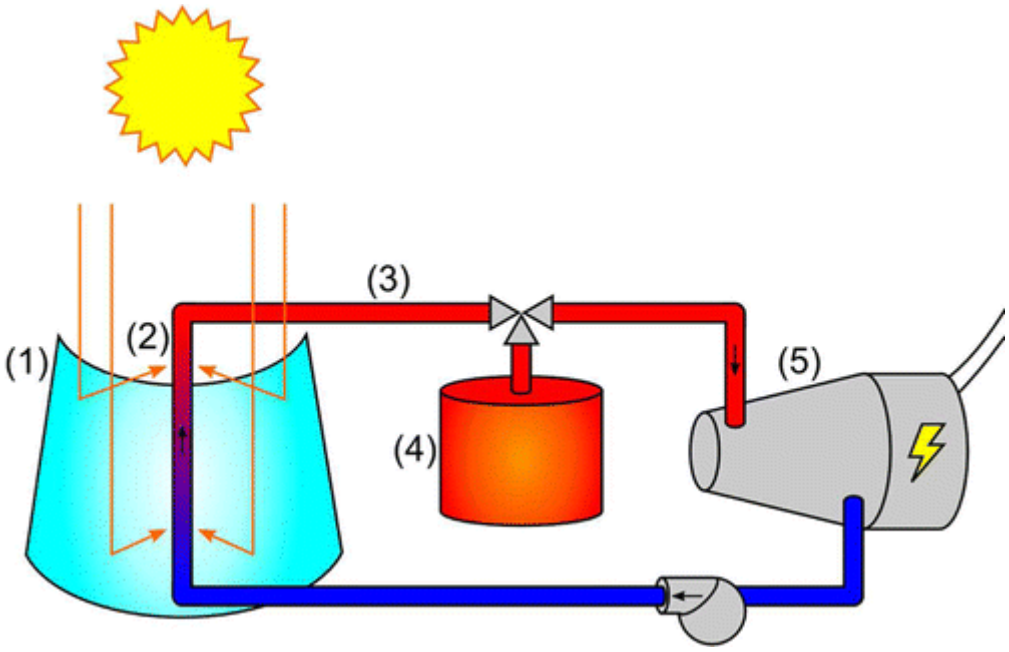

Figure 2.1: Typical components of a traditional CSP system: (1) concentrator, (2) receiver, (3) heat-transfer fluid, (4) thermal energy storage, and (5) heat engine. Reprinted with permission from reference [14]. Copyright 2015 American Chemical Society.

For CSP systems intended solely for thermal energy production, heat engine would not be needed, and in case of immediate use of thermal energy, the absorber could be linked directly with the application device, thereby excluding the need for TES and perhaps HTF. In essence, the real compositions of CSP systems depend on intended application.

Concentrated solar power technologies are usually classified on two broad basis. The first one is the type of tracking mechanism adopted. There are some collectors that track the sun only along its main axis of rotation, from east to west, generally referred to as one-axis tracking [15]. Conversely, other solar collectors track solar rotation both from east-west and north-south axes, generally called two-axis tracking. The solar collectors using one-axis tracking focus solar rays on a line, and are thus called line-focus collectors, with parabolic trough collectors (PTC) and linear Fresnel reflectors (LFR) being the main collector types in this category [16]. On the contrary, collectors using two-

axis tracking focus solar irradiation on a point, and are thus called point-focus collectors, with main types in this category being parabolic dish reflectors (PDR) and heliostatic field (otherwise known as central solar receiver or solar tower). Although point-focus collectors have the advantage of high concentration ratios over their line-focus counterpart, the technical requirement to achieve this is a little bit complicated, and the costs are consequently much higher [17].

The second basis for classifying CSP systems is the nature of collecting surface adopted. Some collectors have their surfaces to be continuous, where the receiver and collectors are assembled to form a single unit, thereby moving together for solar tracking [18]. It is possible to achieve very high concentration ratios with this arrangement, as well as a simple mechanism for tracking. PTC and PDR are the main examples of collectors in this category. Conversely in this respect, other collectors have discrete facets on their surfaces, with stationary receiver clearly distinguished from the collectors. Although the concentration ratios achievable in collectors using discrete facets are lower, they are often installed closer to the ground, and are thus less affected by wind thrust [19]. LFR and heliostatic field fall to this category. It is clear from the foregoing that PTC, LFR, PDR and heliostatic field are the four main types of solar collectors. The aforementioned different classifications are summarised in Figure 2.2.

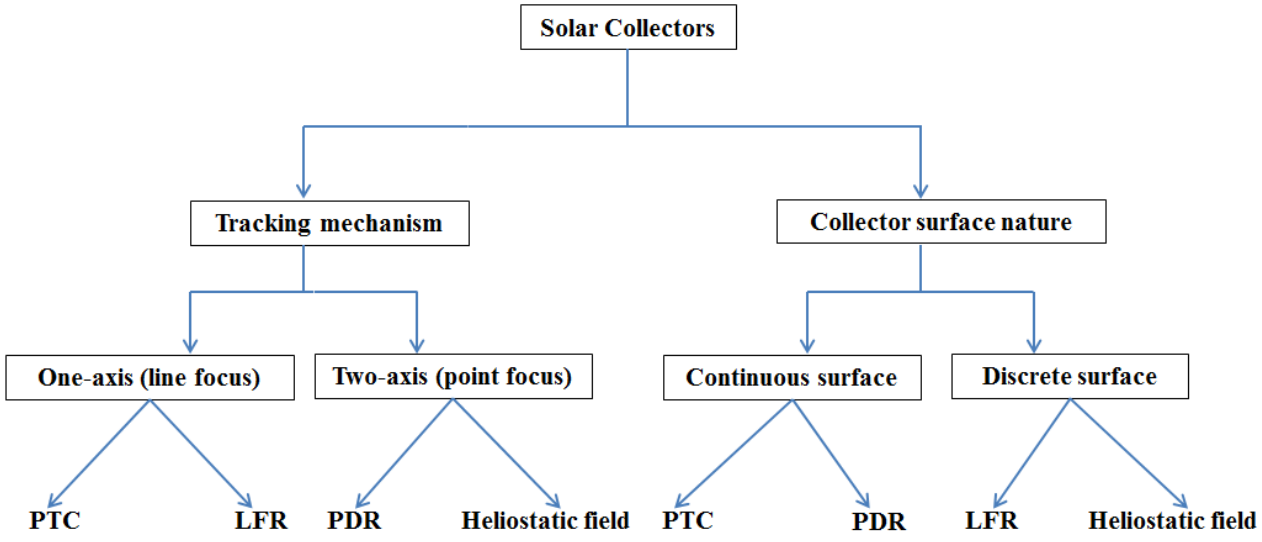

Figure 2.2: Classification of solar collectors.

Parabolic trough collector is by far the most matured CSP technology [20]. This is substantiated by the high number of CSP projects around the world that adopt PTC, relative to other collector types. As at August 2019, about 100 of CSP projects globally are based on PTC technology; about 37 on heliostatic field (Solar Tower); about 15 on LFR; and only about 2 on PDR [21]. The quoted numbers for all collector types also include projects that are currently under development/construction. Given the high level of practical implementation of PTC and heliostatic field and based on the aforementioned classifications of solar collectors, it would be in order to conclude that line-focus and discrete-surface characteristics are desirable features of solar collectors for real applications. However, while PTC is highly matured technically, its continuous surface makes it a bit expensive [22], and it requires high land area for installation [23]. On the other hand, adoption of point-focus mechanism in heliostatic field enhances operations at higher temeperature range, but also at the expense of plant economics [24], which obviously impedes its market penetration. It thus suffices to say that development of collectors with one-axis tracking technique and whose surface are as discrete as possible is a noble adventure, capable of increasing practical implementation and competitiveness of CSP plants. This assertion clearly puts LFR at an advantage, and a lot of developmental efforts are underway to improve their technological capacities by increasing concentration ratios and efficiency [25–27]. In fact, a number of studies have compared PTC and LFR in terms of technical and economic potentials [23,28], and it has been mostly affirmed that LFR holds good prospects in the nearest future [23,27]. Based on this premises, improvement efforts are ongoing on LFR, which has led to scalable and new types of linear collectors in some fronts, such as the compact linear Fresnel reflectors [29,30]. In addition, use of lens in place of reflectors in Fresnel collectors are being assessed in literature, and it has been affirmed that this could provide a more economically-viable alternative relative to conventional LFR [31].

Currently, research efforts on solar collectors are mostly directed at investigating other collector configurations with improved collection/absorption capabilities [32]. Other ongoing research

activities focus on finding ways to reduce efficiency losses due to dirts and film formations on collector surface [33], amongst others. It is generally opined in the state-of-the-art that research efforts should be intensified on reducing costs of small-scale CSP systems, for distributed energy generation in rural and isolated regions [34,35]. In this case, direct use of water as HTF in solar collectors has been hinted to be prospective, for direct steam generation (DSG) applications [35]. More so, future research on CSP-based energy plants should integrate sustainability issues by incorporating life cycle assessments of proposed systems, as well as potential social benefits of installing CSP plants. If this is in place, there is a possibility that policy-making analyses as well as political outlook of CSP projects are improved a bit, which would positively impact decisions in favour of starting new and completing ongoing CSP projects around the world. Furthermore, research efforts aimed at enhancing solar collectors for high-temperature applications should be intensified, implying that materials with higher resistance to thermal stress should be sought and adopted [36].

2.2.2 Thermal energy storage systems

Thermal energy storage systems refer to technologies that are capable of accumulating heat from a thermal source, retaining same over a period of time, and releasing it subsequently for postponed usage. More technically, the accumulation phase of thermal energy in TES systems is known as charging phase; the retaining process is known as storage; while the releasing phase is referred to as discharging phase [37]. TES systems are highly useful technologies, which can be deployed for different applications. First, they serve the purpose of improving dispatchability and competitiveness of energy systems that are based on transient renewable sources, such as solar. These transient renewable energy sources are abundantly and freely available around the world, and huge efforts are currently being deployed to increase their penetration into the global energy mix [38]. However, due to their intermittent nature, reliability and efficiency of their conversion systems are quite low. Thus, TES serves the purpose of intermediating between sources and application

fronts, for improved reliability, which also helps in load shifting to match energy production and demand profiles in domestic applications [38]. In fact, it is widely acknowledged that TES is closely interwoven with future development of CSP plants [39]. Next, TES is highly essential in waste heat recovery in industrial processes, to bridge the availability gap between time of energy recovery from one process and the required time of application by the same or other processes [40–42]. The focus here is however limited to TES for CSP applications, in line with the theme under discussion.

TES systems for CSP applications are commonly classified based on the adopted mode of thermal energy storage, and based on the concept of integration to CSP unit. On the mode of storage, there are three basic kinds of TES systems, known as sensible heat TES systems, latent heat TES systems and thermochemical TES systems [43]. Sensible heat system stores thermal energy by increasing temperature of the storage medium during charging phase, and subsequent decrease in temperature during discharging process, without the storage medium undergoing change of phase [43]. Carefully selected materials with adequate density, specific heat, thermal conductivity and diffusivity, thermal stability, etc. are generally adopted as storage media, usually in solid or liquid phase [44]. One identified impediment of concern with this kind of TES system is low energy density of the commonly used storage materials, thereby necessitating installation of large TES systems with their attendant volume/space consequences. With the aim of ameliorating this setback, research efforts are ongoing aimed at improving energy densities of solid sensible heat TES materials, by integrating encapsulated materials [45] or nanoparticles [46]. It is reported in literature that most of the currently installed CSP plants with TES systems make use of sensible mode of thermal storage [47]. In its stead, latent heat system stores thermal energy by isothermal phase change of storage medium during charging/discharging phases [48]. The phase change material (PCM) can take the form of solid-liquid, solid-gas, or liquid-gas phase transformation during energy accumulation or discharge process [48]. This type of TES systems are known to have higher storage density relative to sensible heat TES systems, thereby requiring lower installed volume [49]. However, more

stringent properties are desired in potential phase change materials, making latent heat TES systems to be a bit more technically risky and costlier relative to sensible heat systems [50]. Also, required charge/discharge duration of PCMs are quite high, due majorly to their low thermal conductivities [51]. Several studies have thus been conducted to investigate adequate additives and new techniques to improve heat transfer processes of PCMs [52]. Contrary to sensible heat and latent heat TES systems that use purely physical processes, thermochemical TES systems store thermal energy by combining or decomposing molecular structures of reactants, through reversible chemical reactions [53]. During charge phase, thermal energy from CSP is expended in an endothermic reaction for storage, and the same energy is recoverable by a reversible exothermic reaction during the discharge process [53]. This way, the entire storage process can take even at low temperatures, in favour of the possible duration of storage. In addition, energy density of commonly used reactants are usually higher than what obtains in latent heat TES systems, and very low storage costs are therefore achievable [54]. Different materials and reactions are possible in thermochemical TES systems, the details of which are contained in the state-of-the-art [54]. Major setbacks of thermochemical TES systems also lie in very slow heat transfer and reduced mass transfer processes, due to poor thermal conductivity and low permeability of suitable materials, respectively [55]. Consequently, many developmental techniques have been proposed in the open literature [56], to enhance heat and mass transfer during decomposition and combination of reactants, while substantial efforts are still ongoing in this respect [57].

Conversely, based on the concept of integration to CSP units, TES systems are classified as active and passive types. In active TES systems, the storage medium flows, driven by forced convection heat transfer process, to interact with thermal source/sink for charging or discharging. Active TES systems could be direct, in which case the HTF circulating through the solar collectors coincides with the flowing storage medium; or indirect, in which case TES storage medium is distinctly different from CSP HTF. Cold and hot storage materials could be stored in different tanks, forming a 2-tank TES system, or in a single tank with cold and hot media separated by temperature

stratification, often reinforced with filler materials to enhance the separation zone between the two regions, called thermocline [58], and to prevent mixing [59]. Adequate filler materials are required, and encapsulated PCMs alongside other innovative solutions are assiduously being investigated in this respect [60]. On the contrary, in passive TES systems, the storage medium, usually in solid state, is stationary, and charge/discharge process takes place by circulating another HTF from/to solar collectors [61]. The different classifications are summarised in Figure 2.3.

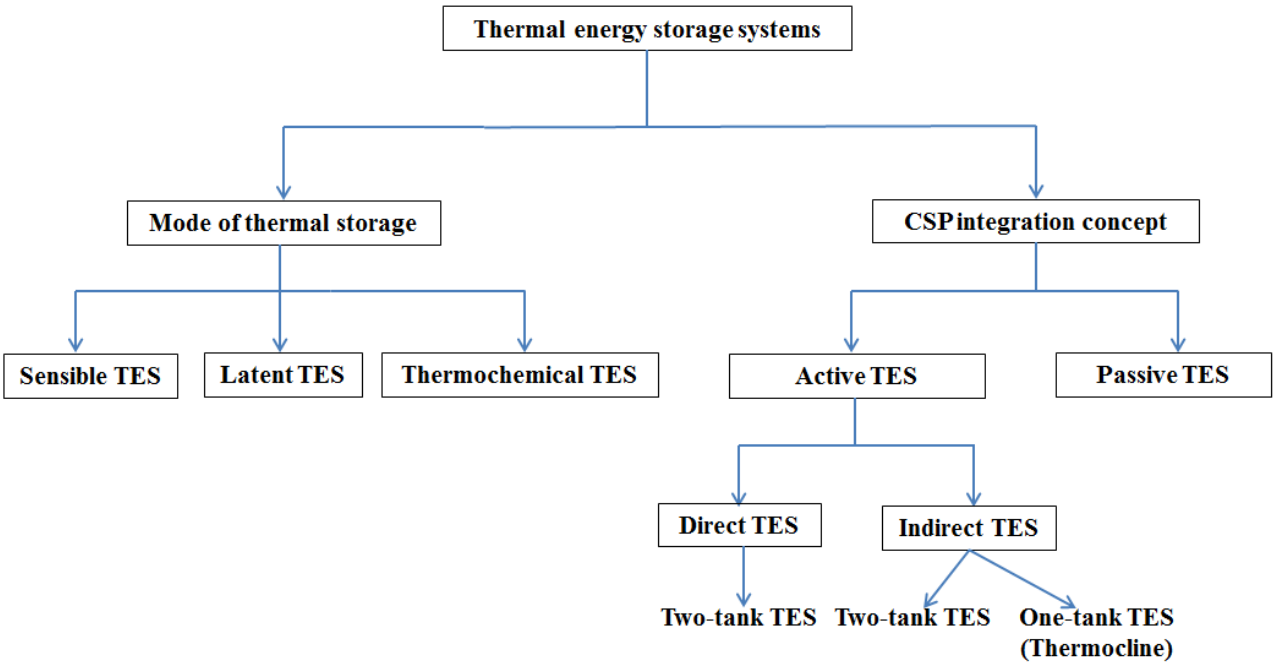

Figure 2.3: Classification of thermal energy storage systems for CSP applications.

Moreover, concerted efforts are ongoing to improve performance of TES systems for CSP applications, with current research activities majorly focusing on enhancement of storage materials for improved heat transfer and ancillary features [62,63]. Also, research efforts are ongoing to develop TES materials that are capable of functioning efficiently at higher temperature range than the current ones [64]. In this regard, hybrid TES schemes that combine two or more modes of thermal storage are being investigated in literature [65–67]. In addition, investigations are ongoing and still needed to develop cost-effective ways of reducing thermal inertial in TES systems, as well as to enhance control of temperature of HTF flowing through the system. In this regard, it has been

proposed that TES systems should be designed and produced in smaller units, in the form of system cascading, instead of combining all the processes involved in one single unit as is currently common [68–70]. However, cascading is yet a more costly solution, and the design and construction intricacies have been reported to be more complicated than what obtain in single units [71,72]. This therefore necessitates further research efforts in this respect. Furthermore, another new area of TES research involve the use of granular particles both as storage media and HTF, adopting mechanical devices to circulate granular particles [73,74].

2.2.3 Biomass energy

Organic resources produced when animate and inanimate living species undergo metabolic processes are generally referred to as biomass [75]. Based on their origin, biomass resources can be classified as agricultural biomass, forest biomass and renewable wastes, which encompass industrial and municipal wastes [76]. Agricultural biomass are typified by energy and rotation crops and their residues, while raw forest woods and their residues are generally grouped under forest biomass [77]. Biomass resources can take any of solid, liquid or gaseous states, depending on the generation source. It is however widely acknowledged that solid biomass resources are the most abundant and commonly used ones [78], and they are the focal point in this study as well. Depending on intended application, biomass resources could be used directly as obtained from their sources, and they could be further treated and upgraded before usage [79]. Common upgrading mechanism of solid biomass include pelletization, pyrolysis and torrefaction, amongst others [80].

The product streams that are obtainable from biomass could be classified based on targeted sector of application, as: energy biomass products, transportation biomass products and industrial biomass products. In the energy sector, biomass could be processed to produce heat, which could be used directly or converted into electricity as a single product or also in addition to heat, known as combined heat and power (CHP) production. In addition, biomass could be used for producing chemical energy in form of fuels, which could be processed for various applications in the energy

sector. In the transportation sector, biomass could be processed into liquid and gaseous fuels which could be used directly or indirectly to drive vehicular engines. The produced fuels from biomass resources are generally known as biofuels [81]. More so, it has been proven that biomass resources are suited for production of raw materials and fuels needed directly in some industrial processes, such as bio-refining, biomaterials, biochemical and charcoals [82,83]. An overview of various sources and obtainable products from biomass is represented in Figure 2.4.

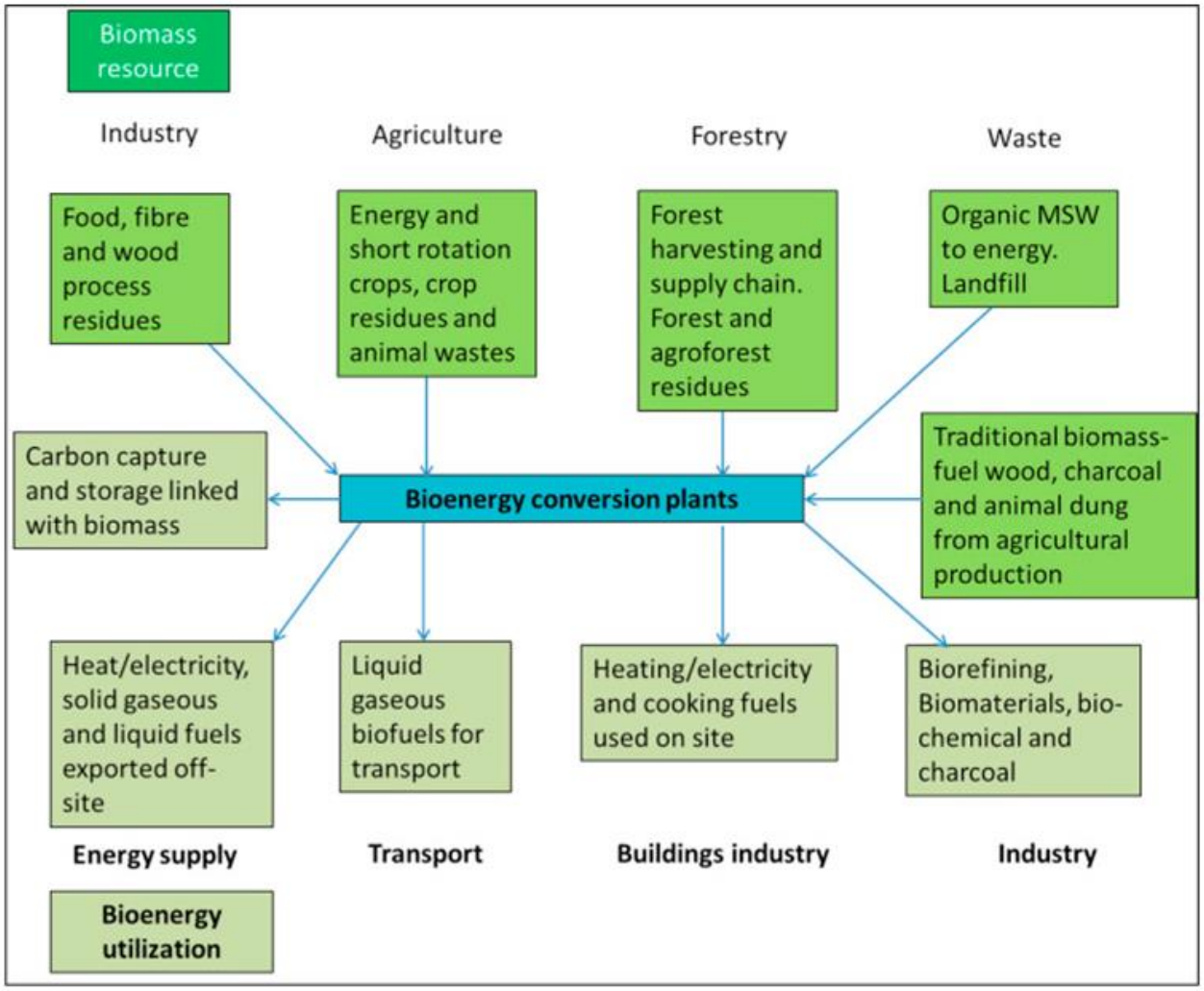

Figure 2.4: Overview of biomass resources and common products [80].

Furthermore, depending on the intended products from biomass conversion, there are generally two conversion processes, known as biochemical and thermochemical conversion processes. In biochemical conversion, biomass resources are either fermented or digested to obtain desired

products [84]. Digestion could take place in the presence of oxygen, in which case it is called aerobic digestion, or in its absence, in which case it is known as anaerobic digestion [85]. On the other hand, thermochemical biomass conversion technologies are used for producing heat from biomass, which is the focal point in this study. The technologies generally employ combustion, gasification and pyrolysis (including liquefaction) processes for biomass conversion [86]. Some studies have also mentioned hydrothermal and hydrolysis processes [87,88], which are however downplayed in this review study. Combustion process could be direct or indirect, depending on whether hot combustion flue gases are used directly for intended applications, or if they are recovered and utilized through other heat transfer processes, for instance in steam production for power production, etc. Different types of devices are applicable for biomass combustion process, such as boilers, furnaces, ovens, driers and kilns [89]. For biomass gasification, solid biomass undergoes thermally-driven phase change conversion to mixture of gases, usually called syngas [90]. The syngas so produced is combustible, and it could thus be burnt for heat, electricity or CHP production [91]. Also, syngas obtained from biomass gasification process could be further processed into fuels and chemicals, such as is done in bio-refining processes [92]. Heat required for biomass gasification process could be obtained externally through heat exchangers, or by partial oxidation reaction [93]. Common biomass gasifiers are in the form of fixed and fluidized bed reactors, which include updraft/downdraft gasifiers and circulating/bubbling fluidized bed reactors, respectively [94]. Other gasifiers include entrained and plasma types [94]. Then, by decomposing biomass in the absence of oxygen, it is possible to transform it simultaneously into liquid, gas and charcoal, a conversion process generally called pyrolysis [95]. It is possible to influence pyrolysis process in favour of one form of the products over the others. For instance, by employing fast heating rate process, more of liquid biofuels are produced (liquefaction process), while extremely slow heating rate process yields charcoal substantially [96]. Several research efforts are ongoing and more are still needed to optimize pyrolysis processes for enhanced techno-economic and market

penetration potentials [97–99]. An overview of common conversion technologies of solid biomass is also represented in Figure 2.5.

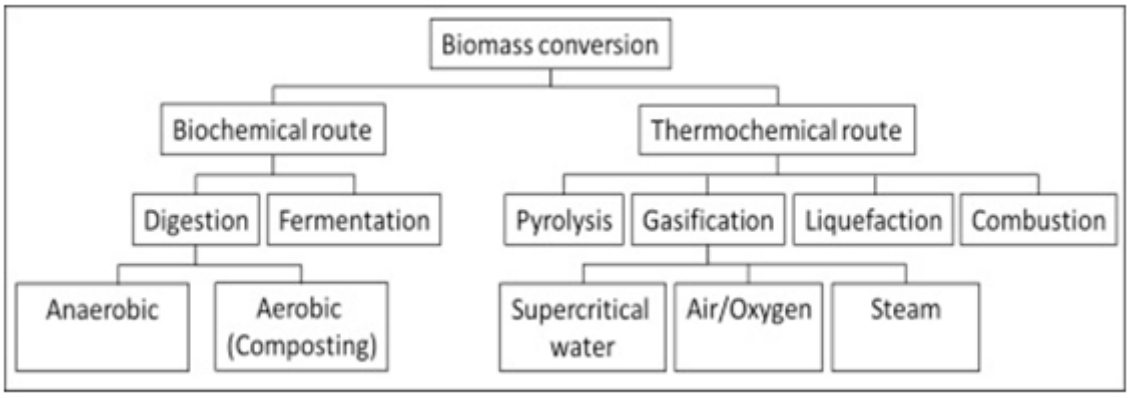

Figure 2.5: Common biomass conversion processes [80].

Overall, current research efforts are directed at improving available conversion technologies of biomass, for enhanced technical, economic, social and environmental performance metrics [86]. Also, suitability and sustainability of different biomass resources for specific industrial applications are being studied widely nowadays, especially as it concerns industrial processes with high-temperature requirements, exemplified by steel and cement industries, etc. [87]. These efforts should be intensified in the nearest future, especially with a mind of promoting new areas of applications of biomass resources, perhaps as direct substitutes for fossil fuels. In addition, integration of biomass-fired or biomass-coal co-fired plants with carbon capture and storage facilities should be examined from technical, economic and environmental points of view, for possible achievement of negative emissions of carbon dioxide. More so, such assessment should be decentralized, as biomass resources available in each country are different, and so are diverse politically-motivated policies and social acceptance that are in place.

2.2.4 Organic Rankine Cycle plant

Organic Rankine Cycle (ORC) refers to a form of classical Rankine cycle plant that uses organic substance as working fluid, in place of water used in conventional cycle, basically for the purpose

of converting low-temperature thermal energy to electrical energy [100]. The history of ORC is dated back to the year 1826, when means were being sought for making valuable use of thermal energy being rejected from condenser of steam reciprocating engines [7]. In particular, the first notable effort proposed that ether should be vapourized by steam condensate from a combined vapour cycle used for ship propulsion [7,101]. However, the progressive development of ORC technology was not consistent, due to myriads of challenges encountered by the first proponents. At a time, scientific activities on the technology were stopped, before the renewal of interest re-surfaced around the year 1935. Steady progress was then recorded between 1975 and the beginning of the 21st century, when rigorous commitments were directed at improving and enhancing commercialization of the technology [101]. Today, it has become a widely investigated technology for exploiting energy sources with low temperature, generally below 500 ^{o}C [7]. In fact, as at the end of the year 2016, there were about 1754 ORC units installed globally, with total capacity of about 2.7 GW, designed and built by about 27 manufacturers who are currently players in the ORC technology business [101]. At the moment, ORC is being widely applied for exploiting thermal energy of various renewable resources, including solar thermal, biomass and geothermal, etc. [102]. In addition, it is being hugely deployed for recovering useful but limited thermal energy from various industrial and ancillary processes [103]. More so, ORC has the advantage of being scalable, which makes it appropriate for medium/small scale applications, as well as for micro applications [104].

Similar to conventional Rankine cycle plants, there are basically four processes involved in power production from ORC. First, organic working fluid at low temperature and pressure is pumped for increased pressure head. Second, the pressurized organic fluid is heated and vaporized in evaporator, by heat exchange process with the adopted heat transfer source. Third, the vapourised organic fluid at high pressure is expanded through a combined expansion device and electricity generator (turbogenerator). Fourth, the expanded organic fluid is cooled to its starting temperature in the condenser, and the cycle continues [102]. Schemes showing the basic ORC components and

processes are illustrated in Figure 2.6. However, some modifications are possible to the above highlighted cycle processes, in order to improve system efficiency and based on the peculiar constraints imposed by the choice of heat source. For instance, it is common nowadays to recover thermal energy of the expanded vapour and use it to preheat organic working fluid before it receives further vaporizing heat from the thermal source [105]. The process is generally referred to as internal recuperation/regeneration, and the heat exchanger used is often called recuperator/regenerator. Similarly, it is common to superheat organic working fluid using thermal energy from the source, prior to the expansion process in turbine, for improved fluid quality at turbine exit, which is aimed at preventing possible damages to the expansion device [106]. In the same vein, expanded working fluid often needs to be subcooled at the end of expansion process, to bring it to the temperature adequate for pressure increase process in the pump [107]. As aforementioned, some of these cycle modifications are often necessitated by the nature of heat source intended to be exploited, and it is thus usual for ORC designers to investigate the appropriate cycle configuration as part of design process [108]. There are now many organic substances that are suitable for applications as working fluid in ORC, including fluid blend/mixture. Design procedures also often include selection of adequate working fluid that would optimize the system for an intended application, considering all of technical, economic and environmental aspects of plant operation [109].

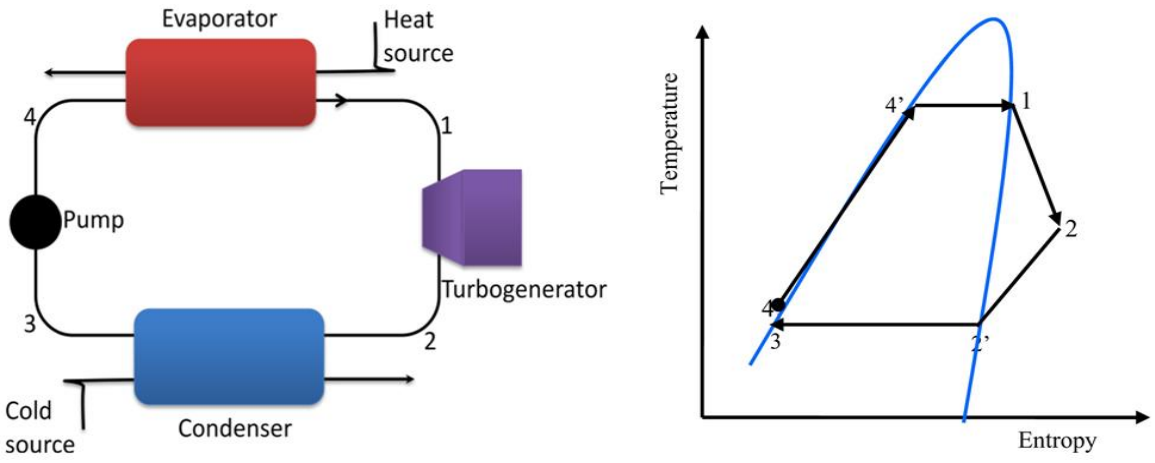

Figure 2.6: Basic ORC components and processes [102].

Furthermore, as hinted earlier, ORC plants are applied for various heat recovery and power production processes in diverse industries. In the maritime industry, ORCs are used for recovering heat from ship propulsion engines, which could then be used to generate heat and/or electricity needed for ship internal operation, thereby promoting energy self-sustenance [110]. A similar thing is now practiced in the oil and gas industry, where ORCs are used for recovering rejected thermal energy from oil and gas offshore platforms, for electricity production [111]. Also, ORC plants are being applied for heat recovery in cement industry [112], ceramic industry [113], glass industry [114] and steel industry [115], just to mention a few. All these are in addition to direct applications for production of electricity, heat and/or CHP from renewable sources by power companies [116]. Clearly, the potential market for ORC technology is enormous, and this justifies the huge efforts being currently deployed for its progressive development in all fronts.

However, there are some notable challenges with ORC plants, especially as it concerns low thermal efficiency, high costs of implementation as well as high energy losses due to thermal instability of sources [117]. Thus, research efforts are ongoing to ameliorate some of these challenges, to pave way for improved market penetration. At the moment, researchers are investigating sustainable ways of integrating ORC plants with various heat sources, leading to hybridization of stable renewable energy sources with transient ones, which is the basis for the research study being reported in this compendium as well [118]. In addition, efforts are being made to investigate novel ways of designing and operating ORC components and units, for improved performance which would lead to increase in efficiency of the overall plant [119,120]. This includes integration of ORC plants to systems using other technologies, as topping or bottoming cycle, to form combined energy and water desalination plants [121], for instance. More so, vast efforts are ongoing to investigate cost-effective working fluid that would optimize performance of ORC components by reducing exergetic losses, thereby improving efficiency. This has attracted huge scientific and financial dedications to the study of fluid mixtures as potential working fluid in ORC applications [122].

All these efforts should be further intensified in the future to make ORC plants more attractive in economic terms, especially in small/micro-scale applications that could be valuable for distributed power generation. Moreover, better control and management strategies should be developed for ORC plants, in order to enhance dispatchability and system stability.

2.3Brief literature review on hybrid CSP-Biomass plants and adopted analyses methods

2.3.1 Review of studies on hybrid CSP-biomass plants

Concentrated solar power is one of the freely available renewable energy sources that are being promoted aggressively for cleaner power production. And as aforementioned, ORC is a key technology that enables power conversion of low thermal power, including CSP systems at small and medium scales. This has led to substantial interest in solar-based ORC plants, as substantiated by the quantity of studies available in the literature on design, analysis and optimization of such systems [123]. However, practical implementations of the studied configurations are not quite embraced as yet. For instance, Petrollese *et al.* reported that only eleven real CSP-ORC plants in the range of 50 kW - 5 MW exist around the world [9], all of which currently perform poorly in thermo-economic terms. One reason that is attributed to difficulty in implementation is diurnal and seasonal fluctuations of solar irradiation. This often leads to low plant reliability and dispatchability, a scenario that badly impact system techno-economic performance.

Consequently, a number of solution strategies are currently being deployed in real CSP-ORC plants. These include integration of thermal energy storage (TES) devices, which has attracted huge scientific and economic efforts in recent times [10]. In addition, hybridizing solar systems with other dispatchable renewable energy resources is another solution strategy being vigorously investigated [11]. And since geothermal and biomass are among the most dispatchable of all renewable energy resources, their suitability for hybridization with solar systems in ORC plants are widely studied. For instance, Heberle *et al.* [124] demonstrated the techno-economic benefits of

retrofitting an existing geothermal ORC plant with a CSP system. Also, the practicality of this concept has been realized at the Still Water hybrid geothermal-CSP project in Nevada, USA [125]. However, in a situation where a solar ORC plant is the base system in existence, hybridizing a geothermal system would be capital intensive. The location of such plant might also not be feasible for exploiting geothermal resources, due to unfavourable ecological features. In this case, biomass hybridization would be a better alternative, and this has necessitated the outlook of this study.

Several authors have analysed different economic and technological perspectives of CSP-biomass hybridization schemes in literature. Powell *et al.* [4] discussed cases of CSP-biomass hybridization in their study, highlighting their merits and setbacks. Also, Hussain *et al.* [126] synthesized the level of technological maturity of different CSP technologies, for hybridization with biomass. They reported that Solar Tower (ST), Parabolic Trough (PT) and Linear Fresnel (LF) configurations are most technically viable, in that order. However, most of the few existing CSP-ORC power plants currently operating around the world adopt PT technology [9]. Although the optical efficiency in LF collectors is lower, as aforementioned, it exhibits much improved economic potentials over the other collector types [127].

In the case of biomass, several studies examined the suitability of different fuels and thermal conversion technologies for hybridization with CSP plants [128,129]. Anvari *et al.* [130] proposed a solar hybrid scheme to enhance power generation in a biomass gas turbine power plant. The hybrid plant is rated at 15 MW, inclusive of a bottoming steam turbine plant. They reported that incorporating solar system to the biomass combined cycle plant increased power generation by 25% and reduced CO_2 emission by 31%. Liu *et al.* [131] analysed two different schemes for hybrid CSP-biomass plants. The two schemes adopt biomass gasification conversion process. CSP is employed in the gasification process, to produce the so called solar fuel. The produced syngas is then converted to electrical power, through combined Brayton-Rankine cycle plant in one case. In the other case, the syngas produced from biomass gasification is fired, for direct utilization of combustion heat by the power block. Similarly, Bai *et al.* [132] analysed the use of CSP-driven

biomass gasification and biomass pyrolysis processes. They demonstrated that integrating CSP system into a two-stage gasifier improved energy efficiency of the system by 26.7%. In another study, Bai *et al.* [133] demonstrated the suitability of direct biomass combustion process for CSP hybridization. The proposed hybrid CSP-biomass power plant is rated at 50 MW. Thermal power obtained from biomass boiler and PT collectors is used in sequence, for producing superheated steam, used for driving a Rankine cycle, for electricity generation. Suffice it to submit that the use of solar power for gasification of biomass to produce syngas is quite interesting. However, in a case where a stand-alone CSP-ORC power plant is already in operation, the gasification technology could be complicated. Furthermore, additional investments might worsen the profitability prospects of the hybrid gasification system. In this light, Hussain *et al.* [126] attempted to evaluate techno-economic suitability of different biomass conversion technologies for CSP hybridization. The authors reported that direct biomass combustion is the most preferred for hybridization with CSP plants. This, according to them, is due to lower capital investment and operational costs, which is able to make up for low technical performance.

From the foregoing, it could be inferred that retrofitting a direct biomass combustion furnace with CSP-ORC plant could allow for techno-economically favourable implementation. Biomass-ORC and CSP-ORC plants have much equipment in common, and this would facilitate existing CSP-ORC plants to be easily retrofitted with biomass furnace, and vice versa. In fact, a number of recent studies have examined different schemes in this context. Sterrer *et al.* [134] proposed hybridization of CSP system with existing biomass-ORC combined heat and power (CHP) plant. The presented plant operates in Salzburg, Austria. Temperatures of some operational points of the biomass-ORC plant markedly deviate from nominal conditions. Thus, PT collectors were proposed for indirect hybridization into the system, to maintain thermal stability. Similarly, Zourellis *et al.* [135] presented operational information for a biomass-ORC CHP plant. They reported the technical performance of integrated PT collectors to the plant, which is located in Denmark. The studied plant is acclaimed to be the first of its kind in the world, and it started operations in the summer of 2017.

Furthermore, Soares and Oliveira [136] analyzed biomass hybridization scheme for a mini ORC power plant, rated at 60 kW. The heat source consists of PT collectors and micro biogas boiler. The study was conducted in the framework of REELCOOP project, which was co-funded by the European Union (EU). The authors submitted that biomass hybridization improved the technical performance of the system, increasing annual energy yield by 6.2 %. Desideri *et al.* [137] presented a mini CSP-biomass-ORC-CHP plant for application in buildings, in the framework of the EU-founded BRICKER project. The employed hybridization scheme is indirect. The heat transfer fluid is first heated in the PT collectors, before the temperature is further raised in biomass boiler. The aim of the project was to demonstrate the potentials to meet energy demands of buildings by fully-renewable energy systems. Pantaleo *et al.* [138] also presented hybrid CSP-biomass scheme for CHP generation. The plant consists of a topping externally-fired gas turbine system, utilizing thermal power from both PT collectors and biomass furnace in series. Then, gas turbine exhaust heat is recovered, for use as heat source for a bottoming ORC-CHP plant. The authors demonstrated the flexibility of the presented system, in terms of both technical and economic performance. However, they reported that incorporation of CSP into existing biomass-only plant reduces economic viability of the plant. In another study, Pantaleo *et al.* [139] presented a similar scheme, with the novelty of using a molten-salt TES systems for transferring exhaust heat from the topping Brayton cycle to the bottoming ORC. They reported levelized cost of electricity of about 140 €/MWh for the system, and investment return rate of around 15%.

All the above-cited studies have clearly demonstrated the viability of CSP-biomass hybridization concept. However, none of them clearly illustrated the techno-economic potentials of retrofitting existing CSP-ORC plants with direct biomass combustion system. In fact, majority of the studies started with biomass system, and then integrated CSP for process upgrade. Since many existing CSP-ORC plants are not able to operate at minimum load and follow scheduled power profile, this study led the focus on the improvement of such systems. Despite the integration of TES systems in modern designs, most CSP-ORC plants are usually shut down for several hours within the year.

This is usually due to insufficient TES capacity, as economic implications of implementing large TES systems and solar fields are often not favourable. Furthermore, TES systems could be characterized with thermal instability, due to imperfect insulation and fluctuating temperature of Heat Transfer Fluid (HTF) from CSP system. It is therefore essential to study a retrofit configuration that is able to better salvage the aforementioned challenges with existing CSP-ORC plants in practice, for enhanced plant management with respect to dispatchability. This essentiality led to the first objective addressed by the study reported in this thesis; to propose and assess a conceptual parallel hybridization scheme, for biomass retrofit to existing CSP-ORC plants, as presented in Chapter 3.

2.3.2 Review of organic mixture as working fluid in solar-biomass ORC applications

As a consequence to the global rise in campaigns for the promotion of ORC for exploiting renewable energy resources, efforts are being hugely deployed to ameliorate the problems of low efficiency and high costs of implementation, as highlighted earlier. Amongst others, one area of potential improvement that has been identified in literature is application of mixture of organic working fluids in ORC systems [140]. In addition to potential improvement of ORC efficiency, adoption of fluid mixtures in ORC expands the selection range of working fluids for different applications [141]. And considering the recent restrictions of some fluorinated pure working fluids due to environmental concerns [142],[143], substantial research efforts are desired for identification and assessment of acceptable mixtures for different ORC applications.

Premised on this reality, several recent studies have focused on the use of mixtures of different classes of fluids as working media in ORC. Aghahosseini and Dincer [144], Chen *et al.* [145], Zhao and Bao [146], Su *et al.* [147] and Chys *et al.* [148] all showed by comparative thermodynamic analyses that mixtures of selected refrigerants are prospective in generic low-temperature ORC power generation plants. Other authors have directed their studies on specific heat source applications. For geothermal ORC plants, Heberle *et al.* [149], Radulovic and Beleno Castaneda

[150], Kang *et al.* [151], Liu *et al.* [152] and Yue *et al.* [153] proved the thermodynamic benefits of using zeotropic mixtures, for different ORC configurations and class of fluids. Notable among their findings is the ability of zeotropic mixtures to reduce irreversibility in condenser, thereby increasing cycle efficiency. The reason for this is non-isothermal phase change process exhibited by zeotropic mixtures in condenser and evaporator. Also, the authors reported that matching temperature difference of cooling medium with condensation temperature glide further improves thermodynamic gains of zeotropic mixtures. Similarly, in the case of ORC plants for waste heat recovery applications, Ge *et al.* [154], Xi *et al.* [155], Song and Gu [156], Li *et al.* [157], Braimakis *et al.* [158], Yang *et al.* [159], Shu *et al.* [160], and Zhang *et al.* [161] all highlighted the thermodynamic merits of zeotropic mixtures over pure fluids. It can be inferred from their diverse studies that temperature range of heat source has considerable effects on selection and performance of mixtures as ORC working fluids. In case of high temperature sources, mixtures of fluids belonging to siloxane class were reportedly suitable, alongside toluene, amongst others. In particular, for siloxane mixtures in ORC waste heat recovery applications, Weith *et al.* [162] studied the potentials of mixtures of hexamethyldisiloxane (MM) and octamethyltrisiloxane (MDM) for power-only and combined heat and power generations. For power-only ORC plant, they reported 1.3% increase in exergetic efficiency when 97/03 wt % MM/MDM-mixture is used, relative to best pure component. In the case of cogeneration, the study highlighted that mixture benefit is even higher, with 60/40 wt % MM/MDM-mixture showing 3% more exergetic efficiency relative to pure fluid. Furthermore, a survey of literature shows that studies are quite few on the adoption of fluid mixtures in solar ORC applications [163]. For this application field, Zheng *et al.* [164], Wang and Zhao [165], Wang *et al.* [166], Mavrou *et al.* [167] and Habka and Ajib [168] all demonstrated that fluid mixtures in ORC are more beneficial to system thermodynamic performance, relative to pure fluids. These include dedicated studies of selected working-fluid mixtures, as well as Computer Aided Molecular Design (CAMD) of working fluid compositions. For biomass and hybrid solar-biomass ORC applications, no dedicated studies on performance of

mixtures as working fluids were found in the state-of-the-art. From the foregoing, it is clear that use of working-fluid mixtures in different ORC applications is favourable to thermodynamic performance.

However, thermodynamic improvement alone is not sufficient to facilitate market penetration of any emerging technology. Beyond performance, investors and policy makers are often more interested in economic viabilities and returns on investments. Based on this reality, economic aspects of supposed benefits of mixtures in ORC applications have attracted some attention in the state-of-the-art in recent times. In their study, Le *et al.* [169] maximized exergy efficiency and minimized levelized cost of electricity (LCOE) in a subcritical ORC power plant. The study considered n-pentane, R245fa and their mixtures as working media, for waste heat recovery application. They reported that thermodynamic and economic performances of 0.95n-pentane/0.05R245fa and 0.9n-pentane/0.1R245fa were comparable to that of n-pentane, which is better than that of R245fa. Heberle and Brüggemann [170] applied thermo-economic principles to evaluate performance of zeotropic mixtures in geothermal ORC power plants. Since it was established that mixtures increase ORC efficiency, the authors aimed to investigate if the efficiency increase overcompensates additional economic requirements on main components. They studied various combinations of popular ORC working fluids, at diverse temperature range of geothermal heat source. As reported, for about 160 ^{o}C geothermal water heat source, mixtures like propane/isobutene, isobutene/isopentane and R227ea/R245fa could be more prospective than most efficient pure fluids, in economic terms. They equally identified prospective mixtures for other temperature values, and submitted that zeotropic mixtures are equally promising for enhanced economics of geothermal ORC plants. In another study, the same authors [171] studied thermo-economic performance of zeotropic mixtures in ORC for waste heat recovery application. For a subcritical ORC with heat source temperature of 150 ^{o}C, they showed that specific cost of power production using pure isobutene is lower than if isobutene/isopentane mixture were the working fluid. However, mixture performed better than R245fa and isopentane, in terms of the ORC specific

cost of power production. Furthermore, Oyewunmi and Markides [172] studied thermo-economic and heat transfer performance of working-fluid mixtures in geothermal ORC applications. For geothermal water of 98 ^{o}C, the authors reported that 0.5n-pentane/0.5n-hexane as well as 0.6R245fa/0.4R227ea were thermodynamically more efficient than all pure components considered. However, these mixtures were reportedly less efficient in economic terms, with costs per unit power output being 14 % more than what was obtained for pure fluids. Feng *et al.* [173] compared thermo-economic optimization of pure and mixture working fluids in generic low-temperature ORC system. With exergy efficiency and levelized energy cost as objective function, optimal operation parameters were identified by Pareto front analysis. The authors reported that better exergy efficiency obtained for mixtures were at the expense of levelized energy costs. In another study, Feng *et al.* [174] presented contrasting results obtained from their study on Pareto-optimal analysis of R245fa, pentane and their mixtures, for generic low-temperature ORC plants. They reported exergy efficiency of 52.12% for 0.5pentane/0.5R245fa mixture, as against 54.25% for pure pentane and 55.02% for pure R245fa. For optimized levelized energy cost, the authors submitted that value obtained for 0.5pentane/0.5R245fa mixture is higher than that of pure pentane by about 3.7%, but lower than that of R245fa by about 2.8%. In their study, Yang *et al.* [175] investigated thermo-economic performance of R1234yf/R32 mixtures in transcritical ORC system for waste heat recovery applications. Composition of the studied mixtures with highest thermodynamic benefit was identified, and by incorporating economic aspects, the authors submitted that mixture performed better than pure fluids in thermo-economic terms. Specifically, they mentioned that mixture thermo-economic performance increased by 1.46% compared to pure R1234yf, and it increased by 4.88% compared to pure R32. Also, Kolahi *et al.* [176] compared thermo-economic performance of pure fluids and mixtures in simple and recuperated ORCs for waste heat recovery applications. They found that 0.6R236ea/0.4cyclohexane performed better than their pure components, and that the benefits are higher for recuperated ORC than non-recuperated ones. However, since addition of extra heat exchanger for internal recuperation amounts to additional

costs, system without recuperator performed better in economic terms. Dong *et al.* [177] reported that adoption of zeotropic mixtures in generic low-temperature ORC systems is not beneficial over pure fluids, considering joint thermodynamic and economic aspects. The authors studied R245fa, R123, R365mfc, R113 and their mixtures, considering 130 ^{o}C heat source temperature. In addition, Li and Dai [178] obtained that use of working-fluid mixtures in both recuperative and non-recuperative ORC provide better economic performance than pure fluids.

From the foregoing, it can be inferred that whether efficiency increase in ORC systems overcompensates additional costs due to larger sizes of components is a function of application area, heat source temperatures, amongst other boundary conditions. Although majority of findings from the detailed literature review summarized above insinuate that adoption of mixtures in ORC is not economically better than pure fluids, none of them included off-design effects in their presented thermo-economic studies. In fact, only three studies are found in literature on off-design analysis of working-fluid mixtures in ORC applications, to the best of author's knowledge [179],[180],[181]. However, none of them investigated economic implications of mixtures under off-design conditions. They focused mainly on thermodynamic effects of heat source, sink and operating parameters on zeotropic performance in ORCs, as well as adjustment/tuning of mixture compositions. Considering that most real ORC plants actually work under off-design conditions, it is necessary to understand if thermodynamic benefits of zeotropic mixtures would outweigh additional economic burdens under these conditions. This knowledge gap is thus the second main scientific contribution addressed in this thesis, as highlighted in the second thesis objective aforementioned in chapter 1. In particular, thermo-economic performance of selected siloxane mixtures has been evaluated for hybrid solar-biomass ORC applications, under both design and off-design operating conditions, which are reported in Chapter 5 of this thesis. Apart from leading the focus on off-design economic analysis of working-fluid mixtures in ORC, this section of the thesis also leads the focus on thermo-economic study of working-fluid mixtures in ORC for hybrid solar-biomass applications.

2.3.3 Exergy-based methodologies for energy system analyses

Exergy is a term used generally to describe quantity of energy available for conversion to work in a process. It is the useful part of energy, and an indication of quality of various energy forms with reference to a specific environment [182]. It is based on the Second Law of Thermodynamics, and the root of its formulation is also traceable to the era of development of the concept of availability of energy, based on the contributions of Clausius, Tait, Thomson, Maxwell and Gibbs in 1868 [182]. Other authors defined similar theoretical hypotheses about the same time and afterwards, but notable practical applications are traceable to the 1930s, as a result of industrial growth and technological development witnessed at that time [182]. It should be particularly highlighted that the term exergy was coined in 1956 by Rant, and it remains a generally accepted terminology for the subject till date [182].

Exergy analysis of systems and processes considers the quality of energy transiting system boundary, and takes due account of internal losses in system components or processes [182]. Thus, exergy balance and methodologies are considered to be more essential for assessing the performance of energy systems nowadays, relative to energy balance and analyses. While energy analysis gives overall conversion efficiency in a multi-component system, exergy analysis goes further to quantify losses and their distributions across the whole system [182]. Such information is being sought in practical applications, to identify system components to which much attention should be directed in order to improve overall system performance.

Application of the concept of exergy traditionally entails establishing exergy balance for each system component, based on the type and functions intended for the respective components. To begin with, inlet and exit exergy entering or leaving each control volume (component/system) are defined. This includes exergy due to thermal energy transfer and actual mechanical work transfer between the control surface and the reference environment [183]. Then, the balance of total input exergy and total output exergy are obtained for each control unit, to quantify loss exergy in the unit. The most popular conventional metric used for assessing exergetic performance of a system is the

exergy efficiency, which is defined as the ratio of total output exergy from a control volume to total input exergy [183]. The concept of exergy method for system analysis has been extended to thermo-economic analysis, in an approach generally known today as exergoeconomic or exergy cost analysis [184–186]. Exergoeconomic analysis integrates economic principles with exergy concepts, to define flow of investment and operational costs in a system, as well as to investigate economic devaluations in a system as well as their locations. The exergoeconomic approaches widely applied nowadays have been termed specific exergy cost (SPECO) approach [187] and the exergy cost theory [188,189]. Similarly, conventional exergy concept has been integrated into environmental impact assessment of systems, in a term generally known as exergo-environmental analysis [190], which includes life cycle assessment of different processes [191,192]. In addition, further development of exergy and exergoeconomic assessments have been proposed in the state of the art, particularly in a bid to examine the parts of destroyed exergy and lost exergy costs that could be avoided, and the parts that are unavoidable [184]. Based on this, exergy and cost losses in a component due to its internal operations (endogenous irreversibility) and those due to its interaction with other components (exogenous irreversibility) are defined, and the concepts of avoidability and unavoidability are integrated [193]. These analyses generally lead to what is now being referred to as advanced exergy and advanced exergoeconomic analyses in the state of the art [194–196].

Furthermore, although the area of application of exergy concept mostly concerned with this study is for energy system analysis; the concept is equally applicable to many other types of systems. For instance, exergy analysis has proven to be a veritable tool in assessing depletion level and flow of natural resources on earth, known generally as exergoecology [197,198]. In fact, a website has been developed for this particular exergy application, amongst others [199], and these concepts are relevant for applications in resource-intensive industries such as manufacturing industry. Also, exergy analysis now finds applications in biomedicine, for assessing human body performance under physical activities [200], including thermal comforts of different body parts [201], and exclusively for studying blood flows in the human heart [202].

Specifically on the application of exergy and derived methodologies for assessing power plants, studies available in the open literature are too numerous to mention, but a few of the relevant ones are summarised here. For solar related systems, Wang *et al*. [203] demonstrated the usefulness of exergy and exergoeconomic assessment of a solar-assisted combined cooling, heating and power gas turbine plant. They stated specifically that energy and exergy efficiencies alone are not sufficient to express the impacts of integrating solar system into the gas turbine plant, but rather by incorporating exergy costs of the different products obtainable from the plant. Similarly, Nemati *et al*. [204] applied exergy and exergoeconomic methods to make an optimal choice between different configurations of a solar-driven organic flash cycles, using different working fluids. In the study, adoption of exergy and exergoeconomic performance metrics was claimed to affirm reliability of the selected optimal choice amongst the studied configurations. In the case of biomass-related systems, Soltani *et al*. [205] adopted exergoeconomic approach to assess and compare an externally-fired biomass plant with a similar plant co-firing biomass and natural gas. They demonstrated that although biomass-only system could be more prospective in exergoeconomic terms, its overall exergy efficiency is lower than when co-fired with natural gas, thereby enabling the adequate choice based on weight of interests. Also, Wang *et al*. [206] integrated system reliability assessment into exergoeconomic analysis in a modified exergoeconomic methodology, to examine cost flow in a biomass trigeneration plant. They reported that the applied modified exergoeconomic approach gave an insight into the fact that failure and repair rates of the gasification system largely influence the cost of products from the electricity generation system and the cooling system. They further stated that the specific exergy cost of the three products with reliability consideration increases by approximately 16%. In addition, for ORC applications, Behzadi *et al*. [207] applied exergoeconomic concepts to optimize a waste-to-energy plant in Tehran. They made comparative analysis on different working fluid that optimize the plant and selected the best, based on exergetic performance, and the components with highest sources of irreversibilities were identified to be gasifier and steam generator. More so, Dai *et al*. [208]

demonstrated the usefulness of advanced approach of applying exergy and exergoeconomic methodologies for assessing energy systems, based on generic ORC with different heat source considerations. Different hydrocarbons were compared, and the best was selected based on exergy analysis. Endogenous avoidable costs for the components were obtained, signalling the areas requiring utmost optimization efforts. The high point of the study is the submission that the exergy efficiency of ORC was improved by about 20% after the system was optimized using advanced exergy analysis. Equally important are the studies on application of exergy and derived methodologies to hybrid solar-biomass power plants. In this respect, Wang and Yang [209] analysed a solar-based biomass gasification combined power plant, highlighting specifically the role of exergy in assessing exploitability of each heat source, as well as their contributions to system thermodynamic and environmental performance. Likewise, Anvari *et al*. [210] studied exergoeconomic and environmental analyses of a solar-biomass combined cycle, by integrating solar system and steam turbine with a biomass plant. The studied exergy and exergoeconomic analyses enable the true measure of thermodynamic and economic impacts of the integrated units.

Based on the foregoing short literature review, it could be affirmed that exergy-based and derived metrics give better insight into true capabilities and optimization potentials of energy and allied systems. And since the hybrid plant proposed in this study comprises a new retrofit scheme, it would be very adequate to assess it based on exergy approach, which forms the basis for the exergy, exergoeconomic, enhanced exergy and enhanced exergoeconomic analyses of the hybrid plant reported in Chapter 5. Although the methods are classical, they remain relevant and novel when applied to new system for the first time. Further definitions and mathematical expressions for different concepts of exergy are also reported in Chapter 4, alongside detailed application procedures to power plant analysis, as exemplified by the studied hybrid solar-biomass scheme.

2.3.4 Optimization of energy systems

Optimization is the process of improving a system to facilitate its performance at its best capacity, based on specified criteria, and subject to given practical realities. It is a broad concept that cuts across many field of application, but the discussion here is limited to application to energy systems. In the 21st century, it is desired that energy systems should have the highest possible conversion efficiency based on thermodynamic principles; the investment and operation costs should be very low; and emissions of greenhouse gases should be as minimum as possible, amongst others. These thermodynamic, economic and environmental requirements are thus the basis upon which energy systems are often optimized. The desired criteria in an energy system that prompt formulation of optimization problems are called objective functions [211], while the practical realities such as thermodynamic laws, established safety principles and government policies that must not be violated during optimization are generally known as constraints [211]. The objective function could be any one of the aforementioned desired criteria, to form a single-objective optimization problem [212]. But, based on the clamour for sustainable energy systems, it is required that plants should satisfy two or more of the aforementioned thermodynamic, economic and environmental criteria, which generally lead to formulation of multi-objective optimization problems [213]. In formulating optimization problems, the parameters of the system that could be varied to obtain the desired optimum system are called the decision or design variables, while those that must not alter are called independent variables [211]. The optimization procedures are often integrated as part of design process for new systems [214], in which case it is possible to obtain optimum process and geometric design parameters. However, it is also a common practice to optimize existing systems on the field for improved performance, in form of plant upgrade or retrofit [214].

The methods generally used for energy system optimization are in three categories: technical/analytical approach, mathematical methods and metaheuristic approach (artificial intelligence) [214,215]. Analytical approach to system optimization entails development of dedicated methods for improving the structures and parametric functions of a system. Suffice it to

mention that the aforementioned exergy, exergoeconomic and accompanying derived methods are in this category. Other examples of methods that have been formulated in this respect are: entropy generation minimization [216] and constructal theory for sizing energy systems [217], amongst others. Mathematical optimization techniques are quite vast and often require exclusive dedication for different applications. For application to energy systems, the most common methods include linear and non-linear programming [218], dynamic and integer programming [219], as well as combinatorial programming [220], just to mention a few. In the case of metaheuristic approach, it is common to find genetic algorithm [221], particle swarm optimization [222], fuzzy logic [223], and artificial neural networks [224] in application, amongst others. The adopted technique often depends on the nature and complexity of the optimization problem at hand. In most cases, some of these techniques are combined, to form hybrid optimization approach [225].

Furthermore, the open literature is replete with studies adopting the aforementioned techniques for energy system optimization, beyond what could be contained in a single volume. Thus, only brief studies are reviewed here, exemplarily, particularly for systems related to solar, biomass, ORC and hybrid solar-biomass plants which are the focus in this study. Regarding optimization of solar-based energy systems, Bravo and Friedrich [226] presented an hybrid optimization scheme for a TES-integrated combined CSP-photovoltaic (PV) plant in the framework of the Atacama-1 project. In the study, they employed multi-objective linear programming technique to optimize operational processes of the solar plant, while multi-objective genetic algorithms were also used for design optimization in succession. By this concept, the authors showed the importance of integrating design and operational optimization for hybrid renewable energy systems, for informed decision making process. Also, Vakilabadi *et al*. [227] demonstrated a possible structural optimization of a solar thermal power plant by adding heat and water recovery system, showing the possibility of marginally improving energy and exergy efficiencies. They reported that by further applying a genetic algorithm optimization approach, additional 0.91 MW power was perceived obtainable from the power plant. For biomass-based systems, Costa *et al*. [228] applied a model-based design of

experiment approach to improve electrical power output in a micro combined heat and power (CHP) plant powered by combustion of syngas obtained from woodchip gasification process. The micro CHP plant had been in operation, and the study objective was to obtain optimal operational parameters with no adjustment made to the existing plant design. They reported that electric power of the system could be improved by 6 %. Similarly, Han and Kim [229] optimized the process of applying a plant biomass (empty fruit bunch) as fuel in a power plant, by integrating drying process into the design and workings of the power plant. They reported that the implemented process optimization reduced the water content of the biomass fuel, and the conversion efficiency of the optimized plant increased by about 14 %. In the case of hybrid solar-biomass energy plants, Sahoo *et al*. [230] applied genetic algorithm technique to obtain optimal performance of a polygeneration plant, using energy, exergy and economic metrics as objective functions. The presented solar-biomass scheme is indirect, such that solar thermal energy is used to upgrade thermal energy of the biomass heat transfer fluid (water), before it is expanded in steam turbine. They reported that the optimization approach enabled reduction in payback period of the plant. More so, Heydari and Askarzadey [5] showed by optimization study that a PV-biomass system could provide a reliable and economically competitive power plant for an off-grid rural application, using Kerman, Iran as study reference. By optimizing the size of PV and biomass conversion engine capacity, they obtained that the hybrid system is more prospective than either sole PV or sole biomass plants. Lastly for ORC plants, Lee *et al.* [231] presented a multi-objective optimization study based on genetic algorithm, for improving exergetic and safety performance of ORC exploiting cold energy from a liquefied natural gas plant. In particular, the authors adopted genetic algorithm technique to select working fluid that optimizes the ORC plant, using the internal process parameters as decision variables. In addition, Ozahi *et al*. [232] presented a multi-objective optimization scheme for an ORC plant, based on non-dominated sorting genetic algorithm (NSGA-II) technique. The studied ORC plant is a bottoming cycle to an existing solid waste plant, which recovers high temperature exhaust gases from the existing plant and utilizes it as ORC heat source to generate additional

power. By implementing NSGA-II, the authors were able to make informed decision on the working fluid and system parameters that would optimize the bottoming ORC, which was the essence of the study.

As it can be inferred from the foregoing, integrating optimization approach to the design and operation of energy systems is often essential, being it a new system or retrofit. Sequel to this, NSGA-II optimization approach was adopted to obtain design parameters of the biomass system that would optimize the hybrid solar-ORC plant proposed in this study, the details of which are presented in Chapter 6.

2.4Summary

Relevant studies available in the open literature have been briefly synthesized in this chapter. This way, an overview of the different technologies involved in the hybrid plant under discussion has been succinctly presented, including: CSP systems, TES systems, biomass energy systems and ORC plants. More so, the state of the art on CSP-biomass hybridization strategies has been reviewed, including use of mixtures as working fluid in ORC applications. In addition, relevant studies on applications of different exergy, exergoeconomic and optimization methodologies for energy plant design and analyses have been highlighted. All these clearly express the importance and novelty of the hybrid CSP-biomass ORC plant proposed in this study, as well as the essence of the techniques and methodologies adopted for analysing and optimizing the hybrid plant. Moreover, pointers were highlighted on the areas requiring further research based on the reviewed renewable energy technologies.

Page left blank intentionally

Chapter 3
Conceptual Design and Techno-economic Assessment of Hybrid CSP-Biomass Plant

3.1Preamble

The importance of hybridizing a dispatchable renewable energy source with transient solar-based power plants has been earlier underscored. This would enhance plant capacity factor; it would improve flexibility of energy supply and demand profile, thereby enhancing system reliability; it would reduce losses due to frequent shutdown and start-up of the power plant; thereby reducing operational costs of the system, amongst other benefits. This reality has led to extensive studies on hybridization of geothermal and biomass energy sources to other transient sources like wind and solar, as aforementioned in Chapter 2. However, due to geological and economic restrictions of geothermal wells, more emphasis is placed on biomass energy. In this regard, several authors have proposed different schemes of hybrid solar-biomass plants, which have also been reviewed in Chapter 2. However, there has not been a thought on how to improve existing CSP-ORC plants through biomass hybridization, in form of retrofit, which is one of the main contributions of this study. In particular, a hybrid CSP-biomass scheme has been proposed, which could be used in retrofitting existing CSP-ORC plants or in designing new fully-renewable hybrid solar power plants. The proposed hybrid CSP-biomass ORC plant is presented and analysed techno-economically in this chapter. The analysis has been divided into two case studies. The first case study considers the hybrid plant as a retrofit to an existing CSP-ORC plant, using design features of a real system of this kind which currently operates at Ottana (NU), Italy as a study reference. In the second case study, novel strategies are proposed to size the CSP, TES and biomass boiler, as if they would be built newly, but also using the characteristics of the existing ORC plant. Then, the retrofit

and newly-integrated case studies are compared, for comprehensive understanding of the potentials of the proposed hybrid CSP-biomass ORC plant. The specific objectives of this chapter are:

- Identification of efficient biomass retrofit concepts for achieving high full-load operating hours in CSP-ORC plants;
- Evaluation of these measures under economic aspects;
- Application of ORC off-design models at component level and their validation by real power plant data;
- Techno-economic comparison of the retrofit and newly integrated design case studies of the hybrid ORC power plant.

Section 3.2 contains a more detailed description of the proposed hybrid CSP-biomass ORC plant; and methodologies implemented for design, off-design and techno-economic analyses of the plant, both for the retrofit and newly integrated design case studies. The results obtained for the two case studies are presented and discussed in section 3.3, while section 3.4 contains chapter summary.

3.2Methodology

3.2.1 Current system configuration and the proposed hybridization

The CSP-ORC plant currently running in Ottana (Italy) comprises of three main sections: the solar field, the two-tank TES system and the ORC plant. The solar field is based on six linear Fresnel collectors and it is characterized by an overall net collecting area of about 8400 m^2. The Heat Transfer Fluid (HTF) is thermal oil with inlet and outlet solar field temperature of 165 °C and 275 °C, respectively. The TES system is characterized by a storage capacity of 15.2 MWh, which corresponds to about 5 hours of ORC plant operation at nominal condition. The power generation plant is based on a regenerative Rankine cycle with a turbogenerator operated by an organic fluid (hexamethyldisiloxane) and characterized by an electrical net power of about 630 kW. Table 3.1 reports the main characteristics of the reference CSP-ORC plant.

Table 3.1: Design characteristics of solar field, TES system and ORC unit at the Ottana solar facility [9]

Plant location data		TES system	
Location	Ottana (Italy)	Storage medium	Therminol
Latitude/longitude angle	$40.23^{o}/9.23^{o}$	Storage capacity	15.2 MWh
Mean ambient temperature	17 ^{o}C	Tank useful volume	330 m^3
Solar field		ORC unit (design conditions)	
Heat transfer fluid	Therminol	HTF mass flow rate	11 kg/s
HTF inlet/outlet temp.	165^{o}C /275^{o}C	HTF inlet/outlet temp.	275/165°C
Collector focal length (FL)	4.97 m	Organic fluid	$C_6H_{18}OSi_2$
Collector length (L)	99.45 m	Cooling fluid	Water
Reference optical efficiency (η_{opt})	65.5%	Cooling inlet/outlet temp.	20/35°C
Cleanliness efficiency (η_{cln})	98%	Net electrical power	630 kW

Starting from the current configuration, the conceptual scheme of the proposed hybrid solar-biomass system is schematically shown in Figure 3.1. It involves placing a modular biomass combustion furnace in parallel to the solar field, such that both heat sources can directly and independently satisfy fractional thermal input requirement of the ORC plant. In the solar section, the thermal energy produced by the solar field is directly sent to the ORC unit as a first option. In case of an overproduction with respect to the ORC nominal thermal energy requirement, the surplus energy is stored in the TES hot tank for a postponed usage. A three-way valve located upstream the ORC inlet side manages the HTF mass flow rates between solar (HTF_S) and biomass (HTF_B) sections. The total HTF mass flow rate (HTF_T) supplied to the ORC depends on the management strategy adopted for biomass furnace operation. For the assumed subcritical configuration for the existing ORC plant, heat addition process takes place in separate single-phase (pre-heating) and

two-phase (evaporation) heat exchangers. After evaporation process, the organic fluid is expanded in a turbogenerator, for power production. Some residual heat available in the expanded organic fluid is recovered internally before condensation of the organic fluid using water as cooling medium. Then, pressure of the liquid organic fluid is raised by a pump. Its temperature is increased using the internally recovered heat in the recuperator, before exploiting external thermal energy from hybrid solar-biomass system for cycle continuation.

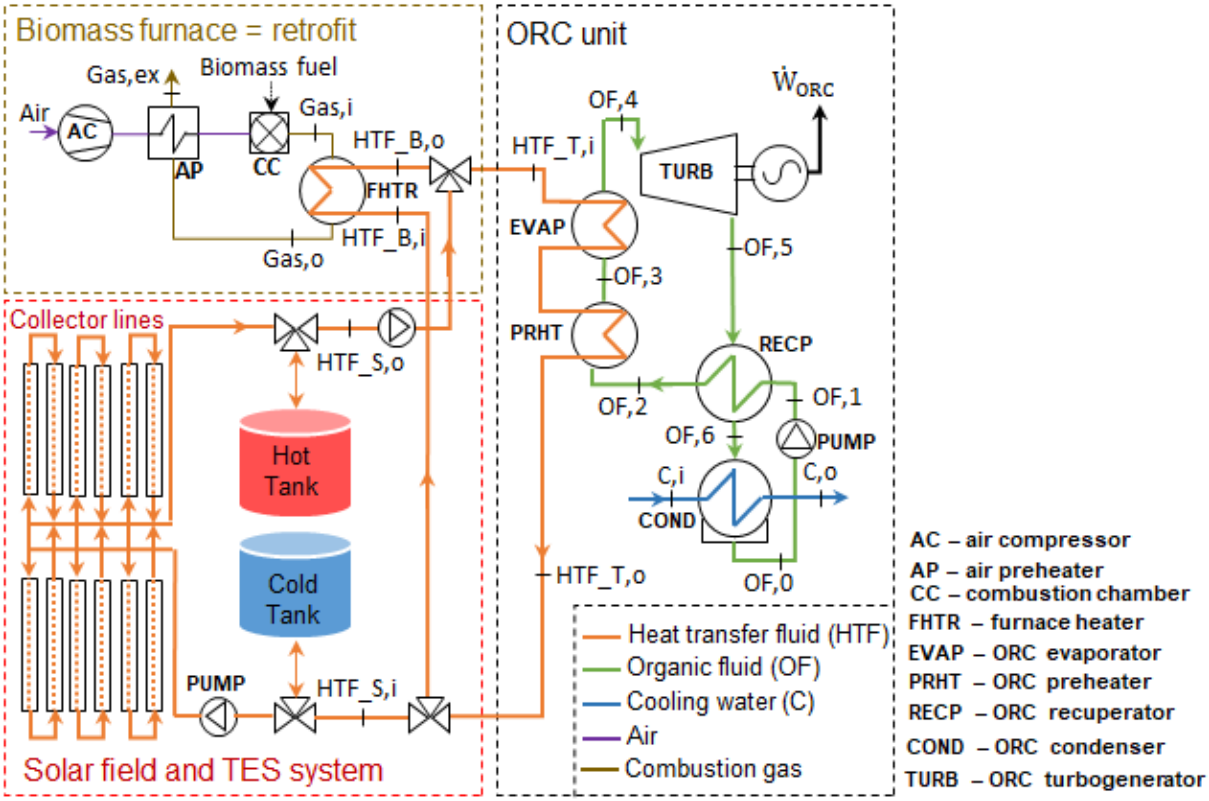

Figure 3.1: Conceptual scheme for hybrid CSP-biomass ORC plant.

3.2.2 Biomass hybridization as retrofit to an existing CSP-ORC plant

For the retrofit case study, the furnace was designed such that it is able to constantly supply a specified fraction of the thermal input requirement of the ORC, with the remaining fraction being satisfied by solar field and TES, depending on availability. In this study, two hybridization approaches based on two different plant management criteria were proposed:

- Fixed Hybridization Approach - fixed biomass supply, where biomass furnace constantly supplies a specified fraction of ORC thermal requirement, as minimum load. The share of ORC thermal power demand not covered by biomass furnace is supplied by thermal power from solar field at first. In the event that full-load ORC thermal requirement is yet to be satisfied, TES is discharged. Accordingly, biomass furnace nominal power ($\dot{Q}_F^D$) is determined as a share of the design thermal requirement of the ORC ($\dot{Q}_{ORC}^D$), by introducing a biomass retrofit fraction, b_{RF}*:*

$$b_{RF} = \frac{\dot{Q}_F^D}{\dot{Q}_{ORC}^D} \tag{3.1}$$

  For a given b_{RF}, biomass supplies equivalent fraction of the specified value, relative to design thermal input requirement of the ORC. Minimum fraction of 40% was considered, to coincide with the minimum load thermal power required for the reference real ORC operation. In this case, about 1270 kW of thermal power is supplied by biomass furnace.

- Modulating Hybridization Approach – modulating biomass supply, where biomass thermal contribution differs per time, such that it is able to make up the balance of thermal power required to satisfy ORC thermal input always at full load. Accordingly, the biomass furnace is sized to match the nominal ORC thermal power input.

Specific mathematical models were developed in MATLAB [233], for evaluating the performance of CSP, TES and biomass systems, under both design and off-design operating conditions. Design, off-design and yearly performance of the ORC plant were simulated, using a combination of ASPEN Plus 8.8 and Aspen Simulation Workbook (ASW) [234].

The following modeling assumptions were made in the study:

i. The system operates at quasi-steady state.

ii. All heat exchangers are thermally insulated to the environment, and pressure drops during operation are negligible.

iii. Empirically based on the existing plant, heat loss in TES due to imperfect insulation is 2% [9].

iv. Modular biomass combustion furnace with model-based control is considered [235]. The thermodynamic inefficiency is ameliorated by adjusting fuel consumption rate. Inefficiency due to unburned fuel and heat loss is 1%.

v. Existing characterization of biomass fuel (Sardinian Eucalyptus) is adopted [236].

Specific methods for modelling different sections of the hybrid plant are highlighted below.

3.2.2.1 Solar field modelling

The thermal power produced by a linear Fresnel CSP field per unit of collecting area ($\dot{q}_{SF}$) was obtained, using eq. (3.2) [23],[28]:

$$\dot{q}_{SF} = DNI \cdot \eta_{opt} \cdot IAM_T \cdot IAM_L \cdot \eta_{cln} \cdot \eta_{end} - a_1(T_{av} - T_{amb}) - a_2(T_{av} - T_{amb})^2 - \dot{q}_{pl} \quad (3.2)$$

where DNI is the direct normal solar irradiation; η_{opt}, η_{cln}, and η_{end} are the reference optical, cleanliness, and end-losses efficiencies of the solar collectors, respectively; IAM_T and IAM_L are transverse and longitudinal Incidence Angle Modifier, which are functions of the respective transverse and longitudinal components of solar incidence angle (θ_L and θ_T); a_1 and a_2 are coefficients of receiver thermal losses (assumed equal to 0.056 W/m^{2}K and 0.213·10^{-3} W/m^{2}K^2 respectively [23]); T_{av} is the mean of inlet and exit HTF temperatures in the solar field; T_{amb} is the ambient temperature; and $\dot{q}_{pl}$ represents piping thermal losses. The IAM_T and IAM_L were computed according to the correlations provided by the LFC manufacturer of real solar ORC plant [9], as shown in Figure 3.2. In addition, end-losses efficiency was calculated as a function of θ_L, focal length (FL) and collector length (L):

$$\eta_{end} = 1 - \frac{FL}{L} tan\,\theta_L \quad (3.3)$$

For other parameters in eq. (3.2), specifications of the real Ottana solar ORC plant were implemented for initial sizing of the solar field, as shown in Table 3.1.

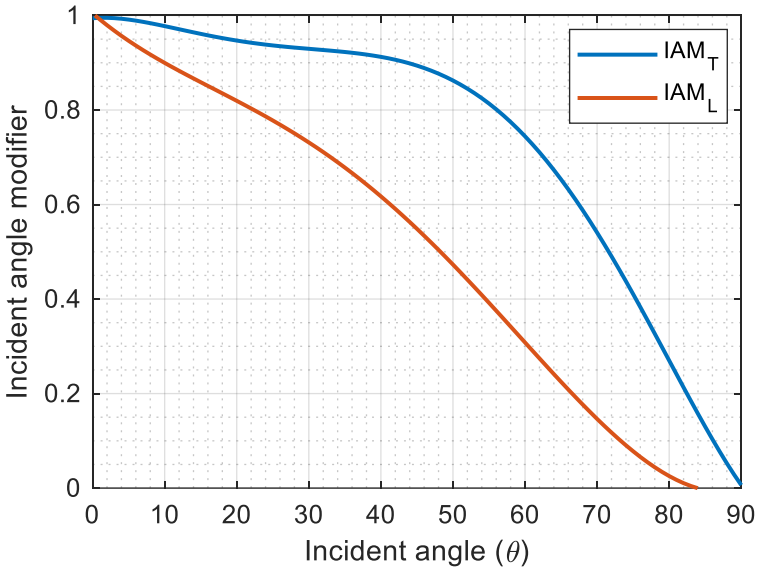

Figure 3.2: IAM correlations with solar incidence angle.

3.2.2.2 Biomass furnace modelling

Characteristics of a small-scale biomass boiler were assumed for design and analysis, where combustion zone is separated from liquid-gas heat exchanger. HTF flowing at the liquid side is heated up by the hot combustion gases, predominantly through convective heat transfer. Residual thermal energy of the hot exhaust gases exiting the furnace is used for preheating inlet air. This boiler type is particularly suited for this study, owing to its model-based control capability [235].

Sardinian Eucalyptus was considered as the biomass fuel in this study, due to its local availability at the plant location. Its detailed characterization had been reported by Mureddu *et al.* [236]. Table 3.2 reports the fuel composition in dry basis, together with the main combustion furnace characteristics. An excess air value of 50 % was considered. With this value, the mass flow rate and temperature of hot combustion gases were obtained, through mass and energy balance of the combustion side:

$$\dot{m}_{Bio} + \dot{m}_{Air} = \dot{m}_{Gas} + \dot{m}_{Ash} + \dot{m}_{umb} \tag{3.4}$$

$$\dot{m}_{Bio}(LHV + h_{Bio}) + \dot{m}_{Air}h_{Air} = \dot{m}_{Gas}h_{Gas,i} + \dot{m}_{Ash}h_{Ash} + \dot{m}_{umb}LHV + \dot{Q}_{Loss} \tag{3.5}$$

where $\dot{m}_{Bio}$, $\dot{m}_{Air}$, $\dot{m}_{Ash}$ and $\dot{m}_{Gas}$ are mass flow rates of biomass fuel, air, ash formed from biomass fuel combustion and combustion gases, respectively, while $\dot{m}_{umb}$ and $\dot{Q}_{Loss}$ are the unburned fuel mass flow rate and the thermal losses due to imperfect insulation of the combustion chamber respectively. Overall, these two energy losses were assumed to be 1% of the primary energy introduced in the furnace.

It is worth highlighting that both the mass and energy balance of the furnace are satisfied during both design and off-design conditions. Thus, by assuming a constant air-fuel ratio, the gas temperature remains constant even during part-load operation of the biomass furnace. The modular biomass boiler regulates flow of biomass fuel at off-design conditions, such that the efficiency and technical parameters of the boiler are preserved.

A counter-flow liquid-gas heat exchanger was considered for transferring biomass thermal energy to the HTF. The HTF inlet and outlet temperatures were taken to coincide with exit and entry temperatures of the ORC at design conditions. Based on the thermal power required from biomass furnace, HTF mass flow rate was thus obtainable. The heat exchanger behaviour at part load has been simulated, using the $\varepsilon - \text{NTU}$ method. Starting from the required heat to be transferred to the HTF, the variation of convective heat transfer coefficients with mass flow rates was calculated. By direct consequence, the actual effectiveness of the counter-flow heat exchanger and the outlet gas temperature were obtained.

Table 3.2: Main characteristics of the biomass furnace [236].

Combustion furnace	
Fuel composition (dry basis)	48.3 %C, 5.9 %H, 0.12 %N_2, 38.47 %O_2, 7.21 %Ash
Lower heating value (dry basis)	16.3 MJ/kg
Moisture content	20 %
Stoichiometric air-fuel ratio	5
Excess air	50 %
Specific heat capacity of ash	0.84 kJ/kgK
Specific heat capacity of gas	1.36 kJ/kgK
Temperature of hot gases (calculated)	1062 °C
Liquid-gas heat exchanger	
HTF inlet/exit temperature	165/275 ^{o}C
Minimum temperature difference	50 °C (design conditions)
Gas heat transfer coefficient	150 W/m^{2}K
HTF heat transfer coefficient	900 W/m^{2}K

3.2.2.3 ORC modelling

The technical parameters used in the ORC design correspond to those of the Ottana Solar Facility [9] and presented in Table 3.1. The complete design specifications are detailed in Table 3.3. The parameters tagged ‘obtained’ are output from the modelling tool, required to achieve the ‘specified’ parameters, which are real parameters of the reference plant.

Given the intermittent nature of solar energy availability, solar ORC would normally perform at conditions that markedly deviate from those assumed for system design. It is therefore necessary to incorporate off-design analysis into ORC models, for comprehensive performance assessment. The

approach employed to account for off-design characteristics of the main ORC components are highlighted below.

Table 3.3: Main characteristics of ORC design.

Specified parameters		Obtained parameters	
Evaporation pressure	10 bar	Evaporator pinch point	34.8 K
Pump isentropic efficiency	80 %	Recuperator pinch point	32.4 K
Pump motor efficiency	98 %	Condenser pinch point	12 K
Turbine isentropic efficiency	85 %	Condensation pressure	0.145 bar
Electromechanical efficiency	92 %	Cooling water mass flow rate	59.6 kg/s
		Working fluid mass flow rate	9.3 kg/s
		Design net efficiency	19.8 %
		Design thermal power input	3177 kW

3.2.2.3.1 Heat exchangers

The correlation proposed by Manente *et al.* [237] was adopted in this study, to account for off-design behaviour of heat exchangers, as given by eq. (3.6):

$$U^{off} = U^{D}\left(\frac{\dot{m}_{OF}^{off}}{\dot{m}_{OF}^{D}}\right)^{z} \tag{3.6}$$

where $\dot{m}_{OF}$ is the mass flow rate of organic fluid in the heat exchanger side of interest; *z* is an index, which depends on the geometry and function of heat exchanger concerned, as well as the working fluid; superscripts '*off*' and '*D*' represent off-design and design conditions, respectively. The values of *z* have been taken to be 0.15 in the evaporator, where the mass flow at the cold side (ORC working fluid) is of interest, 0.60 in the condenser, where the mass flow at the cold side (water) is of interest, and 0.67 in the recuperator, where the cold side (ORC working fluid at pump exit) is of interest. The choice of each of these values was based on information available in literature [237],[238].

3.2.2.3.2 Turbine

In order to model the effects that ORC deviation from design conditions would have on isentropic efficiency of the turbine, the equation proposed by Ghasemi *et al.* [239] was adopted:

$$\eta_T^{off} = \eta_T^D \cdot k_h \cdot k_v \tag{3.7}$$

where η_T^D is the turbine isentropic efficiency under nominal conditions, k_h and k_v relate to enthalpy difference of flow through the turbine and volume flow rate at turbine exit, respectively, definitions of which are expressed in eqs (3.8) and *(*3.9), respectively:

$$k_h = 1.398\Delta h_{T,r}^2 - 5.425\Delta h_{T,r}^{1.5} + 6.274\Delta h_{T,r} - 1.866\Delta h_{T,r}^{0.5} + 0.619 \tag{3.8}$$

$$k_v = 0.038 + 2.588\dot{V}_{Tex,r} - 2.533\dot{V}_{Tex,r}^2 + 1.117\dot{V}_{Tex,r}^3 - 0.21\dot{V}_{Tex,r}^4 \tag{3.9}$$

where $\Delta h_{T,r}$ and $\dot{V}_{Tex,r}$ are the ratios at off-design conditions to those at design conditions, for enthalpy difference of flow through the turbine and volume flow rate at turbine exit, respectively. With decreasing mass flow rate of the heat source, the mass flow rate of ORC working fluid flowing through the turbine is decreased. This leads to decrease in volume flow rate at turbine exit, as well as reduction in enthalpy difference. Overall consequence of this is reduction in turbine isentropic efficiency.

3.2.2.3.3 Pump

Similarly, deviation of mass flow rate of heat source from design value would have considerable effect on the volume flow of organic fluid through the pump. The off-design correlation implemented for the ORC pump relates to volume rate of flow through the pump and the actual isentropic efficiency. On the other hand, an effect of variation of volume flow rate on the pump differential head was assumed negligible. This is due to relatively low auxiliary energy consumptions of the pump. The implemented correlation is as follows:

$$\eta_P^{off} = \eta_P^D \cdot r_c \tag{3.10}$$

where r_c is the normalized curve obtained from a commercial ORC plant, defined by:

$$r_c = 0.00823 + 2.357\dot{V}_{P,r} - 1.710\dot{V}_{P,r}^2 + 0.344\dot{V}_{P,r}^3 \quad (3.11)$$

where $\dot{V}_{P,r}$ is the ratio of volumetric flow rate through the pump at off-design conditions to that at design condition.

3.2.2.4 Yearly performance assessment

For yearly analysis based on the existing solar field area and TES capacity, hourly thermal energy from biomass furnace was simulated, depending on fractional thermal contribution desired from biomass. To obtain hourly thermal energy production from the solar field, Meteonorm software [240] was used for determining the meteorological data needed in eq. (3.2) for each hour of the reference study year. In addition, by integrating the TES capacity into the quasi-steady energy flow analysis, the defocused solar energy at each hour when TES is fully charged was estimated. Consequently, the hourly total thermal energy available for input into the ORC (Q_{ORC}) was obtained, and the heat source mass flow rate was thereby determined, as follows:

$$\dot{m}_{HTF\_T} = \frac{Q_{ORC}}{\left(h_{HTF\_T,i} - h_{HTF\_T,o}\right) \cdot \Delta t} \quad (3.12)$$

where Δt is the time step, assumed equal to 1 hour. It is worth highlighting that a constant HTF mass flow rate (equal to the nominal one) is assuredly supplied to the ORC throughout the year in the modulating hybridization approach. Conversely, the adoption of fixed hybridization approach guarantees the ORC operation under nominal conditions only in such days with high solar irradiation. The major parameters required for ORC simulations were thus obtained in this step and the yearly ORC simulation was carried out by setting up scenario tables in ASW. For the two hybridization approaches, design cases corresponding to biomass fraction equivalent to 40 %, 45 %, 50 %, 60 % and 70 % of ORC nominal thermal input requirement were simulated.

3.2.2.5 System performance evaluation criteria

The annualized net electrical efficiency (*NEE*) of the hybrid plant was employed for technical assessment, while combination of the levelized cost of electricity (*LCOE*), net present value (*NPV*)

and specific payback period (*SPB*) were used for economic assessment. Definitions adopted for these criteria are highlighted as follows [138]:

$$NEE = \frac{W_{ORC}}{\sum_{t=1}^{8760}[\dot{q}_{SF} \cdot A_{SF} + \dot{m}_{Bio} \cdot LHV] \cdot \Delta t} \tag{3.13}$$

$$LCOE = \frac{IC + \sum_{n=1}^{N} \frac{AC}{(1+i)^n}}{\sum_{n=1}^{N} \frac{W_{ORC}}{(1+i)^n}} \tag{3.14}$$

$$NPV = \sum_{n=1}^{N} \frac{FIT_S \cdot W_{ORC,S} + FIT_B \cdot W_{ORC,B} - AC}{(1+i)^n} - IC \tag{3.15}$$

$$SPB = \frac{IC}{FIT_S \cdot W_{ORC,S} + FIT_B \cdot W_{ORC,b} - AC} \tag{3.16}$$

where W_{ORC} is the net electrical energy produced by the plant over one year period; $W_{ORC,S}$ and $W_{ORC,B}$ are the share of the annual net electrical energy produced by solar field and biomass furnace, respectively; IC is the total investment cost incurred on the plant; AC is the annual operating expenditure; FIT_S and FIT_B represent feed-in tariffs for solar power and biomass power, respectively; i is the interest rate and N is the plant lifetime in years. Considering the retrofit case study, marginal economic metrics ($LCOE_M$, NPV_M and SPB_M) were computed, such that only the additional costs and additional energy of biomass retrofit were implemented in eqs (3.14) – (3.16). However, conventional LCOE that includes investment and operating costs of the whole hybrid plant was also computed separately. This is essential to give insight into the overall cost of energy due to the hybrid plant, for informed comparison with other systems. The initial cost of the hybrid plant can be split into direct (IC_{DIR}) and indirect (IC_{IND}) components:

$$IC_{DIR} = c_{SF}A_{SF} + c_{TES}Q_{TES} + (c_{ORC} + c_{BoP})\dot{W}_{ORC}^{D} + IC_F \tag{3.17}$$

$$IC_{IND} = c_{LAND}A_{LAND} + (c_{TAX} + c_{EPC})IC_{DIR} \tag{3.18}$$

The direct component is the investment associated with the ORC unit (c_{ORC}), solar field (c_{SF}), storage system (c_{TES}), biomass furnace (IC_F) and balance of plant (c_{BoP}). The indirect component covers all the remaining costs for the upfront investment that are not directly related to the

equipment. These costs include the purchase of land (c_{LAND}), taxes (c_{TAX}), and the engineering, procurement and construction costs (c_{EPC}). The annual cost includes O&M cost ($c_{O\&M}$ expressed as percentage of the initial cost) and biomass fuel costs (c_{BIO}):

$$AC = c_{O\&M} IC + c_{BIO} \cdot \sum_{t=1}^{8760} \dot{m}_{Bio} \tag{3.19}$$

The main cost assumptions adopted for economic analysis are summarized in Table 3.4. In particular, initial cost for ORC genset was based on information available in [241], which derives from experience with the real solar ORC facility. Together with the cost for ORC Balance of Plant (BoP), this cost assumption is also in agreement with what was obtained from interview with ORC manufacturer (Turboden), for comparable power rating [138]. The initial costs for LFC and TES were obtained from relevant studies in literature [40],[41]. For biomass furnace, cost reported for established furnace obtained from Uniconfort was correlated, using eq. (3.20) [138]:

$$IC_F = IC_{F,ref} \cdot \left(\frac{\dot{Q}_F^D}{\dot{Q}_{F,ref}} \right)^{\gamma} \tag{3.20}$$

where $IC_{F,ref}$, $\dot{Q}_F^D$, $\dot{Q}_{F,ref}$, γ, refer to cost of reference biomass furnace, furnace thermal duty, thermal duty of reference furnace and scale factor, respectively.

Beginning from June 2016 till date, feed-in tariff (*FIT*) obtainable in Italy ranges between 115 €/MWh and 246 €/MWh for electricity produced from biomass, depending on source of biomass fuel [242], and 296 €/MWh for CSP [243]. For woody biomass fuels, *FIT* of 180 €/MWh is appropriate [138].

Table 3.4: Cost assumptions for economic analysis [138,241–246]

Capital costs		Other Indices	
Solar field (c_{SF})	160 €/m^2	Reference furnace cost ($IC_{F,ref}$)	600 k€
TES (c_{TES})	45 €/kWh	Scale factor (γ)	0.8
ORC (c_{ORC})	1000 €/kW	Reference furn. thermal duty ($\dot{Q}_{F,ref}$)	4.52 MW
BoP (c_{BoP})	250 €/kW	Annual interest rate (i)	7%
Land cost (c_{LAND})	2 €/m^2	Plant operational lifetime (N)	25 years
Engineering services (c_{EPC})	8%		
Taxes (c_{TAX})	3%		
Annual costs		Feed-in tariff	
Biomass fuel (c_{BIO})	50 €/t	FIT for solar power (FIT_S)	296 €/MWh
O&M ($c_{O\&M}$)	1.5%	FIT for biomass (FIT_B)	180 €/MWh

3.2.3 Newly integrated design for modified solar field and TES section of the hybrid plant

The methodological analysis of the second case study where solar field and TES were newly sized is presented in this section. This analysis could be valuable for potential expansion of the solar field of the existing plant, or in case a new similar plant is planned. New design objective was thus implemented in this regard, that depart slightly from that of the retrofit case study. The new objective imposes all-day full-load operation of the ORC power plant, on a given reference day (June 21) with clear sky conditions. This should be obtained without having to dissipate any solar thermal energy, considering also the fractional thermal energy contribution from biomass furnace. Thus, depending on the specified thermal contribution from biomass and the method adopted for plant management, the solar field area and TES capacity were determined to satisfy the aforementioned design objective. For the given plant location, clear sky DNI profile for June 21 was obtained using the established model proposed by Hottel [247]. The solar field specific thermal

power (thermal power per unit of collecting area) during the reference day was therefore computed using *eq*. (3.2). The biomass fraction, *b*, was introduced to determine the solar and biomass contribution to the ORC, as follows:

$$b = \frac{\sum_{t=1}^{24} \dot{Q}_{Bio}}{24 \cdot \dot{Q}_{ORC}^{D}} \tag{3.21}$$

where $\dot{Q}_{ORC}^{D}$ is the design thermal hourly requirement of the ORC and $\dot{Q}_{Bio}$ is the hourly thermal supply from biomass furnace. The aforementioned fixed and modular management approach were preserved for this case study as well. For fixed hybridization approach, *b* was set by imposing a proportion of ORC input demand at nominal conditions as biomass thermal contribution. In the case of modular approach, *b* was obtained by the balance of thermal energy required to satisfy ORC input demand on chosen design day, after utilizing all the solar thermal energy produced and stored, such that the design objective is satisfied. In other words, for fixed approach, *b* relates to power and was calculated instantaneously, while for modular approach, it relates to energy and calculated on a daily basis. In particular, the required collecting area (A_{SF}) was calculated to satisfy full-day thermal demands on the reference day, considering also thermal losses from the TES tank, as follows:

$$A_{SF} = \frac{\dot{Q}_{ORC}^{D}(1-b) \cdot 24 + Q_{TES}(1-\eta_{TES})}{\sum_{t=1}^{24} \dot{q}_{SF}^{D} \cdot \Delta t} \tag{3.22}$$

where Δt is the time step, $\dot{q}_{SF,D}$ is the specific solar field production during the reference day, η_{TES} is the TES efficiency, considering the imperfect insulation of the tanks (imposed equal to 98%) and Q_{TES} is the TES capacity. The latter was calculated as a function of the plant management criteria chosen. Specifically, by following the fixed hybridization approach, TES capacity, sized relative to solar energy availability on the assumed reference day, was obtained as follows:

$$Q_{TES} = \sum_{t=1}^{24} max\left(\dot{q}_{SF}^{D} A_{SF} - \dot{Q}_{ORC}^{D}(1-b), 0\right) \cdot \Delta t \tag{3.23}$$

On the other hand, by applying the modular hybridization approach, biomass fraction of zero is a possibility with high solar availability, and the TES was calculated as:

$$Q_{TES} = \sum_{t=1}^{24} max\left(\dot{q}_{SF}^{D} A_{SF} - \dot{Q}_{ORC}^{D}, 0\right) \cdot \Delta t \quad (3.24)$$

Similar to the retrofit case study, five design cases of biomass contribution were considered for each approach. This corresponds to biomass fraction equivalent to 40 %, 45 %, 50 %, 60 % and 70 % of ORC nominal thermal input requirement, respectively. Unlike the retrofit case study, the modular approach in the newly integrated design case study is sensitive to variation in biomass fractions, even at design stage.

Also, similar procedure was implemented for yearly analysis of the newly integrated design, as for the retrofit case study. However, in this case, newly obtained solar field area and TES size were implemented in eq. (3.2), depending on adopted hybridization approach and biomass fraction. To obtain hourly thermal power production from the solar field, Meteonorm software [38] was equally used for determining the meteorological data needed in eq. (3.2), for each hour of the reference study year. Also for determining the heat source mass flow rate in this case, imposed TES efficiency and TES capacities obtained at design stage were implemented simultaneously.

3.3Results and Discussion

3.3.1 ORC simulation and validation

3.3.1.1 Off-design behaviour of ORC components

While the overall heat transfer coefficient in recuperator and evaporator reacted to deviation of ORC organic fluid mass flow rate from design conditions, the effect was observed insignificant in condenser, for off-design variations of mass flow rate of heat sink (water). Mass flow rate of the heat source was observed to be directly proportional to organic fluid mass flow rate through the process, for both evaporator and recuperator.

The behaviours of pump and turbine at off-design conditions are reflected in Figure 3.3. For the two components, deviation of heat source mass flow rates from design conditions decreases isentropic efficiencies. This trend is quite in agreement with what obtains in practical ORC power plants. The use of the turbine off-design correlations proposed by Ghasemi *et al*. [239] is thus justified. This is regardless of the fact that boundary conditions in the referenced study by Ghasemi *et al*. are different from those considered in this study, particularly regarding working fluid and plant capacity. Furthermore, these trends are congruent with those obtained from experimental studies reported in [248], for axial turbines in micro ORC for waste heat recovery, using hexamethyldisiloxane (MM) as organic fluid. Again, the differences are in the reduced values of isentropic efficiencies in the experimental studies, due to variation in ORC capacity.

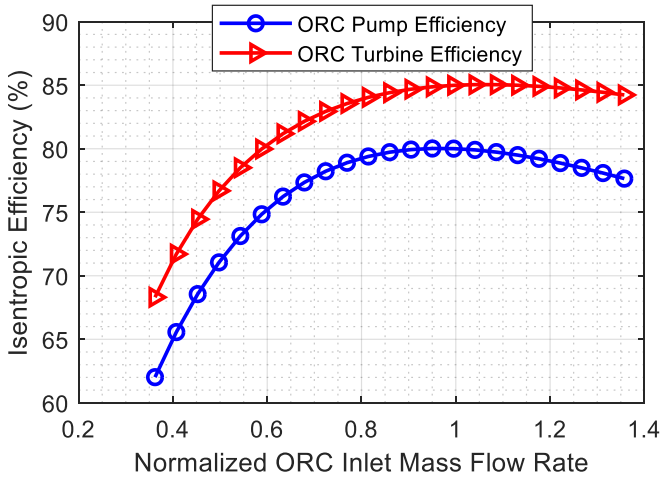

Figure 3.3: Off-design isentropic efficiencies of ORC pump and turbine.

3.3.1.2 Part-load behaviour and comparison with real power plant data

Either due to insufficient thermal energy input for full-load operation or due to reduced energy demands from users, it is common to operate thermal power plants at part-load conditions. This situation obviously affects overall thermal efficiency. For the hybrid solar ORC plant presented in this study, effects of part-load thermal input on gross efficiency of the ORC is shown in Figure 3.4(a). In addition, as a way of validating the ORC model, the simulation results have been compared with first measured data from the real ORC plant (Ottana Solar Facility). Percentages of

the input thermal energy into the ORC were computed, relative to the value at nominal conditions. In a similar manner, effects of water temperature at condenser inlet were simulated, and then compared with real power plant measured data, the results of which are presented in Figure 3.4(b). In addition, to further establish the validity of the implemented ORC off-design models, comparisons were made at component level. Therefore, Figure 3.5 shows temperatures of ORC working fluid at preheater inlet ($T_{OF,2}$) and evaporator exit ($T_{OF,4}$), for simulation and real power plant data, at varying temperature of the source HTF. In particular, HTF inlet temperature ($T_{HTF\_T,i}$) and outlet temperature ($T_{HTF\_T,o}$) corresponding to different ORC inlet gross power were used as input for off-design calculations. As evident in these figures, simulation results depart just slightly relative to data measured from the real power plant. This can be explained by a number of points. For instance, the effects of system start-up/shutdown were not considered for simulations, having assumed a quasi-steady operating condition. Also, pressure drop and heat loss in heat exchangers were not taken into account in the ORC simulation. However, it is worth highlighting that a number of points of the simulation results correlate quite well with approximate measured data. For instance, only 1% and 5% mean deviations in simulation results were obtained for $T_{OF,4}$ and $T_{OF,2}$ respectively, relative to real plant data. In the case of ORC gross efficiency, 3% mean relative deviation was obtained between simulation results and real operational data with respect to Figure 3.4(b).

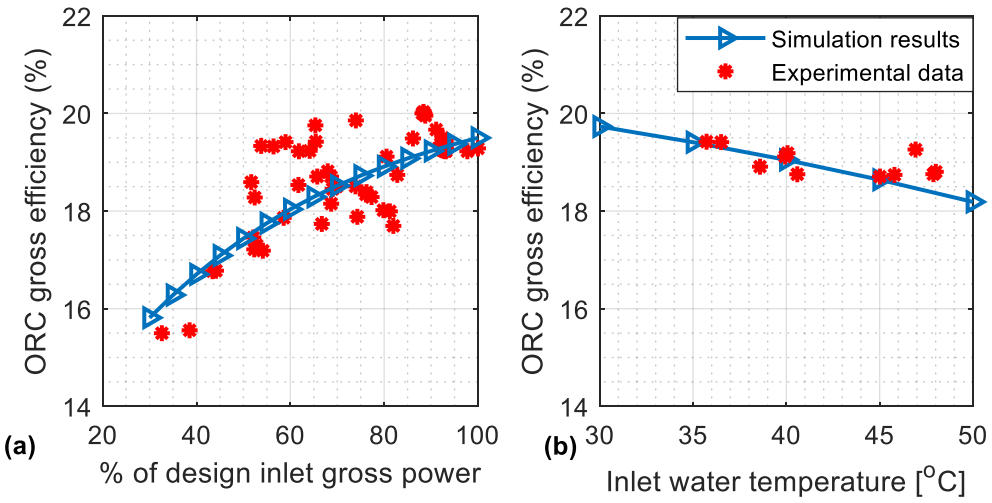

Figure 3.4: (a) ORC performance at part load conditions and (b) Effect of water inlet into the condenser on ORC gross efficiency.

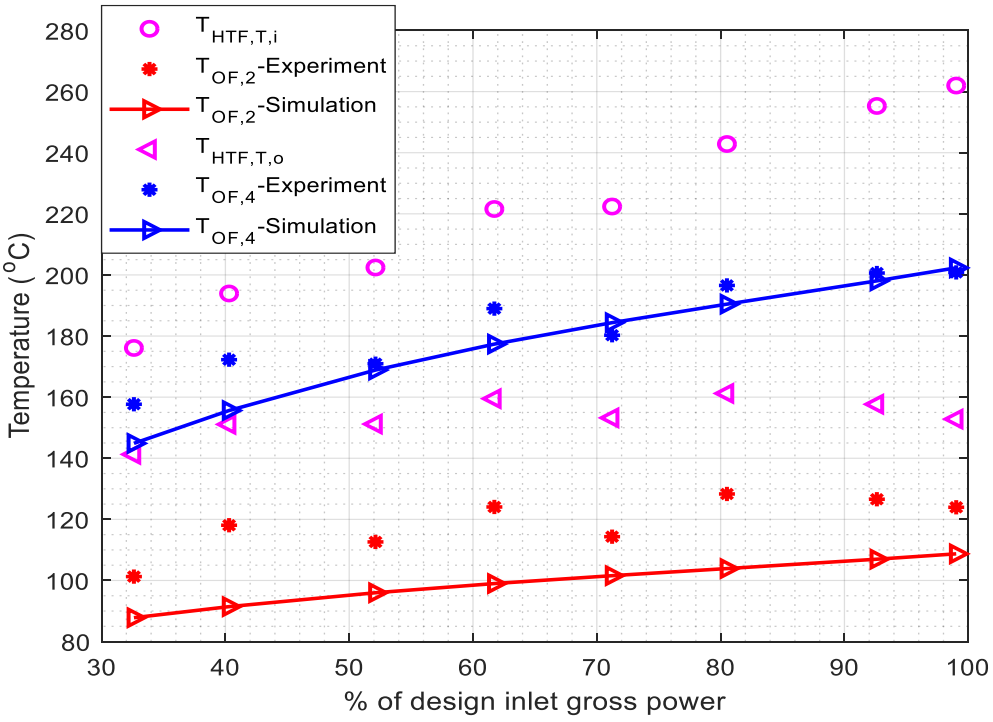

Figure 3.5: Comparison of real plant and simulation temperatures at different values of input thermal power.

3.3.2 Techno-economic performance of biomass retrofit for the existing CSP-ORC plant

The results of techno-economic effects of biomass retrofit for the existing solar-ORC plant, running at Ottana (Italy), are presented here. As aforementioned, the actual size of solar field (8400 m^2) and TES (15.2 MWh, corresponding to about 5 equivalent hours) of the running solar ORC plant have been implemented for retrofit case study.

As a first design case, the fixed hybridization approach with a biomass thermal supply of 40% of ORC nominal requirement was assumed, with the aim of keeping the ORC in operation throughout the year. For this case study, hourly profile of ORC net electrical power production for one year and frequency distribution of production ratings are depicted in Figure 3.6. As shown, the ORC is able to operate at a minimum load throughout the year, and the net electrical power production is controlled never to exceed the nominal value. The nominal electrical power is often reached at the hours of the year with high thermal power production from the solar field. In addition, the frequency distribution plot shows that the most recurrent ORC net electrical power production within the year is close to the minimum load, in the range of 215 kW to 280 kW. It represents about 65% of hourly ORC power production rating. This is closely followed by peak ORC production in the range of 595 kW to 630 kW, representing about 20%. The implication of 65% of plant operation close to minimum load is that without biomass hybridization, the ORC plant would be inoperable for more than half of the year. This is expected to pose consequential challenge on losses due to frequent plant start-up/shutdown, as well as difficulties with dynamical controls. Obviously, increasing biomass contribution for the fixed biomass hybridization approach would lead to increase in minimum-load electrical power production of the plant, as well as increase in frequency distribution of ORC power production rating close to the nominal condition.

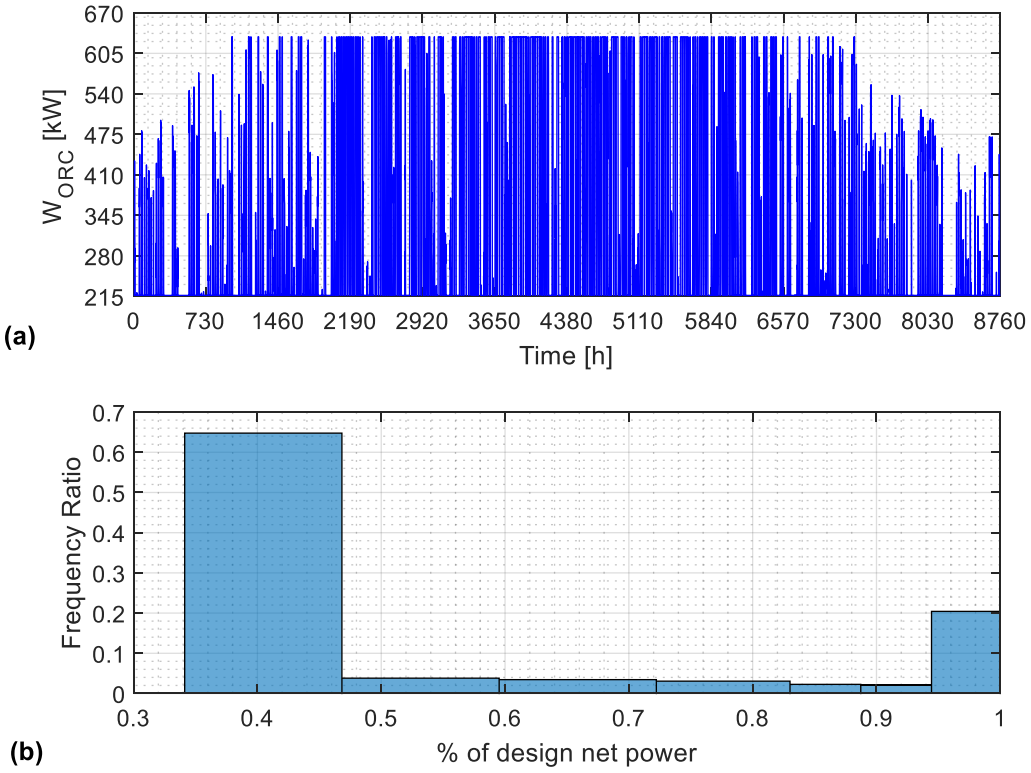

Figure 3.6: (a) ORC hourly net electrical power production and (b) Frequency distribution of ORC power production for fixed 40% biomass contribution

Figure 3.7 shows the monthly profile during the reference study year, for thermal energy production from solar field and biomass, ORC electrical energy production, as well as total energy dissipated due to insufficient storage capacity. This figure illustrates a case for 40% biomass contribution, but similar trend obtains for other biomass fractions. The results obtained for ORC electrical production reflects that a power output higher than 215 kW is guaranteed. This is as a result of continuous supply of biomass thermal energy at a specified minimum level. This is because, as envisaged, biomass hybridization with the CSP-ORC plant stabilizes electrical energy production at minimum load. However, this is with the consequence of wasting some solar thermal energy in summer months, as shown in the figure. For instance, about 5% of solar field production in June is lost to defocusing of some solar collector lines.

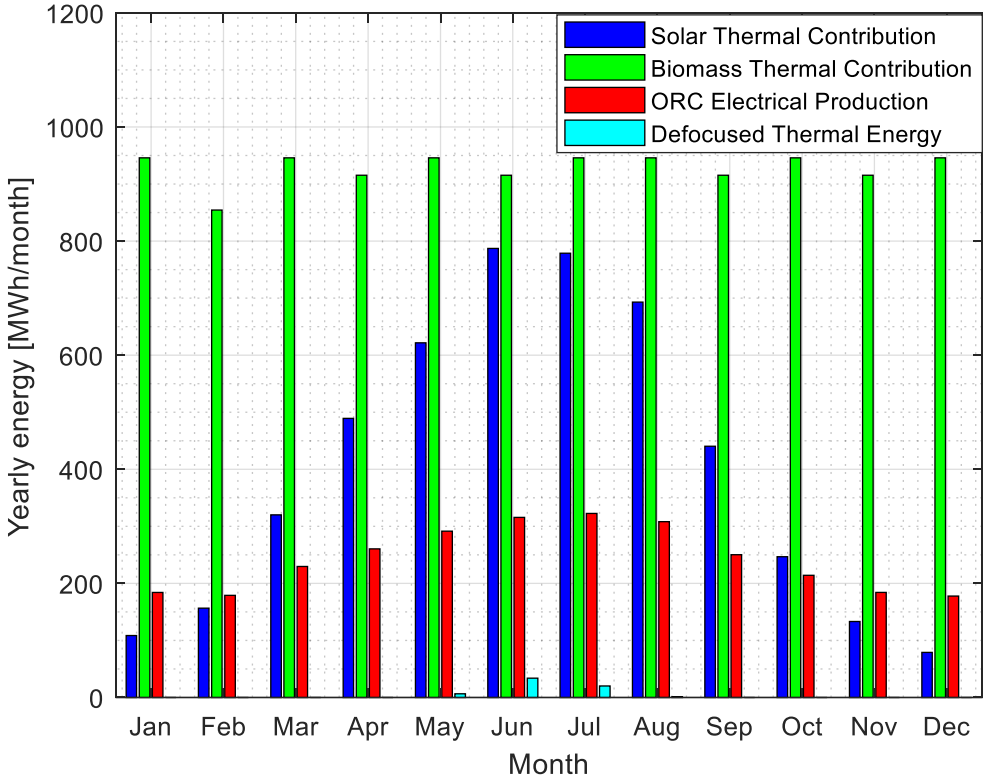

Figure 3.7: Yearly energy production – 40% fixed biomass contribution, real plant data.

3.3.2.1 Effects of biomass fraction for the retrofit

As aforementioned, five cases were simulated for hybridization by following the fixed approach, corresponding to biomass thermal supply of 40 %, 45 %, 50 %, 60 % and 70 % of ORC nominal requirement, in addition to the simulation obtained by following the modular approach. Annual performances of the six cases were thus compared with the existing solar-only case. The point of minimum load power production with biomass retrofit is further reflected in Figure 3.8, which shows the trend of ORC electrical power production for solar-only and retrofit cases, on a typical winter day. As shown, increase in biomass fraction leads to higher minimum load power production, which is a direct consequence of the implemented hybridization scheme. Implementing biomass fraction of 70% kept the ORC working at its nominal condition between 9:00 and 16:00 hours, regardless of the season. Comprehensive techno-economic performance of the plant for this case study is reported in Table 3.5. Annualized operating hours presented in this table refer to the

equivalent number of hours in a year when the plant operates at its nominal capacity, obtained as fraction of total annual production of the plant to nominal power (630 kW).

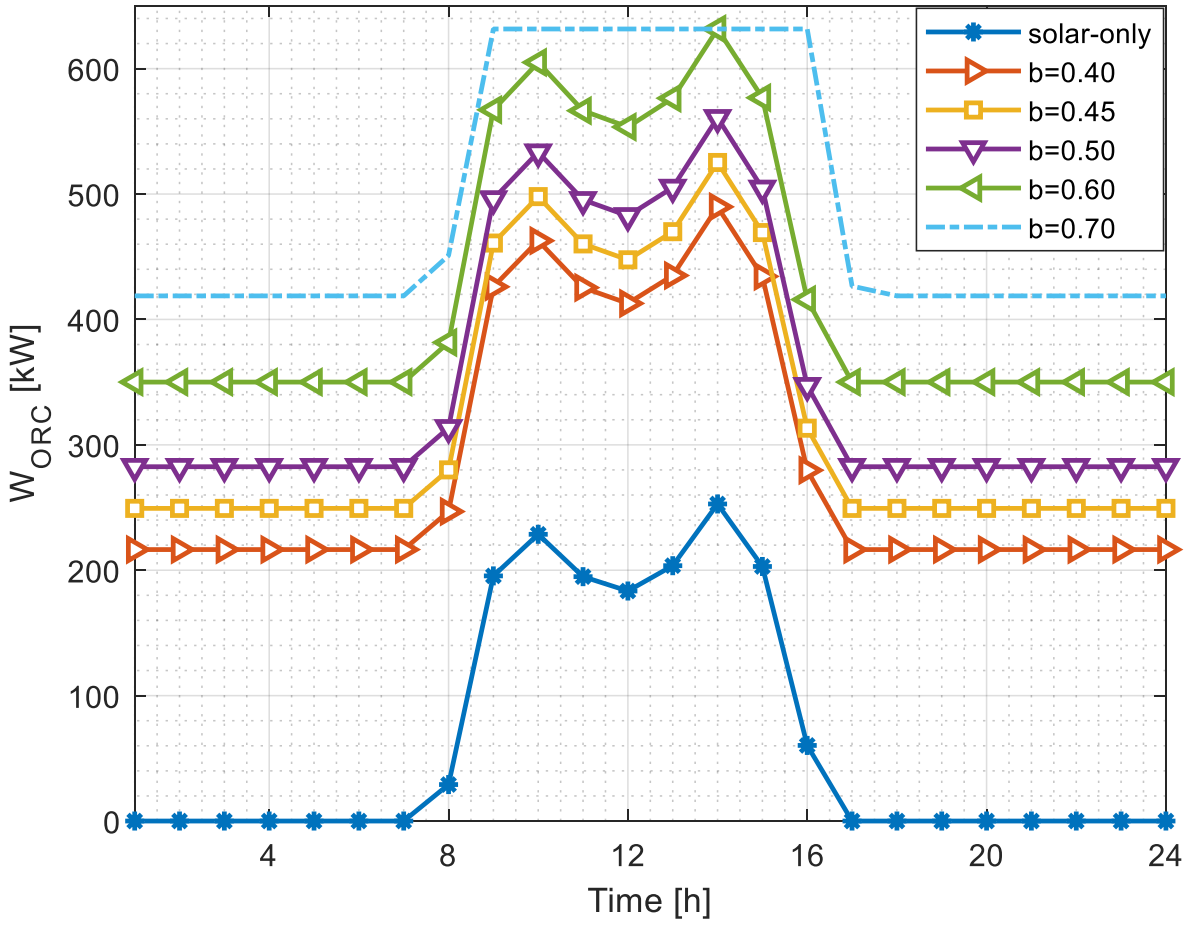

Figure 3.8: ORC electrical power production on a typical winter day.

Table 3.5: System performance of biomass retrofit for the real Ottana plant configuration.

	CSP only	Modular Appr.	Fixed Approach				
			Biomass retrofit fraction (b_{RF})				
			40%	45%	50%	60%	70%
Design stage							
Solar field collecting area (m^2)	8400	8400	8400	8400	8400	8400	8400
Solar field land area (ha)	11.76	11.76	11.76	11.76	11.76	11.76	11.76
Rated furnace power (MW)	-	3.18	1.27	1.43	1.59	1.91	2.23
TES size (h)	4.9	4.9	4.9	4.9	4.9	4.9	4.9
Annual energy performance							
Solar energy input (GWh/y)	4.85	4.85	4.85	4.85	4.85	4.85	4.85
Biomass energy input (GWh/y)	-	23.00	11.14	12.53	13.92	16.71	19.49
Defocused energy (GWh/y)	0	0	0.06	0.10	0.16	0.30	0.59
Annual solar contribution (%)	100	17.4	30.0	27.3	25.0	21.1	17.5
Biomass quantity (t/y)	-	8941	4341	4884	5426	6512	7597
Electricity production (GWh/y)	0.70	5.51	2.92	3.20	3.48	4.03	4.65
Annual NEE (%)	14.5	19.8	18.3	18.5	18.7	19.0	19.2
Annualized operating hours (h)	1117	8760	4635	5079	5524	6397	7238
Economic performance							
Marginal initial costs (M€)	-	0.502	0.241	0.265	0.289	0.334	0.378
Marginal annual costs (M€/y)	-	0.455	0.221	0.248	0.276	0.331	0.386
$LCOE_M$ (€/MWh)	-	103.5	109.0	108.6	108.2	107.9	108.4
SPB_M (years)	-	1.2	1.4	1.3	1.3	1.2	1.2
NPV_M (M€)	-	4.286	1.832	2.076	2.320	2.800	3.218
LCOE	-	148.3	192.2	184.6	178.2	168.2	161.7

As shown, fixed approach of biomass thermal retrofit would increase annual net electrical efficiency of the plant, for all the cases of biomass fraction considered. In particular, constant supplies of 40% of ORC nominal thermal requirement would increase annual net electrical efficiency of the plant by about 4 percent points. This increase improves steadily for higher biomass fractions, and it reaches the peak for the modular biomass hybridization approach, with increase of about 5 percent points. However, implementing high biomass fraction would increase wastages in the solar system, due to increase in defocused thermal energy. Suffice it to mention that, based on the manufacturer's specification for the studied ORC; the minimum thermal power that would keep the plant running is equivalent to 40% of nominal value, below which ORC would not work. This influenced the choice of 40% as the minimum biomass fraction in this study, since one of the key objectives was to keep the plant running continuously. For clearer illustration, trends of annual solar contribution and defocused thermal energy with biomass fraction are shown in Figure 3.9(a), for fixed approach. As it can be observed, increasing biomass fraction decreases percentage solar contribution, while defocused thermal energy increases drastically from biomass fraction beyond 50%. Also, it could be observed that annual solar contribution of the modular approach is equivalent to that of the fixed approach at 70% biomass fraction. Obviously, a further increase in biomass fraction for the fixed approach would reduce solar contribution below that of modular approach, in addition to huge defocused thermal energy. In addition, based on the presented technical results, one major thermodynamic benefit of biomass retrofit is dramatic increase in yearly operating hours of the hybrid plant, for all the retrofit cases, relative to the existing solar-only case.

Furthermore, the economic implications of biomass retrofit for the solar-ORC plant have been quantified. As aforementioned, since the solar ORC is already existing, marginal economic metrics ($LCOE_M$, NPV_M and SPB_M) have been used for assessment for the retrofit case study [249]. In particular, the marginal initial costs represent the additional capital investments required for retrofitting biomass boiler to the existing plant, while the marginal annual costs are the costs associated with operation and maintenance of the biomass boiler, as well as costs of biomass fuels.

Also, the annual net energy values implemented in these equations are those produced additionally by the biomass boiler, for the different biomass contributions. As shown in Table 3.5, the lowest $LCOE_M$ for the retrofit is valued at 103 €/MWh, obtained for the modular approach. The poorest is obtained for 40% fixed hybridization, valued at 109 €/MWh. This could give the modular hybridization approach an advantage, as solar energy produced is also fully utilized, with zero dissipation. It is however with attendant implication of higher biomass consumption, alongside its sustainability concerns. Conversely, NPV_M increases from lowest to highest for the biomass fractions studied, as illustrated in Figure 3.9(b). Between fixed and modular approach, economics results show that modular approach is more prospective, with higher NPV_M in the order of about 30%, relative to the most prospective fixed approach. In addition, in order to enable economic comparison of the implemented biomass retrofit scheme with other scenarios, conventional LCOE has equally been quantified, by adopting the cost assumptions reported in Table 3.4 for the whole plant. As reported in Table 3.5, results show that modular hybridization approach is equally more prospective in this regard, relative to all the fixed approach cases considered. In addition, another potential benefit arising by using the modular approach is the ability of the plant post-retrofit to modulate the power in the whole range of operation and in each operating time. This flexibility in following scheduled profile gives the possibility, not only to supply electric power with nearly zero carbon emissions, but also to provide ancillary services at distribution level.

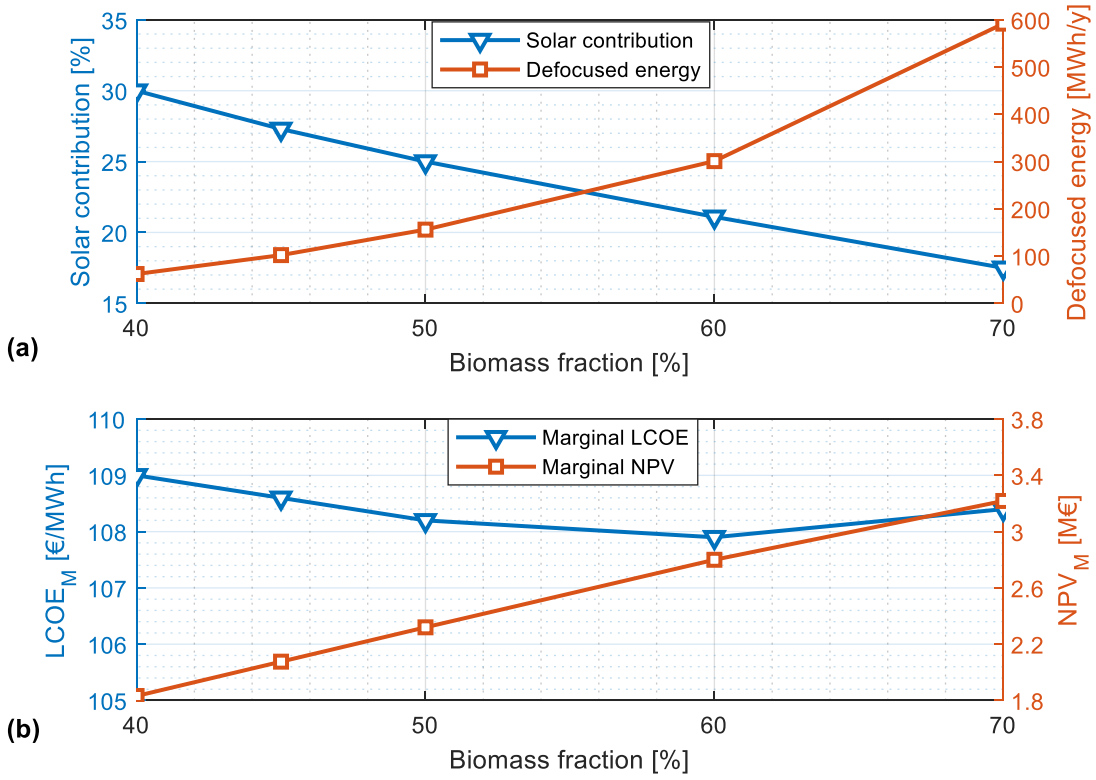

Figure 3.9: (a) Effect of biomass fraction on annual solar contribution and defocused energy and (b) Effect of biomass fraction on marginal LCOE and NPV.

Overall, it is worth noting that the marginal costs obtained are lower than feed-in tariff obtainable for biomass energy in the Italian market, thereby highlighting the benefit of retrofitting biomass with the solar section of the existing plant, for power generation. SPB_M values obtained indicate that it would only take about 1.2 to 1.4 years to repay the additional investment that would be incurred by implementing the retrofit scheme.

3.3.3 Design sensitivity and techno-economic performance of the newly integrated hybrid CSP-biomass plant

3.3.3.1 Sensitivity of CSP-biomass plant design to biomass contribution

For the sake of emphasis, this sensitivity analysis concerns just the newly integrated designs, as aforementioned. Based on the hybridization approaches adopted, solar field and TES sizes are sensitive to biomass fraction implemented, for each design case. To illustrate sensitivity of solar

field area to variation in biomass contribution, Figure 3.10 and Figure 3.11 show the solar field energy production, state of TES charge and discharge, as well as the share of biomass energy production for the two previously proposed (fixed and modular) hybridization approaches. This is illustrated at daily biomass contribution *b* equal to 40%, with respect to the aforementioned chosen reference day for design. The same trend is however obtainable for other biomass fractions. As it can be observed, a more intensive use of the TES system as well as higher TES capacity are required, if the fixed hybridization approach is assumed. Conversely, a lower thermal duty of the biomass furnace is required, and the biomass electricity production is independent of the solar source. The consequent advantage is in the use of a simpler control system and probably longer plant lifetime due to less start-up/shutdown cycle for the biomass section.

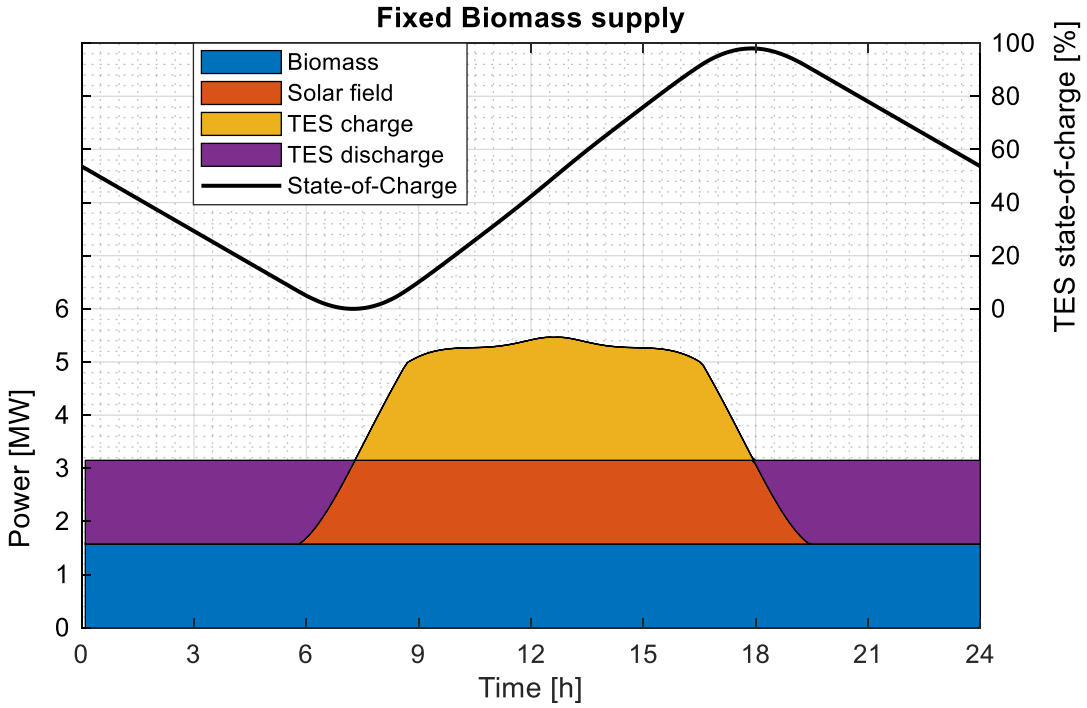

Figure 3.10: Energy flow in solar field, biomass furnace and TES at design condition for fixed biomass supply, b=40%.

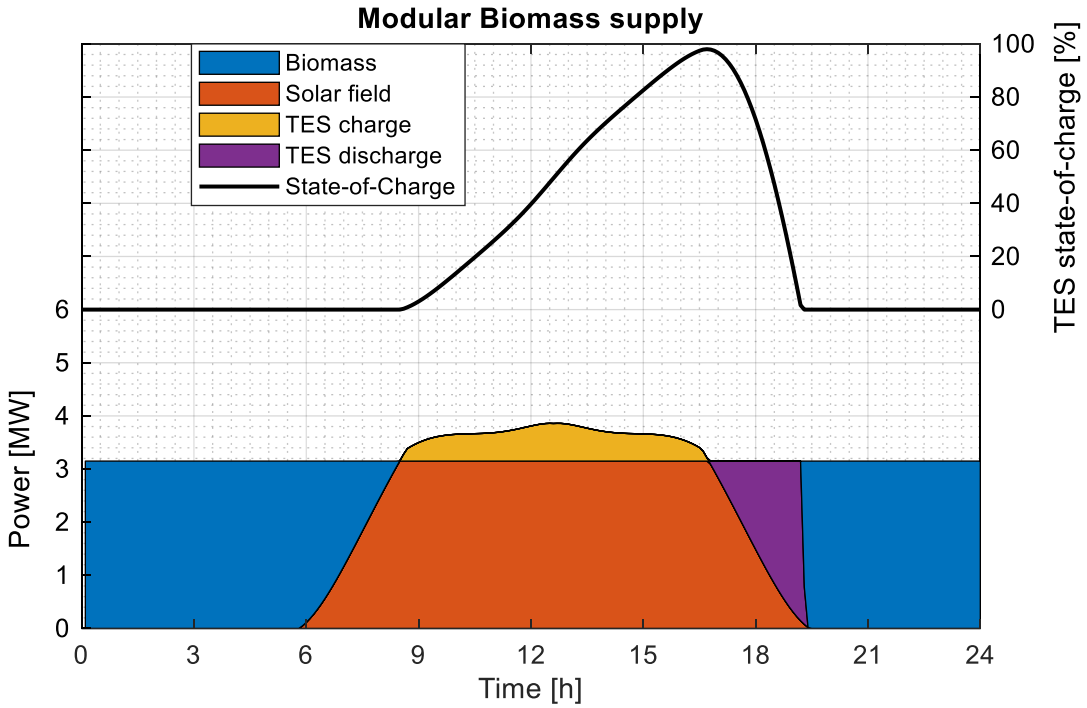

Figure 3.11: Energy flow in solar field, biomass furnace and TES at design condition for modulating biomass supply, b=40%.

The variation of solar field collecting area and design TES capacity with biomass contribution is shown in Figure 3.12. Obviously, the TES capacity required to satisfy design objective decreases with increasing contribution from biomass. As it is expected, the decrease in TES capacity is proportional for the fixed hybridization approach, and it becomes zero only when the plant is operated as exclusive biomass-ORC plant (100% biomass contribution). However, for the modular hybridization approach, no TES would be needed from around 60% biomass thermal contribution. In addition, required TES capacity is always lower in modulating approach. From the area representing solar field production in the figures, it could be understood that solar field area decreases with increasing biomass contribution. The collecting areas required with fixed biomass supply are slightly higher than those of the modulating one, for the same biomass contribution cases. This is due to higher TES capacity required to satisfy stated design objective, with consequent more significant impact of TES thermal losses.

As aforementioned, the required capacity for biomass boiler differs for each of the two hybridization approaches. In the case of fixed biomass supply, it corresponds to the multiple of respective biomass fraction with nominal thermal input requirement of the ORC. However, for the modular biomass supply approach, it always corresponds to ORC nominal thermal input requirement.

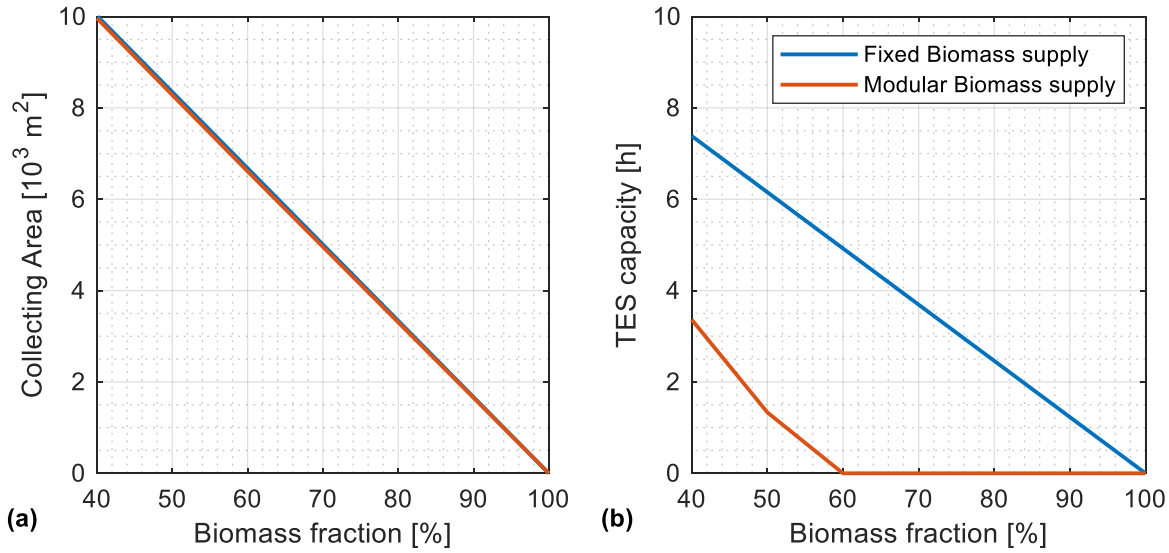

Figure 3.12: Variation of (a) solar field collecting and (b) design TES capacity with biomass fraction.

3.3.3.2 Yearly performance of the hybrid plant for newly integrated design

For the newly integrated design case study, Table 3.6 and

Table 3.7 report the summaries of overall plant performance for different biomass fraction, for fixed and modular hybridization approach, respectively.

Table 3.6: System performance for fixed biomass hybridization approach.

	Biomass contribution (b)				
	40%	45%	50%	60%	70%
Design stage					
Solar field collecting area (m^2)	10108	9266	8423	6739	5054
Solar field land area (ha)	14.15	12.97	11.79	9.44	7.08
Rated furnace power (MW)	1.27	1.43	1.59	1.91	2.23
TES size (h)	7.4	6.8	6.2	4.9	3.7
Annual energy performance					
Solar energy input (GWh/y)	5.84	5.36	4.87	3.90	2.92
Biomass energy input (GWh/y)	11.14	12.53	13.92	16.71	19.49
Defocused energy (GWh/y)	0.06	0.05	0.05	0.04	0.03
Annual solar contribution (%)	34.2	29.7	25.7	18.7	12.9
Biomass quantity (t/y)	4341	4884	5426	6512	7597
Electricity production (GWh/y)	3.11	3.31	3.50	3.89	4.29
Annual NEE (%)	18.4	18.6	18.7	18.9	19.2
Annualized operating hours (h)	4937	5254	5556	6175	6810
Economic performance					
Initial costs (M€)	4.132	3.906	3.680	3.227	2.771
Annual costs (M€/y)	0.279	0.303	0.327	0.374	0.421
LCOE (€/MWh)	203	193	184	167	153
SPB (years)	10.2	9.6	9.0	7.8	6.7
NPV (M€)	0.587	0.828	1.073	1.567	2.076

Table 3.7: System performance for modular biomass hybridization approach.

	Biomass contribution (b)				
	40%	45%	50%	60%	70%
Design stage					
Solar field collecting area (m^2)	10052	9204	8356	6670	5003
Solar field land area (ha)	14.07	12.89	11.70	9.34	7.00
Rated furnace power (MW)	3.18	3.18	3.18	3.18	3.18
TES size (h)	3.4	2.3	1.3	0	0
Annual energy performance					
Solar energy input (GWh/y)	5.81	5.32	4.83	3.86	2.89
Biomass energy input (GWh/y)	22.11	22.57	23.04	23.99	24.95
Defocused energy (GWh/y)	0.02	0.02	0.01	0	0
Annual solar contribution (%)	20.8	19.0	17.3	13.8	10.4
Biomass quantity (t/y)	8597	8775	8956	9322	9697
Electricity production (GWh/y)	5.51	5.51	5.51	5.51	5.51
Annual NEE (%)	19.8	19.8	19.8	19.8	19.8
Annualized operating hours (h)	8760	8760	8760	8760	8760
Economic performance					
Initial costs (M€)	3.745	3.427	3.116	2.600	2.300
Annual costs (M€/y)	0.486	0.490	0.495	0.505	0.519
LCOE (€/MWh)	146	142	138	132	130
SPB (years)	5.9	5.5	5.1	4.5	4.26
NPV (M€)	3.699	3.840	3.970	4.104	3.985

As it would be expected, increasing biomass fraction leads to slight increase in annual net electrical efficiency for the fixed approach, while the annualized efficiency is always at the highest for the modular approach. Actually, the main technical benefits of biomass hybridization concerns increase in plant operating hours during the year, and minimum load plant operation. In addition, it is observed that increasing biomass contribution reduces annual solar contribution to the hybrid plant, for both fixed and modular approach. Also, from the values of annual solar contribution obtained for fixed and modular approach, it could be inferred that solar energy is better utilized in fixed approach, relative to modular one. It is however with the consequence of implementing larger TES system in fixed approach, a situation that is unfavourable to plant economics. In fact, economic results reported in Table 3.6 and

Table 3.7 clearly show that more prospective economic performance is obtained in the modular approach, for all biomass fractions studied. For the two approaches, increasing biomass fraction improves all the computed economic metrics, obviously due to lower solar field and TES requirements. Overall, modular biomass hybridization approach with 70% biomass fraction portends the most prospective economic values for the newly integrated design case study, with LCOE, SPB and NPV obtained at 130 €/MWh, 4.3 years and 3.985 M€, respectively. Obviously, more economic merits could be derived by further increasing biomass fraction, but concerns surrounding biomass fuel availability and sustainability would be higher in that regard.

In addition, future scenario of economic performance has been quantified for the hybrid plant, in the event that current measures being vigorously pursued to reduce investment costs of CSP systems are successful. Thus, possible trend of reduction in LCOE has been obtained, for the newly integrated design case study, in the event of 30% and 50% reduction in CSP investment costs, as shown in Figure 3.13. For the fixed biomass hybridization approach, minimum LCOE of about 126 €/MWh is achievable at 100% biomass contribution, for both 50% and 30% reduction in CSP investment cost. In the case of modular approach, minimum LCOE of 120 €/MWh and 123 €/MWh

are achievable at 60% and 100% biomass contribution, for 50% and 30% reduction in CSP investment cost, respectively.

It is important to point out that, for ORC power plant with rated capacity less than 1 MW, the LCOE, SPB and NPV values obtained here imply an increase in market competitiveness, relative to what obtains in other renewable power plants of comparable ratings. Moreover, for the Italian market used as reference here, the LCOE values obtained for all modular approach case studies are lower than the feed-in tariffs for both biomass and solar energy, which further reiterates the profitability of the hybrid scheme implemented in this study.

Overall, it is worth highlighting also that the strategy adopted for biomass hybridization in this study is particularly versatile, owing to its suitability not only as biomass retrofit for existing solar-ORC plants, but also for development of new systems, as demonstrated in the newly integrated design case study.

Finally, results showed that newly integrated design case study enables higher plant operating hours relative to retrofit case study, with closely matched annualized net electrical efficiency. This is with the consequence of increasing solar field size for biomass fractions lower than 60%, as well as high biomass consumption in all cases of biomass fraction. However, all of these points do not noticeably affect economic prospects of the newly integrated design concept. This is justified by the most prospective LCOE obtained as 148 €/MWh for the retrofit case study, which is poorer than all the LCOE values obtained for modular approach for the newly integrated design case study. Moreover, in terms of biomass fuel availability and sustainability concerns, retrofit case study is more promising than newly integrated design case study, since lower biomass fuel is consumed in the former.

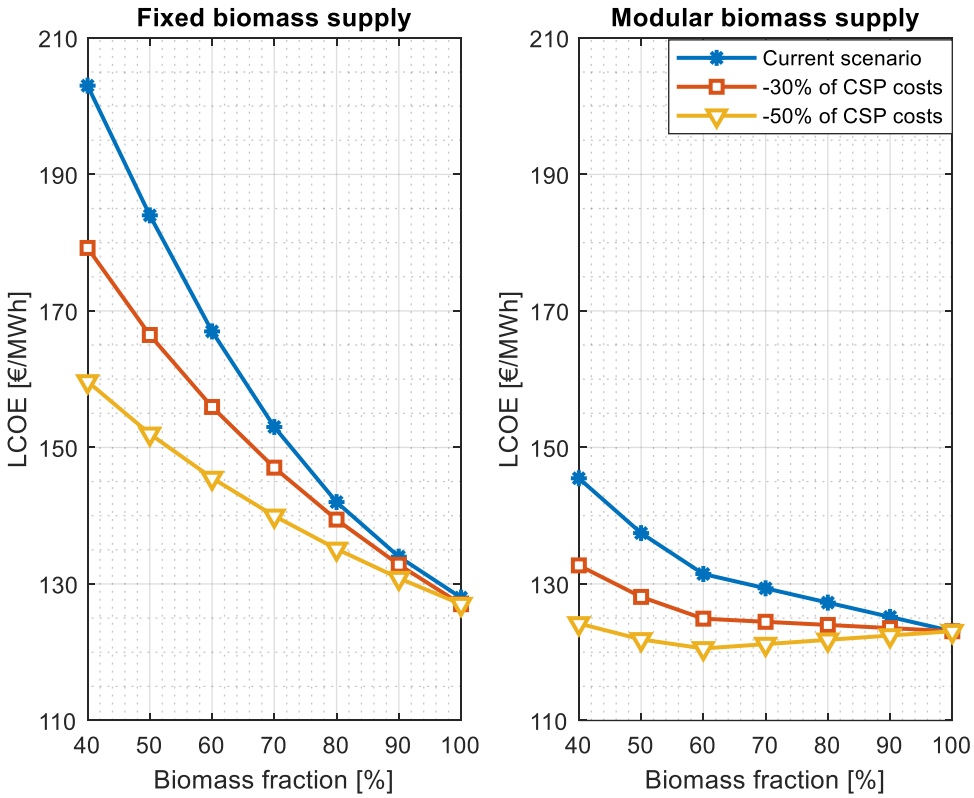

Figure 3.13: Prospective reduction of hybrid plant LCOE with reduced investment cost of CSP.

3.4Summary

Conceptual design of hybrid CSP-biomass ORC plant has been presented in this chapter. Although a number of authors have presented different schemes for hybrid solar-biomass plants, particular attention has not been given to the case of retrofitting existing CSP-ORC plants with biomass combustion process. In this light, a parallel hybridization scheme has been proposed and analysed, where both solar field with TES and biomass furnace are able to independently satisfy fractional thermal requirement of existing ORC power plant. In addition, in order to expand the scope of the study, newly integrated designs were introduced for sizing solar field and TES systems in a separate case study. This gives room for the analyses included in this chapter to be equally relevant, if a new hybrid solar-biomass ORC plant of this type is planned.

Some major results derived from the analyses presented in this chapter are highlighted as follows:

- Supposed biomass retrofit can lead to an increase in electrical efficiency in the order of 5 percent points compared to CSP-ORC plant. Also, the implemented modular approach for biomass retrofit can enable scheduled power profile to be followed, thereby enhancing plant dispatchability.
- Retrofit can increase annualized plant operating duration by about 3,500 hours, with marginal LCOE and NPV of 109 €/MWh and 1.83 M€, respectively. Additional investment cost incurred due to retrofit can be offset in 1.4 years of plant operation.
- Validity of the applied ORC off-design methods is satisfied. This is based on the obtained relative deviation of ORC gross efficiency between simulation results and real power plant data, which is below 3%.
- For the newly integrated design, modular hybridization approach leads to most prospective economic performance and higher plant utilization, compared to fixed approach. This is however at the expense of increased biomass consumption and attendant sustainability issues.
- In comparison with retrofit case study, newly integrated design leads to a more economically-prospective hybrid plant, with LCOE, SPB and NPV obtained at 130 €/MWh, 4.3 years and 3.99 M€, respectively. Also, relative to stand-alone solar ORC power plants of equivalent ratings, these economic values portend market competitiveness [250],[251].

Page left blank intentionally

Chapter 4
Exergy and Exergoeconomic Assessment of the Proposed Hybrid CSP-Biomass ORC Plant

4.1Preamble

The importance of exergy-based assessment of energy systems has been underscored in Chapter 2. Amongst others, it quantifies thermo-economic losses in each system component, thereby providing relevant information on the components to be optimized for technical and economic enhancements. When exergy and exergoeconomic analyses are extended to quantify exergy and economic losses in each components that could not be avoided, better optimization potentials of each system components are obtained. Thus, detailed exergy, exergoeconomic, enhanced exergy and enhanced exergoeconomic analyses had been carried out for the hybrid CSP-biomass ORC plant under investigation, as presented in this chapter. The enhanced analyses bother on separating avoidable lost exergy and exergy cost from the unavoidable ones, following classical and established procedures. The chapter specific objectives are:

- Quantification of exergy rate in each thermodynamic state, and irreversibility in each component of the hybrid plant, as well as assessment of overall exergetic performance of the plant;
- Estimation of exergy cost rates for all thermodynamic states and components of the plant, as well as assessment of exergoeconomic performance of components and the whole plant;
- Comparative analysis of the impacts that integrating energy quality levels of streams to cost formation process would have on exergoeconomic performance of the hybrid plant; and
- Determination of avoidable and unavoidable irreversibility and lost exergy cost in each component, and suggestion of adequate measures to improve the respective components.

The methods applied for the exergy, exergoeconomic, enhanced exergy and enhanced exergoeconomic analyses are presented in section 4.2, while the results and discussions derived therefrom are contained in section 4.3. Section 4.4 summarizes the main issues discussed in this chapter.

4.2Methodology

4.2.1 Exergy analysis

As aforementioned, the system under investigation here is a fall out from experience with a real solar-ORC power plant, and the energetic performance of the ORC had been validated by real data from the existing plant, as presented in Chapter 3. However, mass balance and energy balance of each component of the hybrid plant are also established in this section, prior to the intended component-based exergy analysis of the system. The modified hybrid plant scheme is shown in Figure 4.1, for adequate identification and numbering of different thermodynamic states. The classical mass, energy and exergy rate balance equations at steady state were implemented for each component, as follows [183]:

$$\sum \dot{m}_i = \sum \dot{m}_o \quad (4.1)$$

$$\sum \dot{m}_i h_i + \dot{Q} = \sum \dot{m}_o h_o + \dot{W} \quad (4.2)$$

$$\sum \dot{m}_i e_i + \dot{Q}\left(1 - \frac{T_a}{T_c}\right) = \sum \dot{m}_o e_o + \dot{W} + \dot{I} \quad (4.3)$$

where $\dot{m}$ is mass flow rate of the stream substance, h is the specific enthalpy, $\dot{Q}$ is heat flow through component boundary, T_a is the temperature of the environment (average taken as 25 ^{o}C for exergy analysis), T_c is the temperature at component boundary, at which heat is transferred with the environment, e is the specific exergy of the stream, $\dot{W}$ is work rate of the component, and $\dot{I}$ is the rate of exergy destroyed in the component (irreversibility). Subscripts i and o represent inlet and exit to and from the component, respectively. The specific exergy (e) is expressed as:

$$e = e_{ph} + e_{ch} + e_{ke} + e_{pe} \quad (4.4)$$

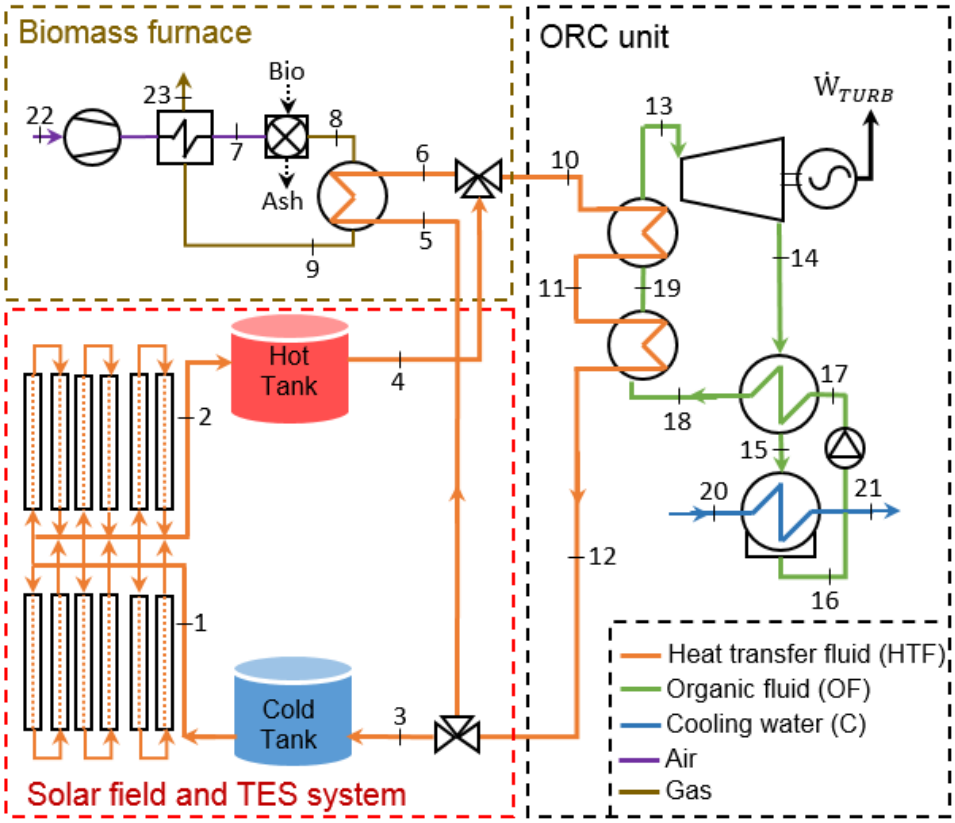

Figure 4.1: Conceptual scheme of the hybrid CSP-biomass ORC plant.

where e_{ph}, e_{ch}, e_{ke}, and e_{pe} represent the physical, chemical, kinetic and potential components of the specific exergy, respectively. The kinetic and potential components are inconsequential to the performance of most system analysis at steady state, and could mostly be acceptably neglected [182]. For streams with notable chemical compositions and interactions with the environment, chemical exergy is quite significant. However, in streams without interactions with the environment, the chemical exergy cancels out between two state points, such that only the physical exergy defines the total specific exergy of such streams [182]. The fundamental equation for estimating physical exergy is given as:

$$e_{ph} = (h - h_a) - T_a(s - s_a) \quad (4.5)$$

where s is the specific entropy of the concerned stream, while h_a and s_a are the specific enthalpy and specific entropy of the environment, respectively. Specific chemical exergy of stream depends on the stream composition, as well as reference state of the environment. A number of authors have

done extensive studies on methodologies for estimating chemical exergy of different solid, liquid and gaseous substances. These have led to development of chemical exergy values for several compounds, at specified reference temperature [182,214]. Mathematical correlation also exists, for adjusting the estimated chemical values at environmental state of interest [182]. In particular, specific chemical exergy (e_{ch}) of flue gases was computed in this study, as follows:

$$e_{ch} = (\sum_i x_i \hat{r}_i + RT_a \sum_i x_i \, lnx_i)/MM \quad (4.6)$$

where x_i and $\hat{r}_i$ represent molar mass and reference standard exergy of each component of the gaseous streams (taken in accordance with [183]), respectively; *R* is the universal gas constant, and *MM* is the average molar mass of the chemical stream. Also, the chemical exergy of biomass fuel ($\dot{E}_{ch,biom}$) was computed as follows [182]:

$$\dot{E}_{ch,biom} = \beta \times LHV \quad (4.7)$$

where β is the index quantifying the chemical exergy in organic fuels, and *LHV* is the lower heating value of the biomass fuel. The expressions adopted for β is as follows [182]:

$$\beta = \frac{1.044 + 0.016\frac{H}{C} - 0.34493\frac{O}{C}(1 + 0.0531\frac{H}{C})}{1 - 0.4124\frac{O}{C}} \quad (4.8)$$

giving a value of 1.141 by assuming the composition of the considered biomass.

For the solar field, fuel exergy is exergy associated with the solar radiation ($\dot{E}_s$), which was obtained from [252]:

$$\dot{E}_s = DNI \cdot A_{sf}\left[1 - \frac{4}{3}\frac{T_a}{T_s} + \frac{1}{3}\frac{{T_a}^4}{{T_s}^4}\right] \quad (4.9)$$

where DNI is the direct normal irradiation, A_{sf} is the solar field collecting area and T_s is the sun temperature (imposed equal to 5770 K). Solar thermal power produced by DNI in excess of what is required to maintain energy balance of the system has been regarded as exergy loss in these analyses. Also, the exergy content of the solar radiation is strongly devalued by irreversibility

(related to the temperature difference between the sun and the receiver) and thermal and optical losses ($\dot{Q}_{loss,sf}$). The latter were calculated as:

$$\dot{Q}_{loss,sf} = [DNI(1-\eta_{opt}) + (a_1(T_{av}-T_a) + a_2(T_{av}-T_a)^2 + \dot{q}_{pl})] \cdot A_{sf} \qquad (4.10)$$

where η_{opt} is the total optical efficiency, T_{av} is the average solar field temperature, a_1 and a_2 are coefficients related to receiver thermal losses (imposed equal to 0.056 W/m^{2}K and 0.213·10^{-3} W/m^{2}K^2 respectively, according to [23]) and $\dot{q}_{pl}$ represents the piping thermal losses (set equal to 5 W/m^2).

Furthermore, due to imperfect insulation in the TES tanks, the temperature of storage fluid drops over time, resulting in thermal losses. This temperature drop was considered in this study, as follows [253]:

$$\frac{T(t)-T_a}{T_i-T_a} = e^{-(U\cdot A_{TES}\cdot t)/(\rho_{HTF}.c_{HTF}.V_{HTF})} \qquad (4.11)$$

where T, ρ_{HTF}, V_{HTF}, and c_{HTF} are the temperature, density, volume and specific heat capacity of heat transfer fluid, respectively; A_{TES} is the heat transfer area of storage thermal oil; t is time; and U is the overall heat transfer coefficient, obtained as follows [254]:

$$U = \frac{d_{ins}}{k_{ins}} + \frac{1}{\alpha_{air}} \qquad (4.12)$$

where d_{ins} (0.5 m) and k_{ins} (0.16 W/m^{2}K) are respectively the thickness and thermal conductivity of the insulation material. The convection heat transfer coefficient of air (α_{air}) was estimated as a function of the wind speed (v_a), as follows:

$$\alpha_{air} = 10.45 - v_a + 10\sqrt{v_a} \qquad (4.13)$$

In addition, having adequately considered design and operational features of each sub-section of the hybrid plant, zero-dimensional models were developed for each component, with reference to eqs (4.1 - 4.3), for mass, energy and exergy balance. Inlet and exit temperatures of thermal source HTF into the ORC were fixed at 275 ^{o}C and 165 ^{o}C respectively, in accordance with the existing real ORC plant. Thermodynamic calculations were performed in Matlab environment, while stream properties were computed using CoolProp [255] as well as based on manufacturer's datasheet for the source HTF.

4.2.1.1 Exergetic performance parameters

In order to examine the exergetic performance of each system component k, rational efficiency (ε_k), efficiency defect (δ_k) and relative irreversibilities (RI_k) were computed as follows:

$$\varepsilon_k = \frac{\dot{E}_{o,k}}{\dot{E}_{i,k}} \tag{4.14}$$

$$\delta_k = \frac{\dot{I}_k}{\dot{E}_{i,k}} \tag{4.15}$$

$$RI_k = \frac{\dot{I}_k}{\sum \dot{I}_k} \tag{4.16}$$

where $\dot{E}_{o,k}$ and $\dot{E}_{i,k}$ are respectively the product and fuel exergy of the k-th component (Table 4.1 reports the expressions for each component), while $\dot{I}_k$ is the corresponding exergy destroyed. For solar field and combustion chamber, where thermal losses to the ambient were considered, the efficiency defect due to losses is the ratio of lost exergy to component fuel.

For the system as a whole, rational efficiency is the ratio of overall product exergy to fuel exergy. The main fuels are the actual solar exergy received by the collectors ($\dot{E}_s$), as well as biomass exergy ($\dot{m}_b e_{ch,b}$). The main products from the system are the turbine work ($\dot{W}_{TURB}$) and warm water

obtained at condenser exit, which is being used for heating office floor at plant location, signalling the possibility of operating the plant in CHP mode.

4.2.2 Exergoeconomic analysis

As stated earlier, exergoeconomic analysis of energy systems is a powerful tool, which integrates exergy-analysis and cost-analysis principles. It is aimed at providing useful insights into the costs of useful and destroyed exergy in each system component, thereby providing vital information on components with high potentials for optimization. In this study, the Specific Exergy Costing (SPECO) methodology was adopted for implementation, in two different approaches. The first one is the conventional approach as proposed originally in [187]. This approach assumes that, for the same working substance entering and leaving a component, unit cost of exergy is the same at inlet and exit streams, regardless of the quality of energy content of the streams. The second approach implemented in this study integrates energy quality of streams to cost formation process in SPECO analysis, and it is termed integrated exergoeconomic approach here. The actual formulations of the two exergoeconomic approaches are summarized below.

4.2.2.1 Conventional exergoeconomic approach

As a prelude to applying SPECO for conventional exergoeconomic analysis, the exergy of each stream and destroyed exergy in each component should be quantified from exergy analysis. Afterwards, the exergoeconomic analysis consists of the following essential steps: (1) the desired exergy output from respective components (product exergy) and net exergy expended in each component (fuel exergy) should be defined; (2) cost rate balance equations should be defined for each component, generally given as follows [187]:

$$\sum c\dot{E}_i + c_q\dot{E}_q + \dot{\mathrm{Z}} = \sum c\dot{E}_o + c_w\dot{W} \tag{4.17}$$

with c, $\dot{E}$ and $\dot{E}_q$ representing stream cost per unit exergy, stream total exergy rate, and exergy rate due to heat transfer with a component, respectively; c_q and c_w are cost per unit exergy of heat and work exchange with a component, respectively; and $\dot{Z}$ is the cost rate due to investment, operation and maintenance of a component, calculated as:

$$\dot{\mathrm{Z}} = \mathrm{Z} \cdot \frac{1}{H_A} \cdot \frac{int(1+int)^N}{(1+int)^N - 1} \cdot (1 + MF) \tag{4.18}$$

where Z is the purchase cost of a component, H_A is the annual equivalent working hours of the plant (taken as 6000 hours in this study), *MF* is the maintenance factor (assumed equal to 6%), *int* is interest rate (7% here) and *N* is the plant life time (25 years here). The purchase costs of solar field and TES were taken as 160 €/m^2 and 45 €/kWh, respectively [244]. For ORC and biomass components, purchase costs were obtained from Turton *et al*. [256]. Shell and tube configuration was assumed for heat exchangers. Costs associated with engineering, procurement and construction (EPC) as well as taxes were factored into *Z*, at 11%. Based on fuel-product principles of SPECO [187], auxiliary equations were defined, to facilitate simultaneous solution of the cost rate balance equations, from where values of *c* for all streams were obtained.

4.2.2.2 Integrated exergoeconomic approach

As aforementioned, conventional SPECO methodology as proposed and as it is being widely applied today follows fuel-product principle that excludes quality of stream energy in cost formation process. Oftentimes, this gives erroneous information regarding the cost required to utilize waste heat meant to be rejected to the surrounding, for generation of another product in form of cogeneration or polygeneration [257]. In an attempt to ameliorate this effect, the energy level methodology developed in [258] had been integrated into cost formation process of SPECO [259]. This was achieved by modifying fuel-product principle used in formulating auxiliary equations, based on the assertion that unit exergy cost of each stream should be linearly proportional to its

energy quality level. Specifically, for the same working substance entering a component from stream *i* and leaving through stream *o*, the fuel-product cost principle based on the integrated exergoeconomic approach is expressed as follows:

$$\frac{c_i}{G_i} = \frac{c_o}{G_o} \tag{4.19}$$

where *G* is the stream thermal energy level, defined as follows [258]:

$$G = 1 - T_a\left(\frac{dS}{dH}\right) = \left|1 - \frac{T_a}{T}\right| \tag{4.20}$$

where *dS* and *dH* are entropy change and enthalpy change, respectively. Based on this concept, all the auxiliary equations needed to obtain unit exergy cost for each stream were re-formulated, which is the only major difference between integrated and conventional exergoeconomic approaches implemented in this study. In addition, the unit cost of loss exergy of flue gas is set as zero under this approach [214]. Although the best way to treat cost of loss exergy in exergoeconomic analysis is an open discourse, it is adequate here to assign zero cost to exergy of the flue gas exiting the system for inclusion in costs of other components, since it could otherwise be recovered for further use in the system.

For the two approaches, the exergoeconomic performance of each component was assessed, using the cost rate of destroyed exergy ($\dot{C}_D$), exergoeconomic factor (*f*) as well as relative cost difference (*r*), defined as follows [214]:

$$\dot{C}_D = c_f \cdot \dot{I} \tag{4.21}$$

$$f = \frac{\dot{Z}}{\dot{Z} + \dot{C}_D + \dot{C}_L} \tag{4.22}$$

$$r = \frac{c_p - c_f}{c_f} \tag{4.23}$$

where c_f, c_p and $\dot{C}_L$ represent cost per unit of fuel exergy (ratio of cost rate of fuel to fuel exergy, €/kWh), cost per unit of product exergy (ratio of cost rate of product to product exergy, €/kWh) and cost rate of lost exergy (€/h), respectively. Indeed, huge exergy is expected to be lost due to inability of solar collectors to fully absorb transmitted solar energy. These losses are somewhat natural and unavoidable, due to atmospheric radiation processes, as well as diffusion on impinging the focused solar collectors. In essence, it would be inappropriate to insinuate that all losses in such unit are due to decrease in exergy transfer as a result of inefficiency of the unit, and distinctions between lost and destroyed exergy have thus been made in this regard. However, since solar energy is treated as free fuel (zero cost), it is acceptable to disregard cost due to lost exergy for this unit. The cost of exergy lost to diffusion of solar irradiation was thus taken as zero.

For the whole system, *f* and unit cost of turbine work have been used as main evaluation criteria. While the unit cost of turbine work is obtainable directly from SPECO, the definition of *f* given in eq. (4.22) had been applied, with $\dot{Z}$, $\dot{C}_D$ and $\dot{C}_L$ taken as the sum for all system components. For each component, expressions for cost rate balance as well as auxiliary equations for conventional and integrated exergoeconomic approaches are highlighted in Table 4.2.

Table 4.1: Component fuel and product exergy

Component (abbreviation)	Fuel exergy	Product exergy
Solar field (SF)	$\dot{E}_s$	$\dot{m}_2 e_2 - \dot{m}_1 e_1$
Hot tank (HT)	$\dot{m}_2 e_2$	$\dot{m}_4 e_4$
Cold tank (CT)	$\dot{m}_3 e_3$	$\dot{m}_1 e_1$
Air preheater (AP)	$\dot{m}_9 e_9 - \dot{m}_{23} e_{23}$	$\dot{m}_7 e_7 - \dot{m}_{22} e_{22}$
Combustion chamber (CC)	$\dot{m}_b e_{ch,b} + \dot{m}_7 e_7$	$\dot{m}_8 e_8$
Furnace heater (FH)	$\dot{m}_8 e_8 - \dot{m}_9 e_9$	$\dot{m}_6 e_6 - \dot{m}_5 e_5$
ORC preheater (PRHT)	$\dot{m}_{11} e_{11} - \dot{m}_{12} e_{12}$	$\dot{m}_{19} e_{19} - \dot{m}_{18} e_{18}$
Evaporator (EVAP)	$\dot{m}_{10} e_{10} - \dot{m}_{11} e_{11}$	$\dot{m}_{13} e_{13} - \dot{m}_{19} e_{19}$
Recuperator (RECP)	$\dot{m}_{14} e_{14} - \dot{m}_{15} e_{15}$	$\dot{m}_{18} e_{18} - \dot{m}_{17} e_{17}$
Condenser (COND)	$\dot{m}_{15} e_{15} - \dot{m}_{16} e_{16}$	$\dot{m}_{21} e_{21} - \dot{m}_{20} e_{20}$
Pump (PUMP)	$\dot{W}_{PUMP}$	$\dot{m}_{17} e_{17} - \dot{m}_{16} e_{16}$
Turbine (TURB)	$\dot{m}_{13} e_{13} - \dot{m}_{14} e_{14}$	$\dot{W}_{TURB}$
Valve 1 (V1)	$\dot{m}_4 e_4 + \dot{m}_6 e_6$	$\dot{m}_{10} e_{10}$
Valve 2 (V2)	$\dot{m}_{12} e_{12}$	$\dot{m}_3 e_3 + \dot{m}_5 e_5$

Table 4.2: Component fuel, product, cost rate balance and auxiliary equations.

Component (abbreviation)	**Cost rate balance equation**	**Auxiliary equation (conventional)**	**Auxiliary equation (integrated)**
Solar field (SF)	$\dot{C}_1 + \dot{Z}_{SF} = \dot{C}_2$	$c_s = 0$	$c_s = 0$
Hot tank (HT)	$\dot{C}_2 + \dot{Z}_{HT} = \dot{C}_4$		
Cold tank (CT)	$\dot{C}_3 + \dot{Z}_{CT} = \dot{C}_1$		
Air preheater (AP)	$\dot{C}_{22} + \dot{C}_9 + \dot{Z}_{AP} = \dot{C}_{23} + \dot{C}_7$	$c_{22} = 0;$ $c_9 = c_{23}$	$c_{22} = 0;$ $c_{23} = 0$
Combustion chamber (CC)	$\dot{C}_7 + \dot{C}_b + \dot{Z}_{CC} = \dot{C}_8$	$c_b = 1.1 \frac{\text{c€}}{\text{kWh}}$	$c_b = 1.1 \frac{\text{c€}}{\text{kWh}}$
Furnace heater (FH)	$\dot{C}_8 + \dot{C}_5 + \dot{Z}_{FH} = \dot{C}_9 + \dot{C}_6$	$c_8 = c_9$	$\frac{c_8}{G_8} = \frac{c_9}{G_9}$
ORC preheater (PRHT)	$\dot{C}_{11} + \dot{C}_{18} + \dot{Z}_{PRHT} = \dot{C}_{19} + \dot{C}_{12}$	$c_{11} = c_{12}$	$\frac{c_{11}}{G_{11}} = \frac{c_{12}}{G_{12}}$
Evaporator (EVAP)	$\dot{C}_{10} + \dot{C}_{19} + \dot{Z}_{EVAP} = \dot{C}_{11} + \dot{C}_{13}$	$c_{10} = c_{11}$	$\frac{c_{10}}{G_{10}} = \frac{c_{11}}{G_{11}}$
Recuperator (RECP)	$\dot{C}_{14} + \dot{C}_{17} + \dot{Z}_{RECP} = \dot{C}_{15} + \dot{C}_{18}$	$c_{14} = c_{15}$	$\frac{c_{14}}{G_{14}} = \frac{c_{15}}{G_{15}}$
Condenser (COND)	$\dot{C}_{15} + \dot{C}_{20} + \dot{Z}_{COND} = \dot{C}_{16} + \dot{C}_{21}$	$c_{20} = 0;$ $c_{15} = c_{16}$	$c_{20} = 0;$ $\frac{c_{15}}{G_{15}} = \frac{c_{16}}{G_{16}}$
Pump (PUMP)	$\dot{C}_{16} + \dot{C}_{w,p} + \dot{Z}_{PUMP} = \dot{C}_{17}$	$c_{w,p} = c_{w,T}$	$c_{w,p} = c_{w,T}$
Turbine (TURB)	$\dot{C}_{13} + \dot{Z}_{TURB} = \dot{C}_{w,T} + \dot{C}_{14}$	$c_{13} = c_{14}$	$\frac{c_{13}}{G_{13}} = \frac{c_{14}}{G_{14}}$
Valve 1 (V1)	$\dot{C}_4 + \dot{C}_6 + \dot{Z}_{V1} = \dot{C}_{10}$		
Valve 2 (V2)	$\dot{C}_{12} + \dot{Z}_{V2} = \dot{C}_3 + \dot{C}_5$	$c_{12} = c_3 = c_5$	$c_{12} = c_3 = c_5$

4.2.3 Enhanced exergy analysis

The assessment of optimization potentials in each component using exergy analysis quantifies the rate of exergy destruction in each system component, with the erroneous assumption that all these irreversibilities could be recovered. In actual fact, some irreversibilities are intrinsic in energy system components, due to systemic and economic constraints imposed by thermodynamic laws. In essence, this unavoidable exergy destruction should be regarded, when applying exergy analysis for assessing optimization potentials in energy systems. To estimate unavoidable part of destroyed exergy in a component *k*, the best possible performance characteristics of component *k* are imposed during exergy analysis, while other system components remain at their real states [184]. The ratio of destroyed exergy to product exergy of component *k* obtained under this circumstance, $\left(\frac{\dot{\mathrm{E}}_D}{\dot{\mathrm{E}}_P}\right)_{\boldsymbol{k}}^{UN}$, is then used for estimating unavoidable part of exergy destruction in component *k*, as follows [184]:

$$\dot{E}_{D,k}^{UN} = \dot{E}_{o,k} \times \left(\frac{\dot{\mathrm{E}}_D}{\dot{\mathrm{E}}_P}\right)_k^{UN} \tag{4.24}$$

This leaves the part of destroyed exergy in *k* that could be eliminated by optimization efforts (avoidable part of destroyed exergy) as:

$$\dot{E}_{D,k}^{AV} = \dot{I}_k - \dot{E}_{D,k}^{UN} \tag{4.25}$$

The enhanced exergy efficiency (ε^*) under this condition is given by:

$$\varepsilon^* = \frac{\dot{E}_{o,k}}{\dot{E}_{i,k} - \dot{E}_{D,k}^{UN}} \tag{4.26}$$

Assumptions for the best performance characteristics applied for obtaining unavoidable irreversibilities in this study are based both on empirical judgement and literature, as highlighted in Table 4.3.

Table 4.3: Assumptions for unavoidable conditions of system components.

Component	Unavoidable conditions	Component	Unavoidable conditions
Solar field	$\left(\frac{\dot{E}_D}{\dot{E}_P}\right)_{sf}^{UN} = 0.7638$ [194]	Furnace heater	ΔT_{min} = 3 K
Hot tank	Perfect insulation	ORC preheater	ΔT_{min} = 3 K
Cold tank	Perfect insulation	Evaporator	ΔT_{min} = 5 K
Air preheater	ΔT_{min} = 12 K	Recuperator	*effectiveness* = 0.9
	Adiabatic condition; air-fuel ratio = 1 (high gas temperature)	Condenser	ΔT_{min} = 3 K
Combustion chamber		Pump	η_{is} = 0.95; η_{mech} = 1
		Turbine	η_{is} = 0.97; η_{mech} = 1

4.2.4 Enhanced exergoeconomic analysis

Similar to the avoidable and unavoidable irreversibility estimated with enhance exergy analysis, avoidable and unavoidable cost rates were also determined, due to both destroyed exergy and investment made on the system, using the enhanced exergoeconomic analysis. In particular, the avoidable cost rate due to destroyed exergy ($\dot{C}_D^{AV}$) was obtained for each component, as follows:

$$\dot{C}_D^{AV} = c_f \cdot \dot{E}_D^{AV} \quad (4.27)$$

In order to split the investment cost rate ($\dot{Z}$) for each component into avoidable ($\dot{Z}^{AV}$) and unavoidable ($\dot{Z}^{UN}$) parts, unavoidable investment cost per unit of product exergy $\left(\dot{Z}/\dot{E}_P\right)^{UN}$ was obtained for each component, by assuming exceedingly inefficient thermodynamic parameters for the respective components. Then, the unavoidable investment costs for the components were calculated as:

$$\dot{Z}^{UN} = \dot{E}_P \cdot \left(\dot{Z}/\dot{E}_P\right)^{UN} \quad (4.28)$$

where $\dot{E}_P$ is product exergy for the component under real thermodynamic conditions. Avoidable investment costs were obtained by subtracting unavoidable costs from the total costs in the respective components:

$$\dot{Z}^{AV} = \dot{Z} - \dot{Z}^{UN} \quad (4.29)$$

The performance of the hybrid solar-biomass ORC plant in this case was assessed using the enhanced exergoeconomic factor (f^e) and relative avoidable cost rates (R_{cr}), given by:

$$f^e = \frac{\dot{Z}^{AV}}{\dot{Z}^{AV} + \dot{C}_D^{AV}} \quad (4.30)$$

$$R_{cr} = \frac{\dot{Z}^{AV} + \dot{C}_D^{AV}}{\dot{Z} + (c_f \cdot \dot{E}_D)} \quad (4.31)$$

Based on eq. (4.20) and eq. (4.28), informed comparative analysis was made to underscore the additional importance of enhanced exergoeconomic analysis. The assumed conditions implemented for obtaining unavoidable investment cost rates in this study are highlighted in Table 4.4.

Table 4.4: Assumptions for unavoidable conditions for investment cost rates.

Solar field	$\dot{Z}^{UN} = 0.98 \cdot \dot{Z}$	Furnace heater	ΔT_{min} = 80 K
Hot tank	10% heat loss	ORC preheater	ΔT_{min} = 45 K
Cold tank	8% heat loss	Evaporator	ΔT_{min} = 50 K
Air preheater	ΔT_{min} = 200 K	Recuperator	*effectiveness* = 0.70
	Ambient properties at	Condenser	ΔT_{min} = 20 K
Combustion chamber	inlet; Exit gas	Pump	η_{is} = 0.70
	temperature = 750 K	Turbine	η_{is} = 0.70

4.3Results and Discussion

4.3.1 Conventional exergy, conventional and integrated exergoeconomic analysis

4.3.1.1 Conventional exergy analysis

The flows of exergy (kW) in different streams and components are illustrated in Figure 4.2. The values in brackets represent destroyed exergy in each component. For solar field and combustion chamber, these values include exergy losses to the environment. Figure 4.2 is self-revealing of the

components with highest and lowest destroyed exergy. For the whole system, exergetic efficiency of 7.1 % was obtained. Furthermore, for comparing dissimilar components in exergy analysis of energy systems, it is established that efficiency defect and relative irreversibility are better metrics than exergy efficiency [182,214]. Thus, Figure 4.3 shows these metrics for different components of the hybrid plant. As shown, the efficiency defect is highest in the solar field, as with relative irreversibility.

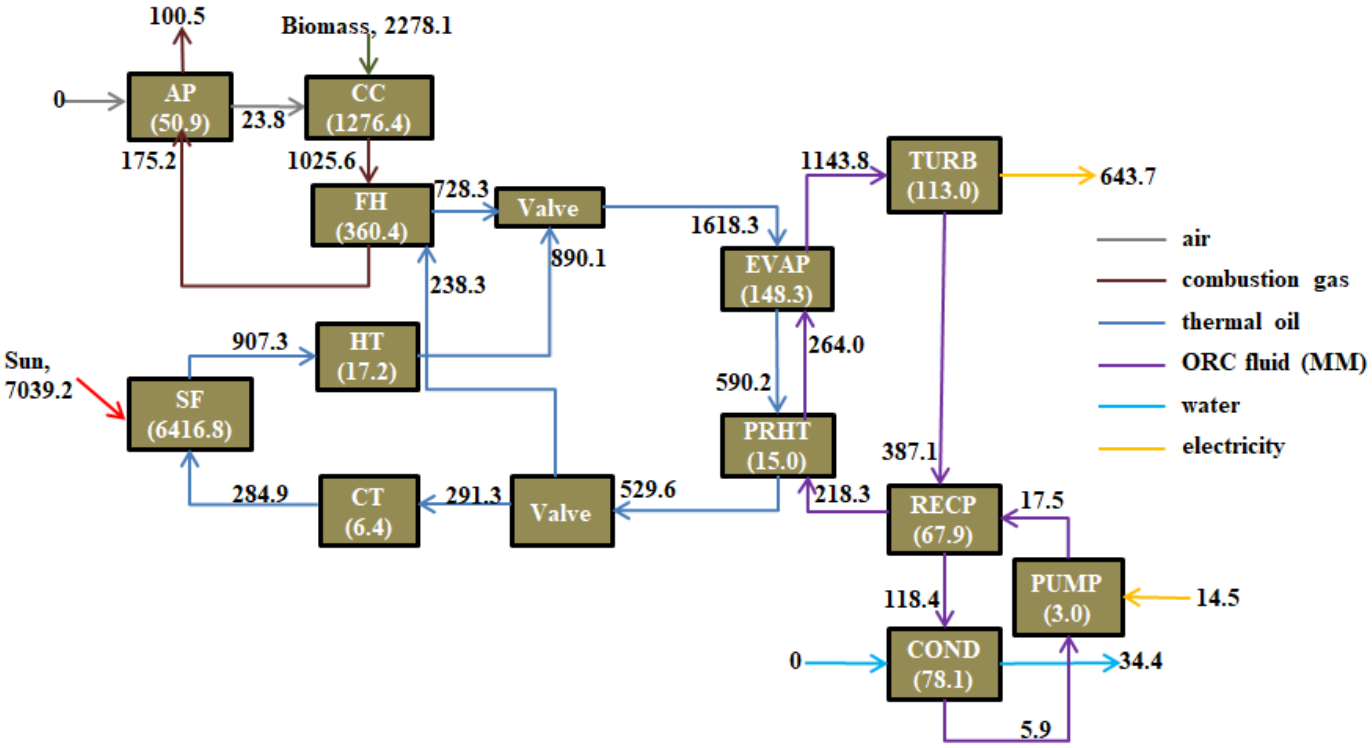

Figure 4.2: Block diagram for exergy flow in the hybrid plant (kW).

This is consequent to high loss of exergy of the sun to the environment, due to transmission and radiation processes, as well as diffusion on impinging the focused solar collectors. This suggests that it requires adequate attention for overall system improvement. This trend is however not a general rule. Although the efficiency defect in air preheater is higher than that of the combustion chamber, relative irreversibility is lower in air preheater, meaning that its absolute irreversibility is quite small, after all. A successful improvement of combustion chamber, furnace heater, evaporator,

condenser and turbine would result in better optimization of the whole system, relative to air preheater, TES tanks, ORC preheater and pump.

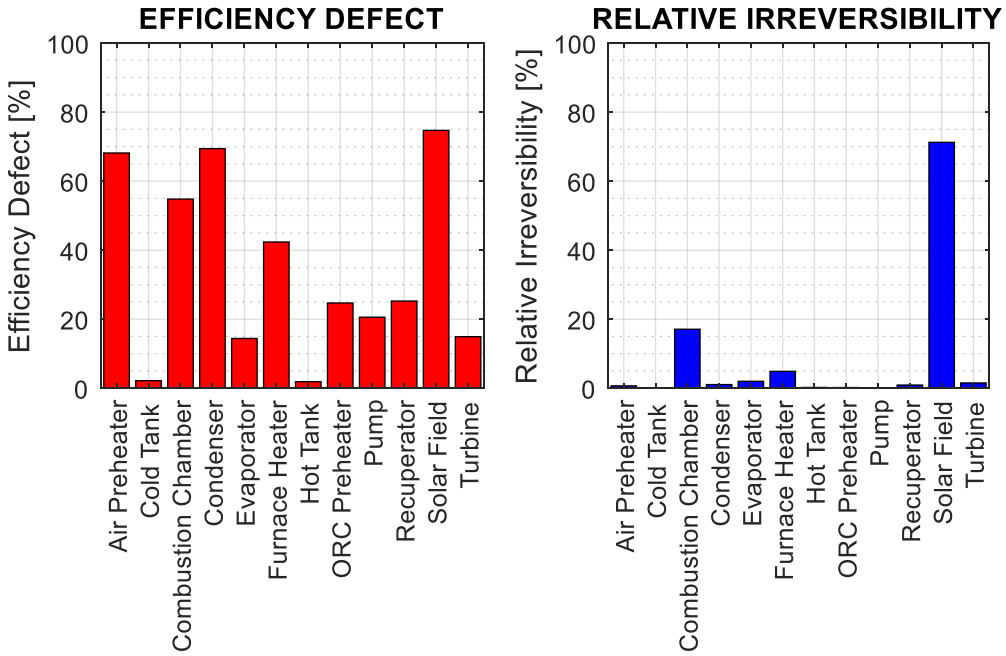

Figure 4.3: Efficiency defect and relative irreversibilities of system components.

4.3.1.2 Conventional exergoeconomic analysis

The flows of cost rate, $\dot{C}$ (€/h) in different streams and components are illustrated in Figure 4.4 for conventional exergoeconomic approach. The values in brackets are the levelized cost rate due to investment, operation and maintenance ($\dot{Z}$**)** of the respective components. Here too, the figure is self-revealing of the cost implications of purchasing and operating different components of the hybrid plant. For instance, in furnace heater, the sum of cost rates of fuel streams into the component (30.27 €/h and 13.33 €/h) and cost rate due to investment (1.69 €/h) is equal to the sum of cost rates of product streams emanating from the component (40.12 €/h and 5.17 €/h). The same analysis holds for other components. Table 4.5 shows the fuel and product costs of system components, as well as their performance based on conventional exergoeconomic approach. The total exergoeconomic cost rates are obtained for each component by the sum of cost rates of destroyed and lost exergy as well as investment and operation cost rates, reported in Table 4.5.

Exergoeconomic performance of system components is thus ranked using this sum. It is desired to be as low as possible for all components, for optimal exergoeconomic performance of the system. For components with high total cost rates, substitution with other cheaper devices with comparable exergetic performance should be considered. In this regard, system improvement requires that due attention be focused on solar field, combustion chamber, furnace heater, ORC heat exchangers, turbine, furnace heater and TES tanks, for possible replacement with cheaper components. For *f*, the values obtained for each component is a trade-off between the capital investment cost and exergetic performance of the component. High values imply that exergoeconomic cost rates is substantially due to investment costs, while low values indicate that total cost rates are due majorly to irreversibility and exergy losses. In this regard, investment costs play substantial role in exergoeconomic underperformance of solar field, TES tanks and ORC preheater. Conversely, for other components with relatively low *f* values, the significance is that large chunk of their investment costs results in losses due to thermodynamic irreversibilities, and optimization efforts should therefore be focused on improving exergetic performance. Moreover, *r* values in system components signify the relativity of unit product cost to unit fuel cost, and particular attention should be given to components with high *r* as reported in Table 4.5. One result of interest obtained in this study is the cost of producing electrical energy by the hybrid plant, which is valued at 10.50 c€/kWh. For the overall system, *f* value of 47.05 % was obtained, implying that more than half of the total investment costs result in thermodynamic losses.

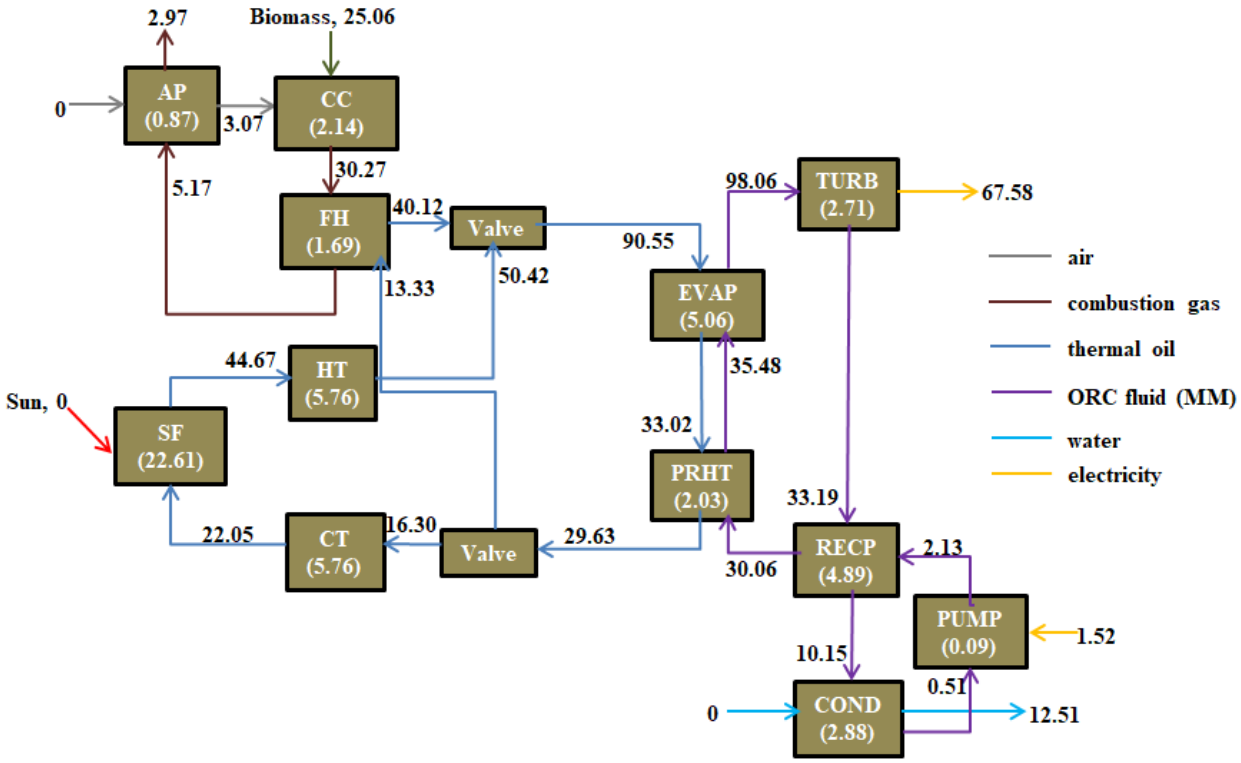

Figure 4.4: Block diagram for cost rate flow in the hybrid plant for conventional approach (€/h).

Table 4.5: Conventional exergoeconomic results for system components.

Components	c_f (€/kWh)	c_p (€/kWh)	$\dot{C}_D$ (€/h)	$\dot{C}_L$ (€/h)	$\dot{Z}$ (€/h)	$\dot{Z} + \dot{C}_D + \dot{C}_L$ (€/h)	f (%)	r (%)
Solar field	0	0.0363	0	0	22.62	22.62	100	Infinity
Hot tank	0.0492	0.0566	0.85	0	5.76	6.61	87.16	15.07
Cold tank	0.0559	0.0774	0.36	0	5.76	6.12	94.15	38.35
Air preheater	0.0295	0.1293	1.50	0	0.87	2.37	36.68	338.19
Combustion chamber	0.0122	0.0295	15.42	0.18	2.14	17.74	12.06	141.52
Furnace heater	0.0295	0.0547	10.64	0	1.69	12.33	13.70	85.24
ORC preheater	0.0559	0.1187	0.84	0	2.03	2.87	70.75	112.14
Evaporator	0.0559	0.0711	8.30	0	5.06	13.36	37.87	27.13
Recuperator	0.0857	0.1391	5.82	0	4.89	10.71	45.66	62.21
Condenser	0.0857	0.3642	6.69	0	2.88	9.57	30.05	324.82
Pump	0.1050	0.1403	0.31	0	0.094	0.40	23.03	33.67
Turbine	0.0857	0.1050	9.69	0	2.71	12.4	21.85	22.47
Valve 1	0.0559	0.0559	0	0	0	0	0	0
Valve 2	0.0559	0.0559	0	0	0	0	0	0

4.3.1.3 Integrated exergoeconomic analysis

Similar to the conventional approach, flows of cost rates in different streams and compnents are illustrated for the integrated exergoeconomic approach, as shown in Figure 4.5. This is in order to show that the cost rate balance equations are equally satisfied using the integrated approach. In addition, when juxtaposed with Figure 4.4, Figure 4.5 reveals how the cost-rate build-up process differs in each state for conventional and integrated exergoeconomic methodologies. While the cost rate values are higher in some states for conventional approach, the reverse is the case for many other states of the hybrid plant. For instance, the cost rate of organic fluid entering turbine from evaporator exit increases by about 4 % in integrated approach, relative to the conventional approach, while that entering recuperator form turbine exit decreases by about 20 %. These cost rate variations are obviously as a result of the distinction in cost allocation to each stream based on the quality of its energy content, as implemented under the integrated approach. The cumulative effects of these variations are reflected in the unit exergy costs of products, which are electricity and warm water in this study. The difference in these product costs for the two exergoeconomic approaches could be gleaned from the cost rates of electricity and water exit stream from the condenser, based on Figure 4.4 and Figure 4.5. However, for clearer illustration, unit exergy cost values for the two products have been plotted side by side for the two approaches, as shown in Figure 4.6. As can be seen, the cost of producing electricity increases from 10.50 c€/kWh in conventional approach to 12.09 c€/kWh in integrated approach, representing about 15 % increase. Conversely, if the plant would be employed for co-generation of power and warm water, the cost of producing warm water would decrease from 36.42 c€/kWh in conventional approach to 15.97 c€/kWh in integrated approach, representing about 56 % decrease. The credibility of integrated exergoeconomic approach implemented in this study is apparent in the unit cost of warm water, which is far more acceptable than what obtains following the conventional approach. Expending as much as 36 c€ to produce just 1 kWh of warm water at 35 ^{o}C doesn't seem to be economically attractive. In essence, such report as conveyed erroneously by the conventional SPECO methodology could dissuade potential

investors from committing economic resources to the kind of cogeneration plant under investigation in this study.

Furthermore, comprehensive exergoeconomic results have been computed for the integrated exergoeconomic approach, as reported in Table 4.6. Here too, juxtaposing Table 4.5 and Table 4.6 reveals the distinctions in the main exergoeconomic results based on integrated and conventional approaches. Taking f as an example, the values increase in integrated approach relative to conventional approach, for hot tank, cold tank, ORC preheater and condenser. The effect is highest in condenser, with about 30 % increase. The implication of this is that, contrary to the belief that condenser should be improved by focusing majorly on the capital cost as depicted by conventional approach, efforts should actually be made to improve its thermodynamic performance by reducing irreversibility, following the integrated approach. Conversely, with the exception of solar field whose f value is the same for the two approaches, the values decrease marginally in all other components of the hybrid cogeneration plant being studied. Moreover, f value of 48.6 % was obtained for the overall system using the integrated approach, which is more than what obtains in the conventional approach by about 1.5 percent points. This implies that the loss of investment costs is marginally lower by adopting integrated approach.

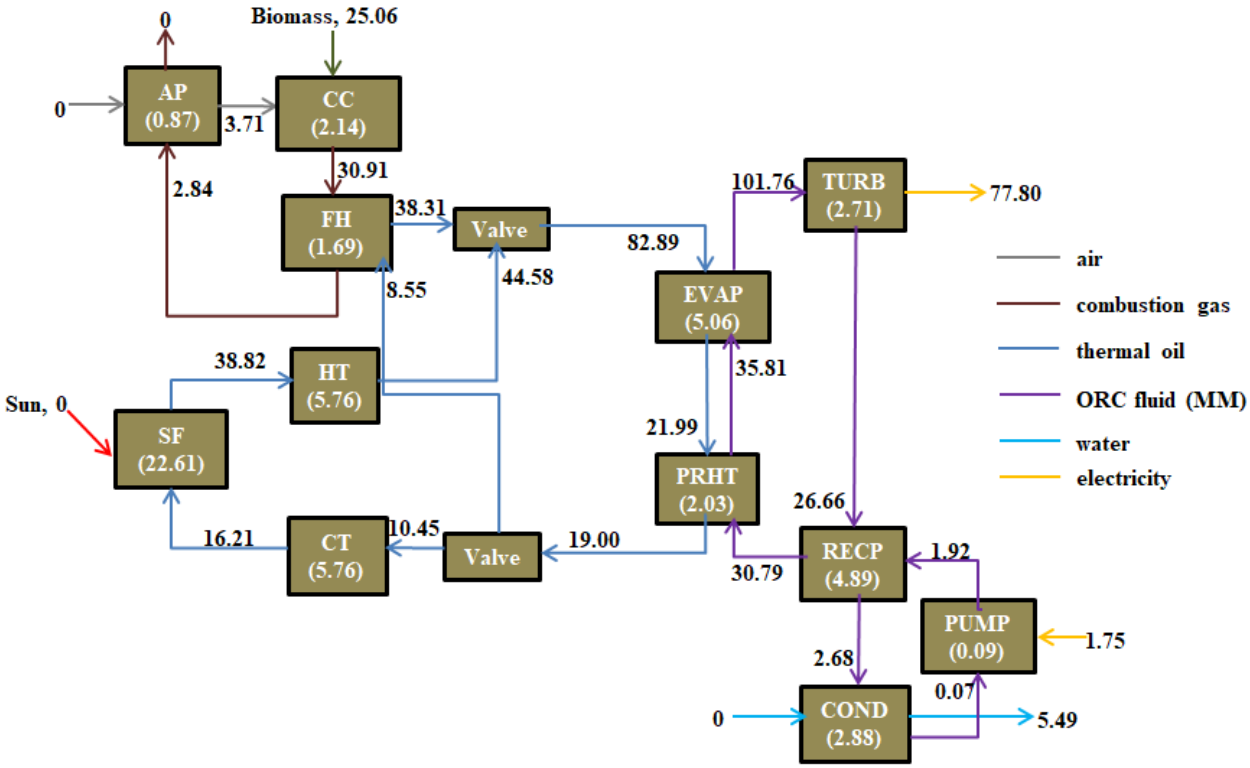

Figure 4.5: Block diagram for cost rate flow in the hybrid plant for integrated approach (€/h).

Table 4.6: Integrated exergoeconomic results for system components

Components	c_f (€/kWh)	c_p (€/kWh)	$\dot{C}_D$ (€/h)	$\dot{C}_L$ (€/h)	$\dot{Z}$ (€/h)	$\dot{Z} + \dot{C}_D + \dot{C}_L$ (€/h)	f (%)	r (%)
Solar field	0	0.0363	0	0	22.62	22.62	100	Infinity
Hot tank	0.0428	0.0501	0.74	0	5.76	6.50	88.65	17.04
Cold tank	0.0359	0.0569	0.23	0	5.76	5.99	96.17	58.54
Air preheater	0.0380	0.1561	1.94	0	0.87	2.81	31.02	310.40
Combustion chamber	0.0125	0.0301	15.77	0.18	2.14	18.09	11.82	141.14
Furnace heater	0.0330	0.0607	11.90	0	1.69	13.59	12.43	84.00
ORC preheater	0.0494	0.1100	0.74	0	2.03	2.77	73.27	122.72
Evaporator	0.0592	0.0750	8.78	0	5.06	13.84	36.55	26.56
Recuperator	0.0892	0.1437	6.06	0	4.89	10.95	44.67	61.10
Condenser	0.0232	0.1597	1.81	0	2.88	4.69	61.32	587.45
Pump	0.1209	0.1603	0.36	0	0.094	0.45	20.63	32.65
Turbine	0.0992	0.1209	11.22	0	2.71	13.93	19.45	21.80
Valve 1	0.0512	0.0512	0	0	0	0	0	0
Valve 2	0.0359	0.0559	0	0	0	0	0	0

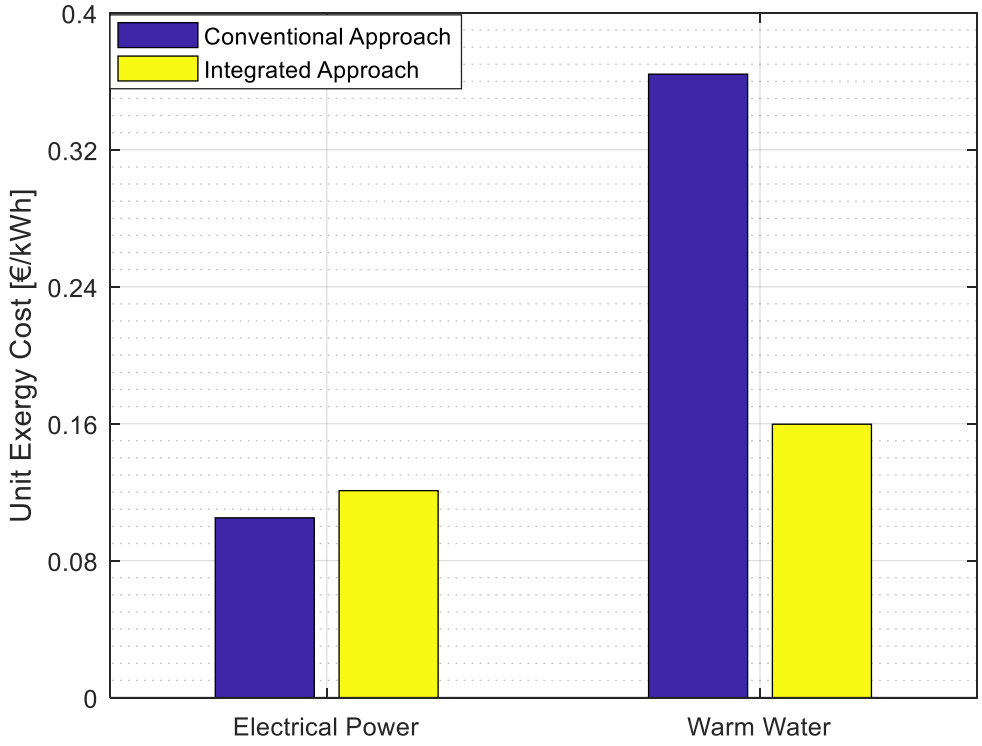

Figure 4.6: Unit exergy costs of products for conventional and integrated approaches.

Enhanced exergy analysis

Table 4.7 contains the avoidable and unavoidable parts of destroyed exergy in system components, which provide a more realistic order of importance of components for system thermodynamic improvement. For instance, results of conventional exergy analysis gave an erroneous impression that furnace heater is deserving of great optimization effort, due to its high rate of destroyed exergy. Actually, only 8.6 % of this destroyed exergy is recoverable by technical optimization. In this regard, more optimization efforts should be channeled to all ORC heat exchangers, relative to furnace heater, for improved performance of the overall system. Also, Figure 4.7 compares the exergetic efficiency under conventional and enhanced analyses. As expected, deducting the unavoidable part of destroyed exergy from fuel exergy increases efficiency slightly, for all components.

Table 4.7: Results of enhanced exergy analysis.

Components	$\dot{E}_f$(kW)	$\dot{E}_p$ (kW)	$\dot{E}_D$ (kW)	$\dot{E}_{loss}$ (kW)	$\dot{E}_D^{UN}$ (kW)	$\dot{E}_D^{AV}$ (kW)
Solar field	7039.2	622.4	5259.0	1157.8	475.41	4783.60
Hot tank	907.3	990.1	17.2	0	0	17.22
Cold tank	291.3	284.8	6.4	0	0	6.39
Air preheater	74.7	23.8	50.9	0	0.44	50.45
Combustion chamber	2301.9	1025.6	1261.8	14.6	269.52	992.24
Furnace heater	850.4	489.9	360.4	0	318.46	41.94
ORC preheater	60.6	45.6	15.0	0	0.64	14.33
Evaporator	1028.2	879.8	148.3	0	17.60	130.71
Recuperator	268.8	200.9	67.9	0	30.61	37.29
Condenser	112.4	34.4	78.1	0	19.93	58.13
Pump	14.5	11.5	3.0	0	0.56	2.42
Turbine	756.7	643.7	113.0	0	14.10	98.93

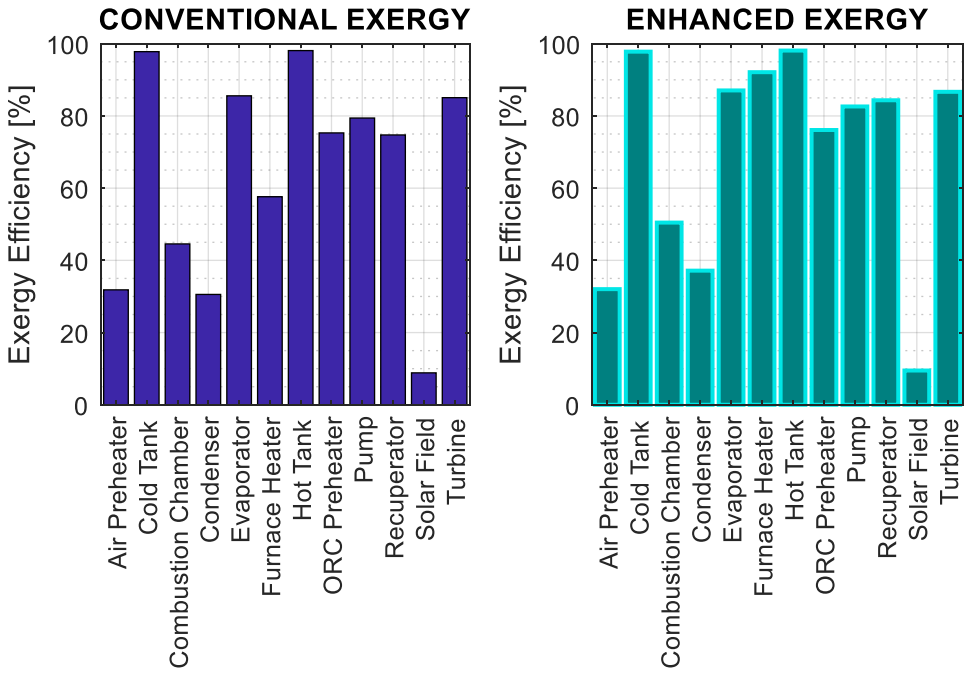

Figure 4.7: Conventional and enhanced exergy efficiencies of system components.

4.3.2 Enhanced exergoeconomic analysis

The cost rates due to destroyed exergy for enhanced exergoeconomic analyses of the hybrid plant are highlighted in Table 4.8. Also, the comparison between exergoeconomic performance of the hybrid solar-biomass ORC plant based on conventional and enhanced analyses is provided in Table 4.9. A valuable insight into the importance of enhanced exergoeconomic analysis is provided by comparing the sum ($\dot{C}_D^{AV}+\dot{Z}^{AV}$) with the sum ($\dot{C}_D+\dot{Z}$), as depicted in Table 4.9. The former (avoidable cost rates) evaluates the cost reduction opportunities in each component of the hybrid solar-biomass ORC plant. The components with high values of avoidable cost rates are more prospective to enhance economic performance of the hybrid plant, and should logically be prioritized for efforts aimed at overall system improvement. In this regard, more attention should be directed at the combustion chamber, turbine, evaporator, recuperator and condenser, amongst others. Premised on the assumptions made for enhanced exergoeconomic analysis in this study, relative avoidable cost rates obtained for the hybrid plant show that between 2 % and 69 % of total cost rates can be theoretically avoided. Furthermore, comparison of conventional and enhanced exergoeconomic factors for each component is shown in Figure 4.8. The contribution of cost of investment to total cost is shown by conventional exergoeconomic factor, for each component, while the enhanced exergoeconomic factor illustrates contribution of avoidable investment cost to total avoidable cost. Except for solar field where both values are equal to 100 % (due to zero cost of solar energy), conventional exergoeconomic factors for all the components are higher than the enhanced ones, for corresponding components. What this implies is that the actual cost improvement that could be achieved for the respective components is partly due to reduction in investment costs, but mostly due to reduction in destroyed exergy and associated costs. In particular, results of enhanced exergoeconomic analysis place emphasis on the need to reduce investment costs of solar field, thermal energy storage tanks, furnace heater recuperator and ORC preheater. Exemplarily for recuperator, conventional exergoeconomic factor shows that about 46 %

of the total costs associated with the component are due to investment expenses. However, enhanced exergoeconomic factor shows that about 27 % of the total avoidable costs associated with the recuperator are due to investment costs. Analyzing this comparison for each system component reveals the best approach to achieve cost improvement for the whole system, either by adopting cheaper components or by optimizing thermodynamic performance for lower irreversibility costs. Thus, the application of enhanced exergoeconomic analysis aids the decision on how to improve performance with more certainty, thereby providing the designer with better iterative cost minimization procedure.

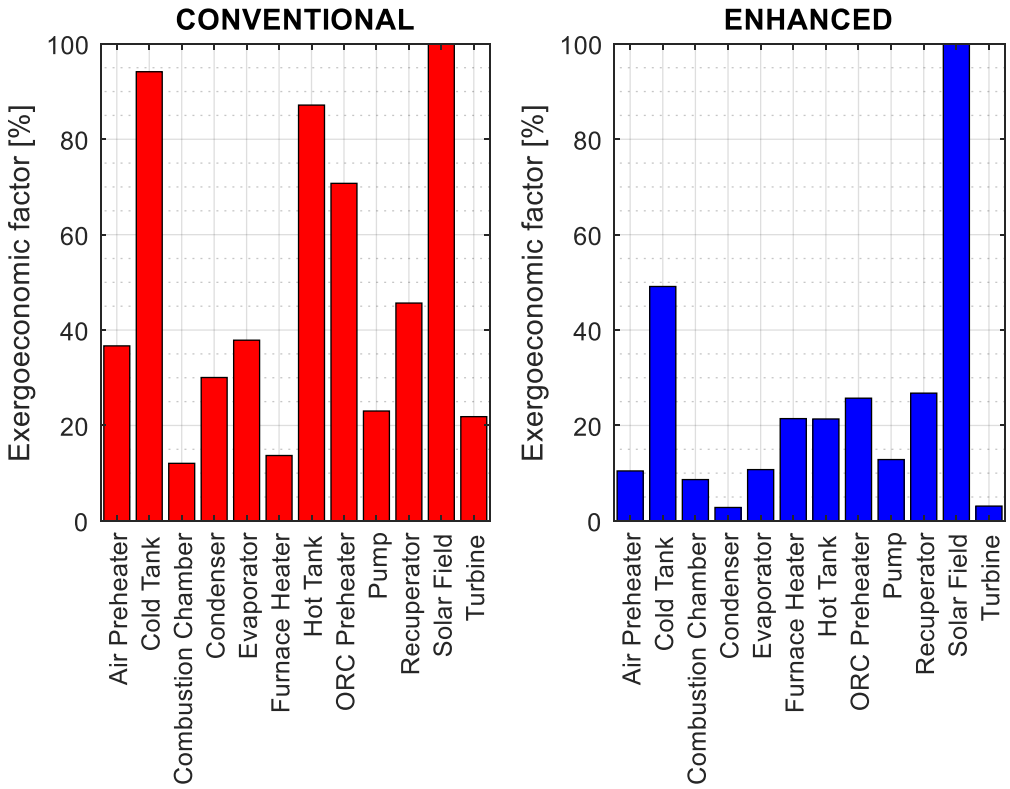

Figure 4.8: Comparison of conventional and enhanced exergoeconomic factors for the hybrid solar-biomass plant.

Table 4.8: Cost rates of destroyed exergy for enhanced exergoeconomic analyses.

Component	c_f (€/kWh)	$\dot{E}_D$ (kW)	$\dot{C}_D$ (€/h)	$\dot{E}_D^{AV}$ (kW)	$\dot{C}_D^{AV}$ (€/h)	$\dot{Z}$ (€/h)
Solar field	0	5259.0	0	4783.6	0	22.62
Hot tank	0.0492	17.2	0.85	17.2	0.85	5.76
Cold tank	0.0559	6.4	0.36	6.4	0.36	5.76
Air preheater	0.0295	50.9	1.50	50.5	1.49	0.87
Combustion chamber	0.0122	1261.8	15.42	992.2	12.13	2.14
Furnace heater	0.0295	360.4	10.64	41.9	1.24	1.69
ORC preheater	0.0559	15.0	0.84	14.3	0.80	2.03
Evaporator	0.0559	148.3	8.30	130.7	7.31	5.06
Recuperator	0.0857	67.9	5.82	37.3	3.20	4.89
Condenser	0.0857	78.1	6.69	58.1	4.98	2.88
Pump	0.1050	3.0	0.31	2.4	0.25	0.094
Turbine	0.0857	113.0	9.69	98.9	8.48	2.71

Table 4.9: Results of enhanced exergoeconomic analysis.

Component	$(\dot{Z}/\dot{E}_P)^{UN}$ (€/kW)	$\dot{Z}^{UN}$ (€/h)	$\dot{Z}^{AV}$ (€/h)	$\dot{C}_D^{AV}$ (€/h)	$\dot{C}_D^{AV}+\dot{Z}^{AV}$ (€/h)	$\dot{C}_D+\dot{Z}$ (€/h)	R_{cr} (%)
Solar field	0.0356	22.16	0.45	0	0.45	22.62	2.0
Hot tank	0.0062	5.52	0.23	0.85	1.08	6.61	16.2
Cold tank	0.0190	5.41	0.35	0.36	0.70	6.12	11.4
Air preheater	0.0293	0.70	0.17	1.49	1.66	2.37	65.0
Combustion chamber	0.0190	0.99	1.15	12.13	13.28	17.56	69.1
Furnace heater	0.0028	1.35	0.34	1.24	1.58	12.33	9.6
ORC preheater	0.0383	1.75	0.28	0.80	1.08	2.87	35.9
Evaporator	0.0047	4.18	0.88	7.31	8.19	13.36	57.5
Recuperator	0.0185	3.72	1.17	3.20	4.37	10.71	36.1
Condenser	0.0795	2.73	0.14	4.98	5.13	9.57	32.5
Pump	0.0049	0.06	0.04	0.25	0.29	0.40	67.5
Turbine	0.0038	2.44	0.27	8.48	8.75	12.40	65.9

4.3.3 Parametric study

4.3.3.1 Effects of ambient temperature on system exergetic and exergoeconomic performance

The sensitivities of system exergy and exergoeconomy to change in ambient temperature are illustrated in Figure 4.9. The solar field, air preheater and combustion chamber interact directly with the environment, and change in atmospheric conditions has cumulative effects on the entire system. As expected, increasing ambient temperature increases efficiency defects due to irreversibility in the system, thereby decreasing exergy efficiencies. The decrease in exergy efficiency is however barely significant, having a similar trend with defects due to losses. Thus, the more the insulation

achieved in the components with direct interaction with the environment, the better the system exergetic performance.

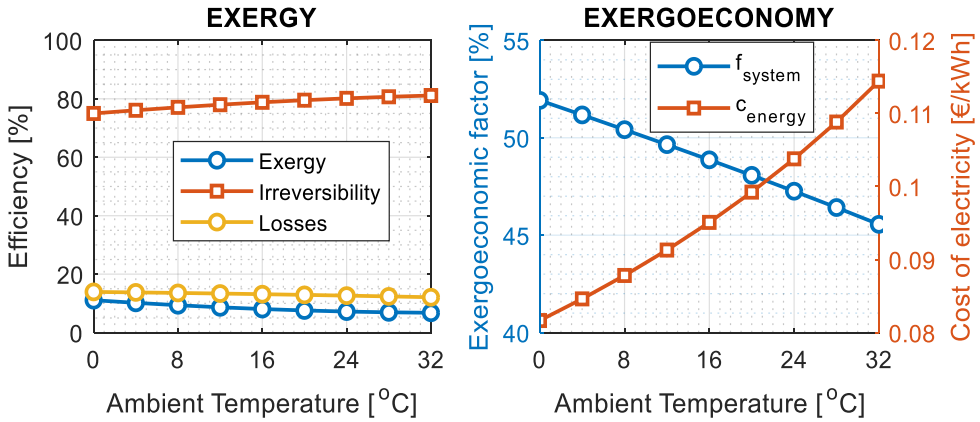

Figure 4.9: Effects of ambient temperature on system exergetic and exergoeconomic performance.

4.3.3.2 Effects of part load on system exergetic and exergoeconomic performance

Variations in turbine and pump efficiencies at off-design conditions had been estimated previously, as presented in Chapter 3. Similar procedure had been followed for off-design performance of heat exchangers. As it can be seen in Figure 4.10, operating the hybrid plant at part load reduces its exergetic performance, due to slightly higher defects of irreversibility and losses. Consequently, the cost of producing electrical energy increases dramatically with decreasing inlet gross power of the hybrid plant, while the exergoeconomic factor increases drastically, thereby keeping most of the investment cost of the system redundant.

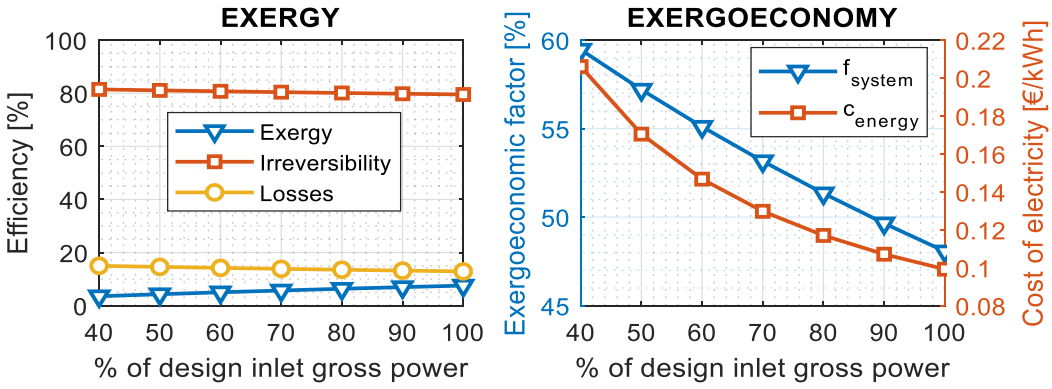

Figure 4.10: Effects of part load on system exergetic and exergoeconomic performance.

4.3.3.3 Effects of DNI on solar field and system exergetic performance

Since the solar field is directly concerned with solar irradiation, its sensitivity to change in DNI is illustrated alongside that of the system, as shown in Figure 4.11. As expected, the more the irradiation concentrated on the solar collectors, the higher the destroyed exergy in the solar field, and thus the less the exergetic efficiency. This trend holds also for the system, albeit with lower degree of sensitivity. Also, the deficiencies due to exergy losses decreases slightly in solar field, with increasing DNI, but this decrease barely has any significance on the whole system.

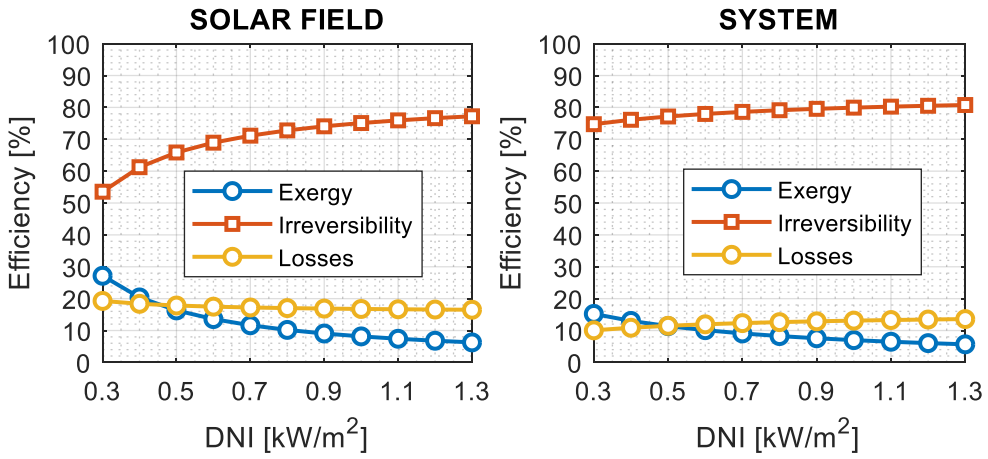

Figure 4.11: Effects of DNI on solar field and system exergetic performance.

4.4Summary

Detailed exergy-based methodologies have been employed in this chapter to assess the proposed hybrid CSP-biomass ORC plant under discussion. Classical and well-established models were implemented for conventional exergy, conventional exergoeconomic, enhanced exergy and enhanced exergoeconomic analyses of the hybrid plant. The main findings are highlighted as follows:

- Exergy flow rates were quantified for all thermodynamic states, and irreversibilities in different components were obtained and illustrated, using Sankey flow diagram. Exergetic efficiency of 7.1 % was obtained for the overall hybrid plant;

- Similarly, flows of exergy cost rates were obtained and illustrated for all thermodynamic states, including investment cost rates for the components and cost rates due to irreversibility. Overall, results showed that the fully-renewable hybrid energy system being studied is capable of producing electrical energy at the rate of between 10.50 to 12.10 euro cents per kWh, depending on the adopted exergoeconomic approach;
- The cost of producing electricity increases in integrated exergoeconomic approach by about 15 %, relative to the conventional approach. Conversely, the cost of producing warm water decreases by about 56 % in integrated approach, which portends a more reasonable analysis, if the plant would be operated for co-generation. Overall, loss of total investment cost of the hybrid plant is marginally lower by adopting integrated approach, relative to the conventional approach;
- The studied enhanced exergy and exergoeconomic analyses facilitated the decision on the best approach to apply thermodynamic and cost improvement measures to each component of the hybrid plant, and thus to the system as a whole. Results showed that relative avoidable cost rates of between 2 % and 69 % of total cost rates could be theoretically avoided. Also, it was obtained that investment costs of solar field, thermal energy storage tanks, furnace heater, recuperator and ORC preheater should be reduced, for acceptable economic performance of the hybrid plant. Efforts should be made to improve thermodynamic performance of all other components, for optimized hybrid power plant. This type of information is highly essential for improved design and quicker market penetration of fully-renewable energy plants.

Page left blank intentionally

Chapter 5
Thermo-economic Assessment of Siloxane Mixtures as ORC Working Fluid in the Proposed Hybrid Plant

5.1Preamble

The foregoing exergy and exergoeconomic analyses revealed amongst others, that efforts should be made to improve thermodynamic performance of the ORC components, for potential optimization of the hybrid plant. One method that has been identified to be adequate for this in literature is application of mixtures as ORC working fluid. In this regard, several studies have been conducted on this topic, and substantial research efforts are still ongoing, as underscored in the literature survey on this topic reported in Chapter 2. Based on the state of the art, the potential thermodynamic gains of mixture applications in ORC plants is a function of type and temperature range of the adopted heat source. For this reason, advantages of mixture applications should be investigated distinctly for different heat sources and temperature ranges. While studies are available for such investigations for medium-temperature and high-temperature solar and biomass heat sources, no study was found for hybrid solar-biomass heat sources in this respect, thereby providing a knowledge gap on this topic. Another knowledge gap on this topic concerns integration of off-design analysis for investigating techno-economic benefits of ORC working fluid mixtures. As also reported in Chapter 2, previous studies have concentrated mostly on thermodynamic and thermo-economic assessment at design conditions, regardless of type of heat source. However, for solar-based heat sources with transient characteristics, ORC plant exploiting them would work mostly at off-design conditions, and it is thus important to equally investigate potential thermo-economic benefits of applying mixtures as working fluid under these conditions. Thus, the applied methods in this study for investigating potential benefits of mixtures as ORC working fluid incorporate both

design and off-design models, which is one other major contribution of this thesis. The specific objectives of this chapter are:

- Preliminary active selection of potential working-fluid mixtures belonging to siloxane family, based on thermo-physical, transport and other properties;
- Exergy-based performance evaluation of selected mixtures relative to pure MM, for the hybrid solar-biomass ORC application;
- Evaluation of economic implications of applying the selected mixtures under design operating conditions;
- Comparison of off-design behaviours of selected mixtures and pure MM;
- Thermo-economic implications of the selected mixtures under off-design operating conditions.

The methodologies employed for these analyses are detailed in section 5.2, including: active selection of siloxane mixtures, sizing of various heat exchangers, off-design modelling for ORC components, as well as thermodynamic and economic evaluations under design and off-design conditions. Results obtained based on the highlighted methods are presented and discussed in section 5.3. Main chapter findings are summarized in section 5.4.

5.2Methodology

5.2.1 Active selection of siloxane mixtures

The criteria proposed by Miao et al. [260] were adapted for active selection of siloxane mixtures in this study. First, siloxane class of fluid was considered because it is employed in the aforementioned real solar-ORC plant, which currently uses pure MM. Then, the selection procedure implemented is termed ‘active’ because it is directed at specific and known characteristics of ORC design conditions. In their study, the authors showed that mixture compositions suitable for each application can be determined directly from thermo-physical properties of pure fluid components. This way, the burden of applying thermodynamic assessment methodologies to several fractional

compositions of different working fluid mixtures is greatly reduced. Adequate temperature match between heat source and working fluid as well as proper temperature glide in the condenser were reported to be the main factors in favour of fluid mixtures in ORC applications. Particularly, mixture compositions with condensation temperature glide equal to temperature rise of cooling medium are reportedly the most efficient ones from thermodynamic points of view. In that case, for ORC systems with known design conditions, comprehensive fluid database such as REFPROP could be used directly to predict prospective mixture compositions. In a separate study, Zhai et al. [261] equally made a similar submission, that fluid database could be used exclusively to obtain thermodynamically efficient mixtures for ORC applications. Suffice it to highlight here that these two studies compared predictions from REFPROP with analyses from simulations for several fluid compositions, including siloxane mixtures. Given the obtained agreement reported independently by the two studies, the proposed methodology based on REFPROP predictions is valid and can be applied with confidence.

Premised on the foregoing, REFPROP 10 [262] was employed for active selection of siloxane mixtures in this study. Vapour pressure, vapour-liquid equilibrium, density and other fluid properties were obtained from REFPROP based on the approach reported in [170], which had been validated by comparison with experimental data from literature for several zeotropic fluids. For each mixture composition, condensation temperature glide was obtained as difference between dew point and bubble point temperatures. Bubble point temperature (T_{bubble}) was obtained as:

$$T_{bubble} = T_{i,sk} + \Delta T_{pp,cond} \tag{5.1}$$

where $T_{i,sk}$ and $\Delta T_{pp,cond}$ represent inlet temperature of cooling medium and minimum pinch point temperature difference in the condenser, respectively. The built-in functions of REFPROP makes it possible to obtain dew point temperature as a function of pressure and mixture concentration. Considering that the temperature difference of cooling water amounts to 10 ^{o}C in this study, fluid mixture compositions with thermo-physical property-based condensation temperature glide in the

range 5-15 ^{o}C were considered for further thermo-economic analyses. In addition, the critical pressure of the selected mixtures should be greater than that of the pure fluid, and should match relatively well with the heat source temperature range.

5.2.2 Thermodynamic performance evaluation of pure fluid and fluid mixtures

Steady-state process simulations were performed for the ORC with different working fluids, using Aspen Plus V8.8 [234]. The same heat source and heat sink conditions were used for comparative analysis, which coincide with the features of the existing ORC plant as presented earlier. Also, minimum temperature difference in heat exchangers, and pump and turbine design characteristics were assumed constant, based on the real plant information. In this respect, internal cycle pressures were adapted using sequential quadratic programing (SQP) optimization subroutines embedded in Aspen Plus. For the optimization process, the objective was to maximize electrical power output, constrained by the aforementioned heat source and sink conditions, as well as design characteristics of ORC components. Effects of composition shift for working-fluid mixtures were neglected. Exergy rate balance equation was established for each ORC component based on the analysis presented in Chapter 4. The net electrical output $\dot{W}_{net}$ and exergy efficiency (ε) were employed for comparative evaluation of ORC with different working fluid compositions. The exergetic efficiency of the ORC unit was calculated here as:

$$\varepsilon = \frac{\dot{W}_{net}}{\dot{m}_i e_i - \dot{m}_o e_o}, \qquad (5.2)$$

where mass flow rate ($\dot{m}$) and exergy parameters (e) represent that of hybrid solar-biomass heat transfer fluid at inlet to and exit from the ORC, respectively.

5.2.3 Sizing of ORC heat exchangers

Shell and tube heat exchanger with counter-flow configuration was assumed, constructed from carbon steel with thermal conductivity of 51 $W/(mK)$ [172]. With the aim of obtaining turbulent flow regimes at lower velocities relative to maximal values, outer tube diameter of 19.05 mm and

wall thickness of 2.11 mm were adopted for calculations. Also, a triangular tube pitch was assumed, with pitch to diameter ratio of 1.25. Heat exchanger with one-pass shell (TEMA type E) was considered. Single segmental baffle types with horizontal cut orientation were considered for modelling. For all heat exchangers, it was assumed that organic working fluid flows inside the tube, while the heat source transfer fluid and cooling medium are led in the shell side. These assumptions were applied in the Log Mean Temperature Difference (LMTD) method of heat exchanger design. In order to obtain overall heat transfer coefficient, different heat transfer correlations were implemented. The correlations depend on composition and phase state of heat transfer fluid, and they provided local heat transfer coefficients in each exchanger side. For single phase flows, the Dittus-Boelter Nusselt number (Nu) correlation was considered, given by:

$$Nu = 0.023 Re^{0.8} \cdot Pr^{n} \tag{5.3}$$

where Re is the Reynolds number, Pr is the Prandtl number and *n* is an index, taken as 0.3 for fluids undergoing cooling process and 0.4 for heating process [7]. For evaporation of pure working fluids in a plain tube, the correlation for flow boiling applied in [171,263] was adopted for the calculation of the convective heat transfer coefficient (α):

$$\frac{\alpha(z)}{\alpha_l} = \left\{ (1-x)^{0.01} \cdot \left[(1-x)^{1.5} + 1.9 \cdot x^{0.4} \cdot \frac{{\rho_l}^{0.37}}{\rho_g} \right]^{-2.2} + x^{0.01} \cdot \left[\frac{\alpha_g}{\alpha_l} \cdot \left(1 + 8 \cdot (1-x)^{0.7} \cdot \frac{{\rho_l}^{0.67}}{\rho_g} \right) \right]^{-2} \right\}^{0.5} \tag{5.4}$$

where ρ and x are density and vapour quality, respectively, and subscripts l and g stand for liquid phase and gaseous phase, respectively. Corresponding heat transfer coefficients α_l and α_g were obtained from eq. (5.3). For evaporation of fluid mixtures, reduction in heat transfer was accounted using the model of Schlünder [264]:

$$\frac{\alpha_{id}}{\alpha} = 1 + \frac{\alpha_{id}}{\dot{q}} \cdot (T_{s2} - T_{s1}) \cdot (y_1 - x_1) \cdot \left(1 - exp\left(-B_0 \cdot \frac{\dot{q}}{\rho_l \cdot \beta \cdot \Delta h_{fg}} \right) \right) \tag{5.5}$$

where β and B_0 are experimentally fitted constants, taken here as $\beta = 2 \times 10^{-4}\ m/s$ and $B_0 = 1$. T_i is the saturation temperature of mixture component, while x_i and y_i are mole fractions of liquid and gaseous phase of component *i*.

The correlation proposed by Shah [265] was implemented to obtain local heat transfer coefficient of working fluid in condenser, as follows:

$$Nu = 0.023 {Re_l}^{0.8} \cdot {Pr_l}^{0.4} \cdot \left[(1-x)^{0.8} + \frac{3.8 \cdot x^{0.76} \cdot (1-x)^{0.04}}{p^{*0.38}}\right] \quad (5.6)$$

where p^* corresponds to the ratio of process pressure to critical pressure. Similar to what obtains in evaporation process, reduction in heat transfer as a result of additional mass transfer for zeotropic mixtures was accounted, using the method of Silver [266] as well as Bell and Ghaly [267]:

$$\frac{1}{\alpha_{eff}} = \frac{1}{\alpha(x)} + \frac{L_g}{\alpha_g} \quad (5.7)$$

where α_{eff} represents the effective local heat transfer coefficient of fluid mixture and $\alpha(x)$ is obtained from eq. (5.6) using the properties of fluid mixture. The gaseous phase heat transfer coefficient (α_g) and ratio between the sensible and latent part of the condensation of fluid mixture (L_g) were obtained as follows:

$$Nu = 0.023 {Re_g}^{0.8} \cdot {Pr_g}^{0.4} \quad (5.8)$$

$$L_g = x \cdot c_{p,g} \cdot \frac{T_{G,Cond}}{\Delta h} \quad (5.9)$$

where $c_{p,g}$ is the heat capacity at gaseous phase, $T_{G,Cond}$ is temperature glide at condensation, and Δh is the corresponding enthalpy difference. As factor of safety, local heat transfer coefficients of shell sides were reduced by combined correction factors according to Bell-Delaware method, taken as 0.65. Then, the overall heat transfer coefficient was obtained for each heat exchanger, using the local heat transfer coefficients of shell and tube sides, as well as thermophysical and geometric properties.

5.2.4 Economic analysis

Comparative economic performance of pure fluid and siloxane mixtures for ORC design was assessed, using energy and exergy-based cost analysis. For exergoeconomy, the specific exergy costing (SPECO) approach [187] was also adopted here, based on the methodology presented earlier in Chapter 4. Since the conditions of hybrid solar-biomass heat source are the same for all cases of ORC working fluids considered, a uniform value of *c* (taken equal to 0.0532 €/kWh, based on the results obtained in Chapter 4) was adopted for analysis here. This cost factor is obtained with the assumption that ORC works at nominal condition, with biomass satisfying 40% of its thermal input requirement. However, improved economic models were implemented in this Chapter, for reliable thermo-economic assessment of potential benefits of mixtures. In particular, the logarithmic correlations of purchased equipment costs (PEC) presented by Sieder *et al*. [268] were adopted for obtaining base cost (Z_B) for ORC components for different working fluids, based on year 2006 data, as follows:

$$\mathrm{Z}_B = (\mathrm{F})\exp\{K_0 + K_1[In\ S] + K_2[In\ S]^2\} \tag{5.10}$$

where *S* is component size factors, while F and K are cost coefficients, highlighted in Table 5.1. For pump, actual Z_B value includes base cost for pump motor (Z_{pm}), obtained as follows:

$$\mathrm{Z}_{pm} = \exp\left\{5.83 + 0.134\left[In\ \dot{W}_{pump}\right] + 0.0533\left[In\ \dot{W}_{pump}\right]^2 + 0.0286\left[In\ \dot{W}_{pump}\right]^3 - 0.00355\left[In\ \dot{W}_{pump}\right]^4\right\} \tag{5.11}$$

where $\dot{W}_{pump}$ is pump consumption expressed in horse power (*hp*) units. The base cost values obtained with eq. (5.10) were adjusted to obtain actual purchase cost (Z) based on current realities, as follows:

$$Z = \mathrm{Z}_B \cdot \frac{I}{I_B}, \tag{5.12}$$

where I and I_B are Chemical Engineering Plant Cost Indices (CEPCI) for 2018 and 2006, given as 603.1 and 500, respectively.

Table 5.1: Cost coefficients for ORC components used in eq. (5.10).

Component	S	F	K_0	K_1	K_2
Preheater/Recuperator	A (m^2)	1.0	10.106	-0.4429	0.0901
Evaporator/Condenser	A (m^2)	1.0	9.5638	0.5320	-0.0002
Turbine	$\dot{W}_{turbine}$(kW)	1.0	6.5106	0.8100	0.0000
Pump	$\dot{V}\sqrt{H}\ \left(m^3 \cdot s^{-1} \cdot m^{1/2}\right)$	2.7	9.0073	0.4636	0.0519

Then, energy-based specific investment costs (SIC), specific exergy costs, net costs of ORC production and exergoeconomic factors (*f*) were adopted for economic comparison of different working-fluid compositions. Specific exergy cost was obtained directly from cost rate balance equations, at turbine production stream. For net costs of ORC production, costs due to exergy loss in the ORC were charged to turbine, and average specific exergy costs of power production was re-calculated. Energy-based SIC and *f* were obtained as follows:

$$\text{SIC} = \frac{Z_{ORC}}{\dot{W}_{net}}, \tag{5.13}$$

$$f = \frac{\dot{Z}}{\dot{Z}+(c_f \cdot \dot{I})} \tag{5.14}$$

where Z_{ORC} represents total costs of investment of ORC (summation of all components), $\dot{W}_{net}$ is net ORC power production and c_f is cost per unit of fuel exergy (ratio of cost rate of fuel to fuel exergy, €/kWh). This is with the assumption that all ORC components are thermally insulated to the environment.

5.2.5 Off-design models

The ORC off-design model proposed by Manente *et al*. [237] was equally used here for heat exchanger analysis, while the model of Ghasemi *et al*. [239] and real plant efficiency curve were implemented for off-design analysis of turbine and pump, respectively. The details of these models have been presented earlier in Chapter 3 and are therefore not repeated here. Also, the validity of

the models had been ascertained by comparing simulation results with operational data obtained from the real ORC plant currently running at Ottana, as reported in Chapter 3.

5.2.6 Annual performance analysis

Similar to what was presented for annual analysis in Chapter 3, annual net electricity production from ORC was simulated for each of the working fluids being evaluated in this chapter, following the aforementioned approach. Furthermore, yearly economic performance was assessed for each ORC working fluid, using levelized cost of electricity (LCOE), net present value (NPV) and specific payback period (SPB) as evaluation criteria, which have also been presented earlier in Chapter 3.

5.3 Results and Discussion

5.3.1 Active selection of siloxane mixtures

Variations of condensation temperature glides of siloxane mixtures with mass fraction of MM are presented in Figure 5.1, as obtained from REFPROP database. As shown, only MM/MDM mixtures have condensation temperature glides within the range 5-15 ^{o}C. In particular, mixtures with 0.1MM/0.9MDM, 0.8MM/0.2MDM and 0.9MM/0.1MDM fall within this range. Also, their critical pressure values are greater than those of pure fluids, which are given as 9.61 bar, 10.93 bar, 11.44 bar, 13.47 bar, 14.38 bar, and 19.31 bar for MD3M, D5, MD2M, D4, MDM and MM, respectively. Moreover, they match quite well with temperature range considered for heat source. Thus, these mixture compositions satisfy the pre-set active selection criteria, and they were adopted for detailed thermo-economic analyses in this study, in comparison with performance of pure MM.

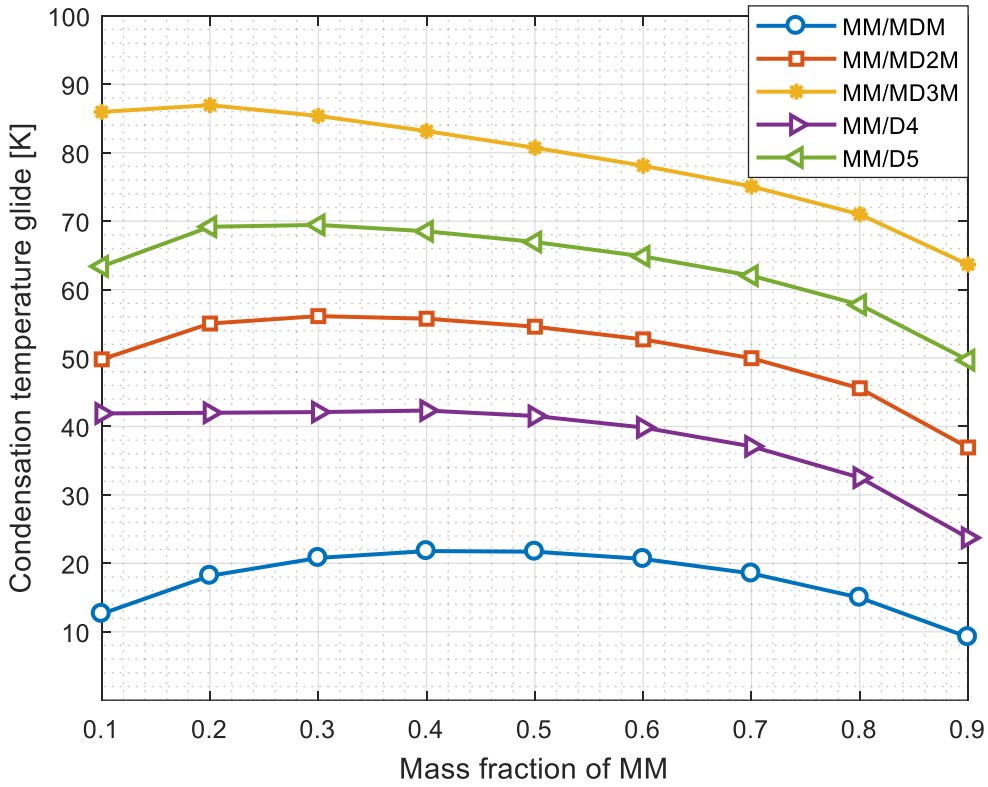

Figure 5.1: Condensation temperature glide of siloxane mixtures.

5.3.2 Thermodynamic performance of selected mixtures relative to pure fluid

In order to assess thermodynamic benefits of using the selected siloxane mixtures relative to pure MM, net power and exergetic efficiencies of the ORC plant were determined for each fluid composition. When using pure MM as ORC working fluid, net power of 629 kW was obtained. For the considered mixture compositions, net ORC power of 621 kW, 638 kW and 641 kW were obtained for 0.1MM/0.9MDM, 0.8MM/0.2MDM and 0.9MM/0.1MDM, respectively. A similar trend was observed for exergetic efficiency of the ORC (ε). For pure MM, it results equal to about 54.1 %. In the case of the selected mixture compositions, results showed that the exergetic efficiency decreases by about 0.8 percent points for 0.1MM/0.9MDM, while it increases by about 0.8 and 1 percent points for 0.8MM/0.2MDM and 0.9MM/0.1MDM, respectively. The optimized cycle design parameters for the selected fluids are highlighted in

Table 5.2.

Table 5.2: Optimized design parameters for selected ORC working fluids.

	MM	0.1MM/0.9MDM	0.8MM/0.2MDM	0.9MM/0.1MDM
Working fluid mass flow rate (kg/s)	9.3	10.6	9.5	9.4
Maximum cycle pressure (bar)	10.0	3.0	7.7	8.8
Maximum working fluid temperature (^{o}C)	204.5	194.4	202.5	203.5

Furthermore, flow of exergy in different streams and components of the ORC are shown in Figure 5.2 to Figure 5.5, for pure MM, 0.1MM/0.9MDM, 0.8MM/0.2MDM and 0.9MM/0.1MDM, respectively. In these figures, the values in bracket in respective labelled components represent destroyed exergy in the components, as done earlier. The essence is to allow objective comparison of thermodynamic performance in different streams and components of the ORC, for the pure and mixture fluid cases considered. Exemplarily, the figures show that exergy of the ORC fluid at turbine entry is higher for pure MM than for all mixture compositions considered. Thus, higher ORC net power obtained for mixtures is due mainly to the internal operations of the ORC, particularly the volumetric expansion capability of the turbine. In addition, it can be observed from the figures that destroyed exergy is reduced in the condenser, preheater and pump for all mixtures, relative to the pure fluid. Conversely, adopting fluid mixture increases destroyed exergy for recuperator and evaporator. Again for turbine, the optimized pressure and molecular weight of mixture compositions are key factors that influence exergy destruction rate, and no common trend is observed. By summing destroyed exergy values in each component, results showed that adopting 0.1MM/0.9MDM increases destroyed exergy in the ORC unit by 9 kW, relative to pure MM.

Conversely, the use of 0.8MM/0.2MDM and 0.9MM/0.1MDM reduce ORC destroyed exergy by 17.7 kW and 19.8 kW respectively, relative to pure MM. This trend is consistent with the net power and exergy efficiency obtained for different fluid cases. Clearly, these results show that adopting fluid mixtures in ORC for hybrid solar-biomass application could marginally improve thermodynamic performance of the plant.

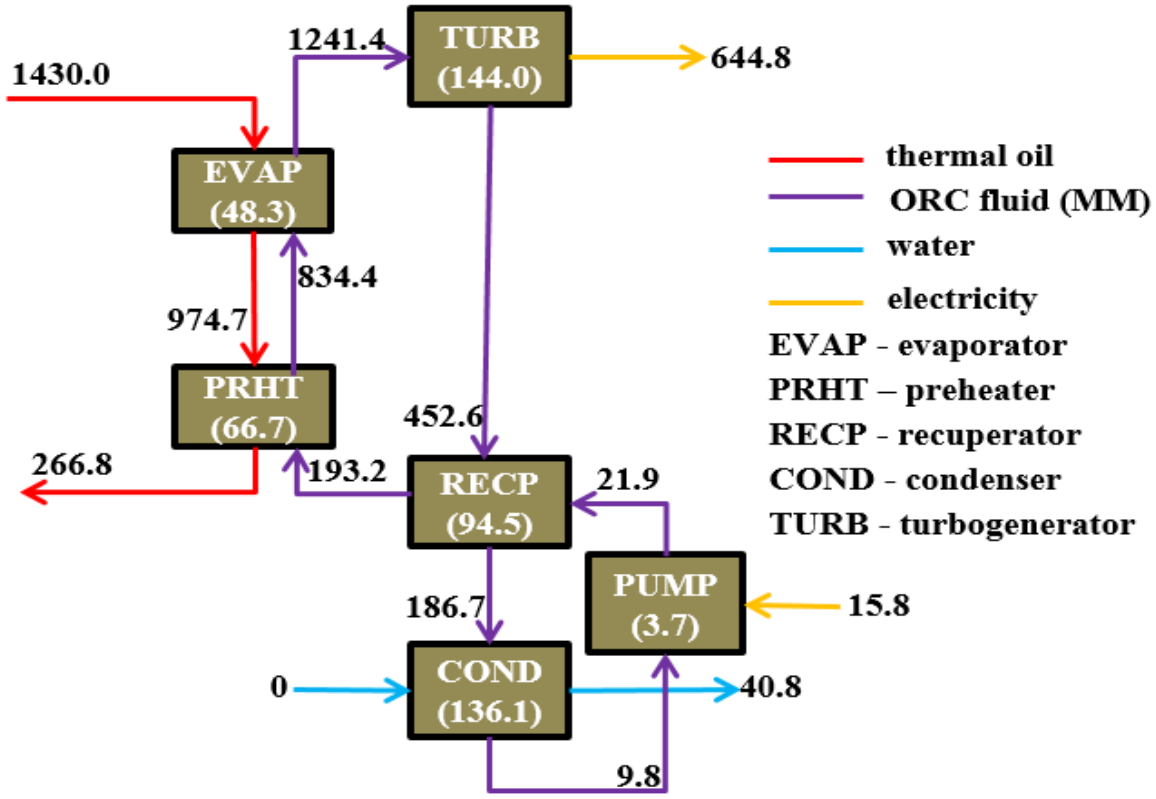

Figure 5.2: Block diagram for exergy flow in the ORC using MM (kW).

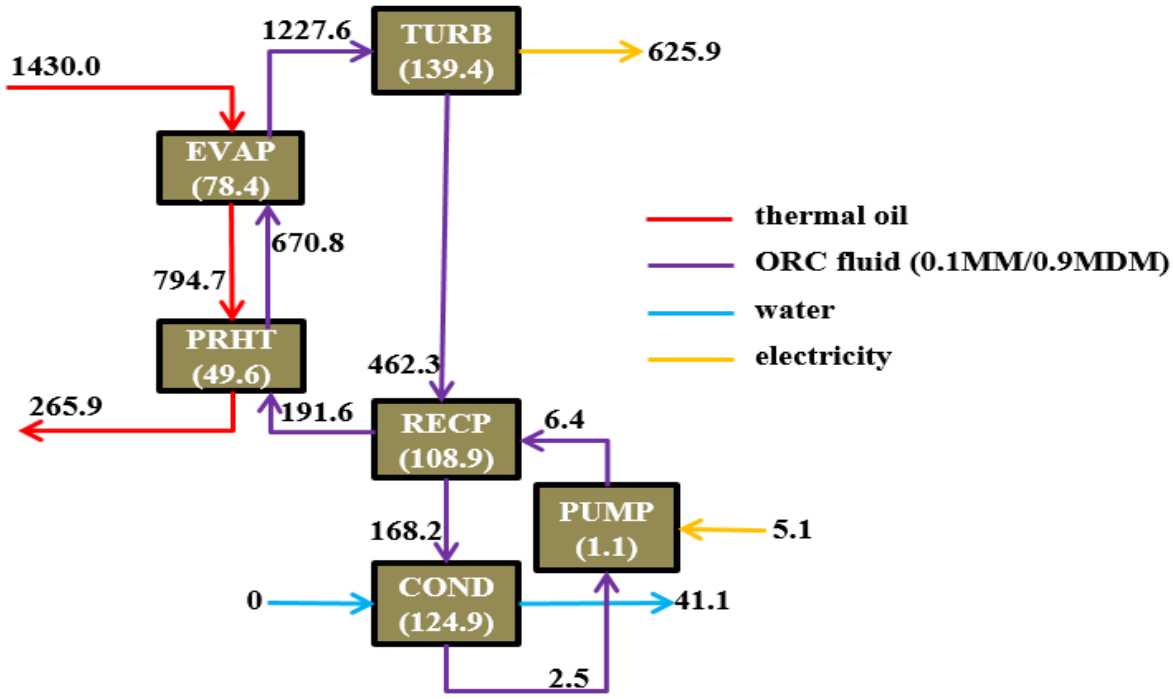

Figure 5.3: Block diagram for exergy flow in the ORC using 0.1MM/0.9MDM (kW).

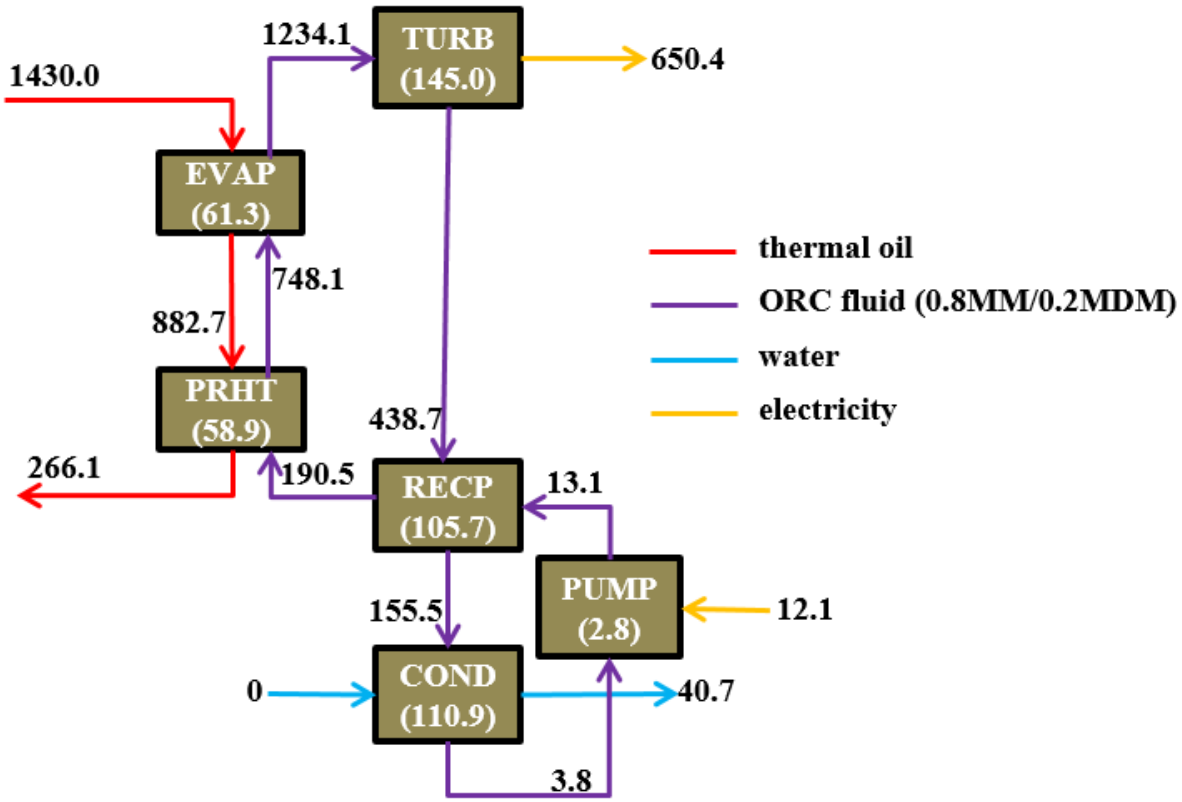

Figure 5.4: Block diagram for exergy flow in the ORC using 0.8MM/0.2MDM (kW).

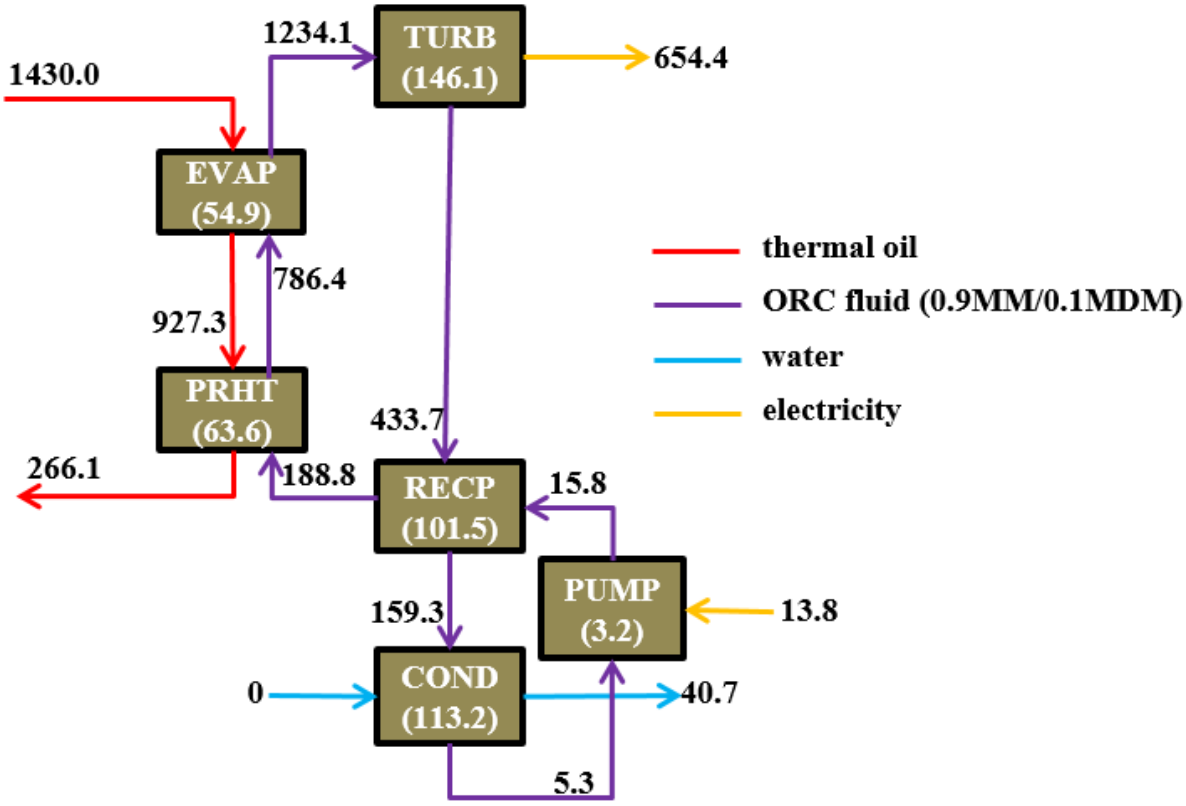

Figure 5.5: Block diagram for exergy flow in the ORC using 0.9MM/0.1MDM (kW).

5.3.3 Effects of mixture working fluid on ORC heat exchange surface

By adopting fluid mixtures in ORC plants, the heat transfer coefficients are reduced in heat exchangers, especially during phase change processes. Consequently, there are significant effects on the heat exchange surface required to achieve set thermodynamic objective. In this regard, the heat exchanger surface area, logarithmic mean temperature difference and heat transfer rate have been quantified for all ORC heat exchangers in this study, as presented in Table 5.3. As it can be observed, a similar trend is obtained for heat exchange surface in condenser and evaporator, where required surface areas for mixtures are higher than those of pure fluid. For heat exchangers with single-phase heat transfer processes, no common trend is observed. In particular, adopting fluid mixtures decreases surface areas in preheater, relative to pure fluid. In the case of recuperator, it is interesting to observe that heat exchange surface reduces for the most thermodynamically efficient mixture (0.9MM/0.1MDM), relative to pure MM, while the contrary is the case for other mixture

compositions. In addition, it can be seen that total heat exchange area increases for all mixture ORC considered, relative to pure MM. In particular, total ORC heat transfer area increases by 18.5 %, 21.3 % and 17.3 % for 0.1MM/0.9MDM, 0.8MM/0.2MDM and 0.9MM/0.1MDM respectively, relative to pure MM. Again, the increase in total surface area is lowest in the most thermodynamically efficient mixture. Moreover, increase in condenser surface for mixture fluids contribute the most to increase in total heat exchange surface areas, obviously due to reduced values obtained for log mean temperature difference.

Clearly, the increase in heat exchange surface area by using mixtures as ORC working fluid would have negative effects on economic performance of the system, and this necessitates the comparative study from economic perspective.

Table 5.3: Effects of mixture on heat transfer surface.

	MM	0.1MM/0.9MDM	0.8MM/0.2MDM	0.9MM/0.1MDM
A_{PRHT} (m^2)	293.1	242.1	266.8	280.0
$\Delta T_{log,PRHT}$ (^oC)	43.3	43.2	43.5	43.6
$\dot{Q}_{PRHT}$ (kW)	2091	1627	1858	1973
A_{EVAP} (m^2)	79.9	151.5	101.4	90.4
$\Delta T_{log,EVAP}$ (^oC)	50.7	54.2	52.0	51.4
$\dot{Q}_{EVAP}$ (kW)	1083	1550	1318	1203
A_{RECP} (m^2)	74.7	80.3	76.0	73.5
$\Delta T_{log,RECP}$ (^oC)	36.9	36.7	37.2	37.1
$\dot{Q}_{RECP}$ (kW)	1161	1324	1269	1224
A_{COND} (m^2)	833.6	1044.2	1109.5	1058.7
$\Delta T_{log,COND}$ (^oC)	16.6	15.7	13.6	13.8
$\dot{Q}_{COND}$ (kW)	2488	2502	2481	2479
A_{total} (m^2)	1281.3	1518.1	1553.7	1502.6

5.3.4 Economic performance of selected mixtures relative to pure fluid

As aforementioned, energy and exergy-based economic assessments were employed for comparative performance evaluation of the different fluid compositions studied. Here, results of

economic performance at design conditions are presented, using mainly exergoeconomic criteria. Flows of exergy cost rates in different streams of the ORC power plant are presented in Figure 5.6 – Figure 5.9, for pure MM and all the selected mixture compositions. Again, the values in brackets inside components are the investment and maintenance cost rates for the respective components. As illustrated in the exergoeconomic cost balance equations, adding the investment and maintenance cost rates to cost rates of streams entering the respective components (fuel) should be equal to the sum of cost rates of streams leaving the components (products). For instance, for evaporator in Figure 5.6, (76.07-14.20) + 2.67 = (86.36 – 59.47). As it would be expected consequent to increase in heat transfer surface for mixture ORC, cost rates due to investment and maintenance increase for condenser and evaporator, for all mixture compositions. For all other components, the change in cost rates due to investment and maintenance are barely distinguishable between pure fluid and mixtures. The specific exergy costs of producing power is obtainable for each fluid case, by the ratio of cost rates of electricity production by the turbine, to turbine power production represented in Figure 5.2 – Figure 5.5. For clearer representation of economic comparisons of the studied fluid, energy-based specific investment costs, specific exergy costs, net costs of ORC production and exergoeconomic factors for respective components are shown in Table 5.4. Results show that energy-based specific investment cost of ORC unit increases by 15 %, 10.3 % and 7.3 % for 0.1MM/0.9MDM, 0.8MM/0.2MDM and 0.9MM/0.1MDM respectively, relative to pure MM. Similarly, specific exergy costs of power production increases by 3.7 %, 1.9 % and 1 % for 0.1MM/0.9MDM, 0.8MM/0.2MDM and 0.9MM/0.1MDM respectively, relative to pure MM.

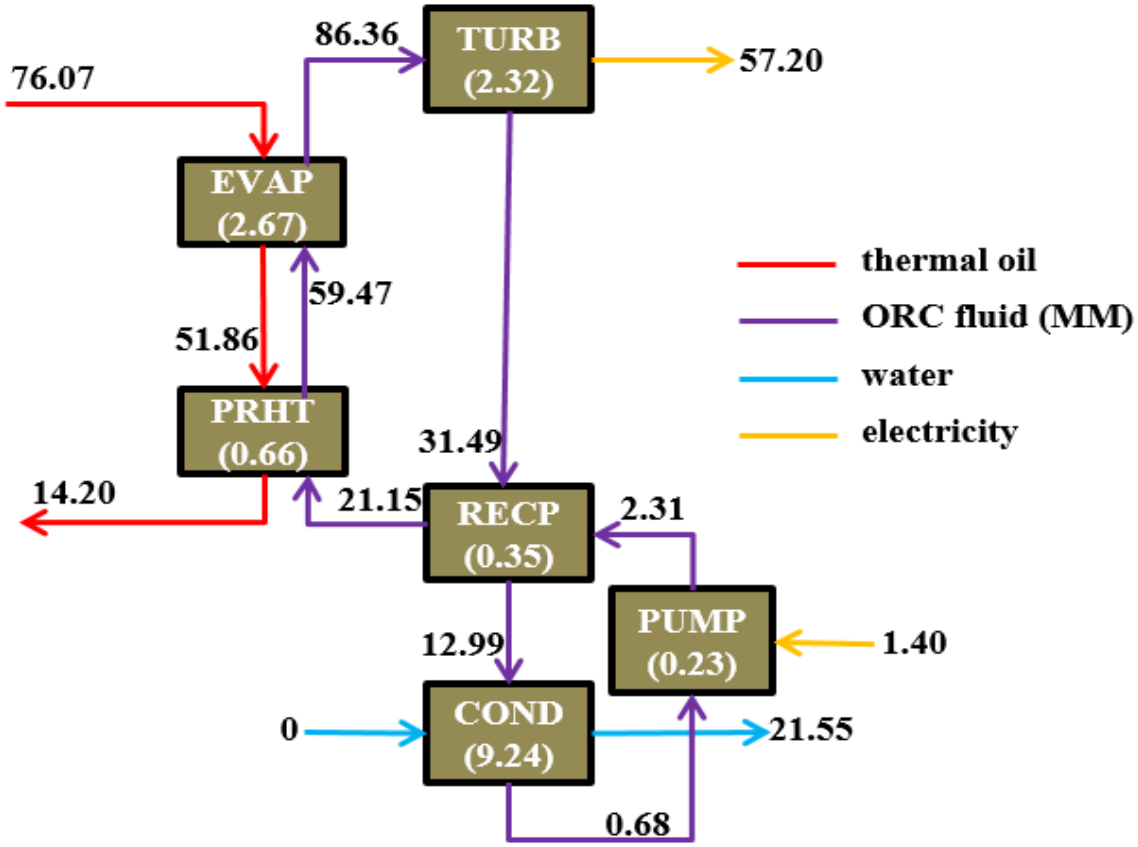

Figure 5.6: Block diagram for cost rate flow in the ORC using MM (€/h).

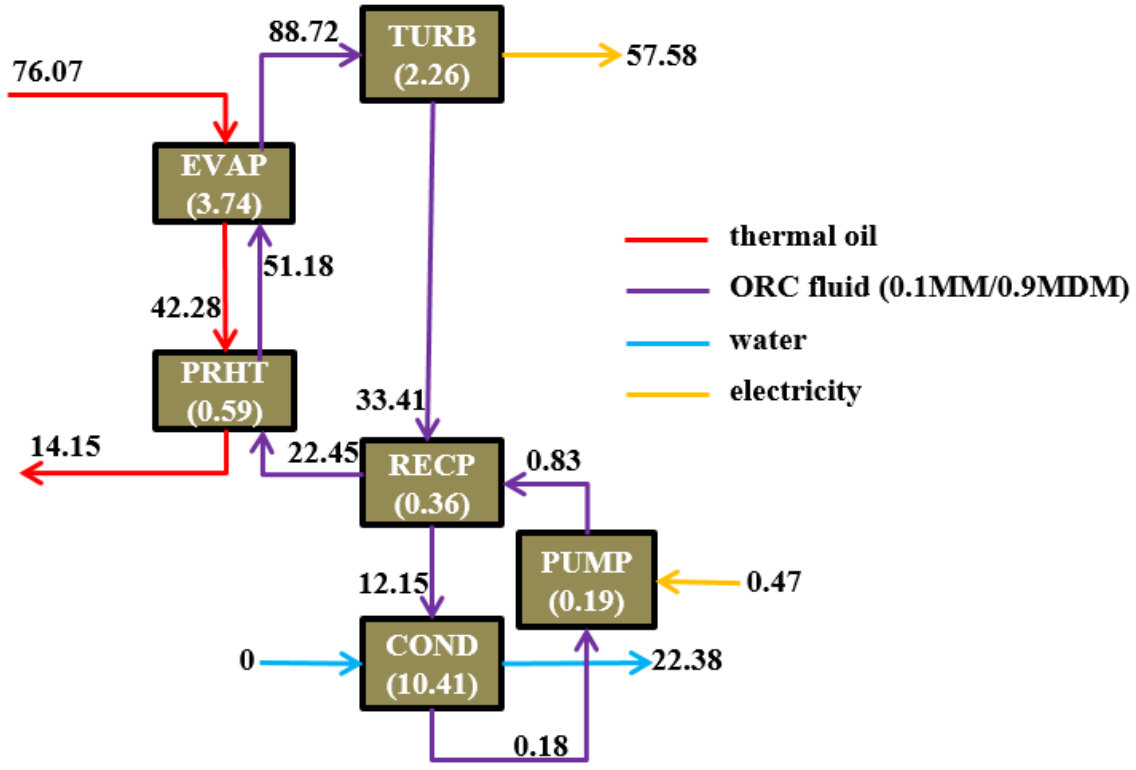

Figure 5.7: Block diagram for cost rate flow in the ORC using 0.1MM/0.9MDM (€/h).

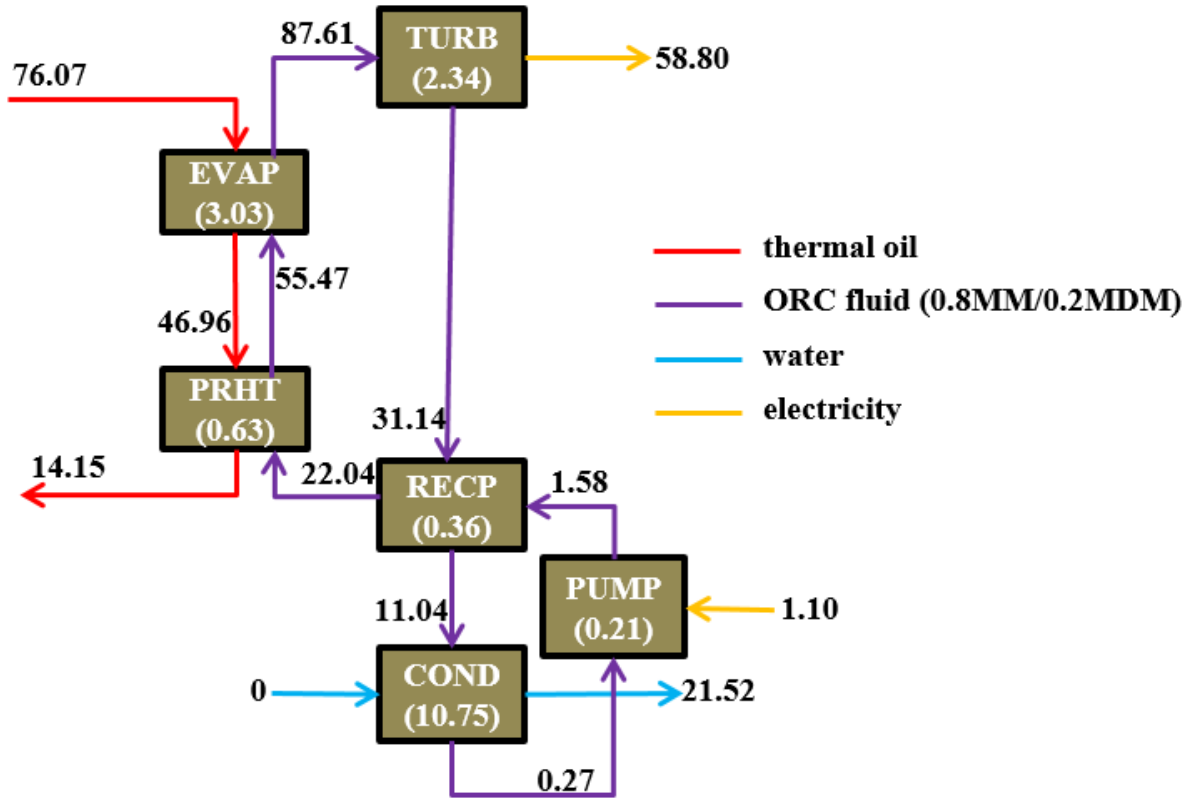

Figure 5.8: Block diagram for cost rate flow in the ORC using 0.8MM/0.2MDM (€/h).

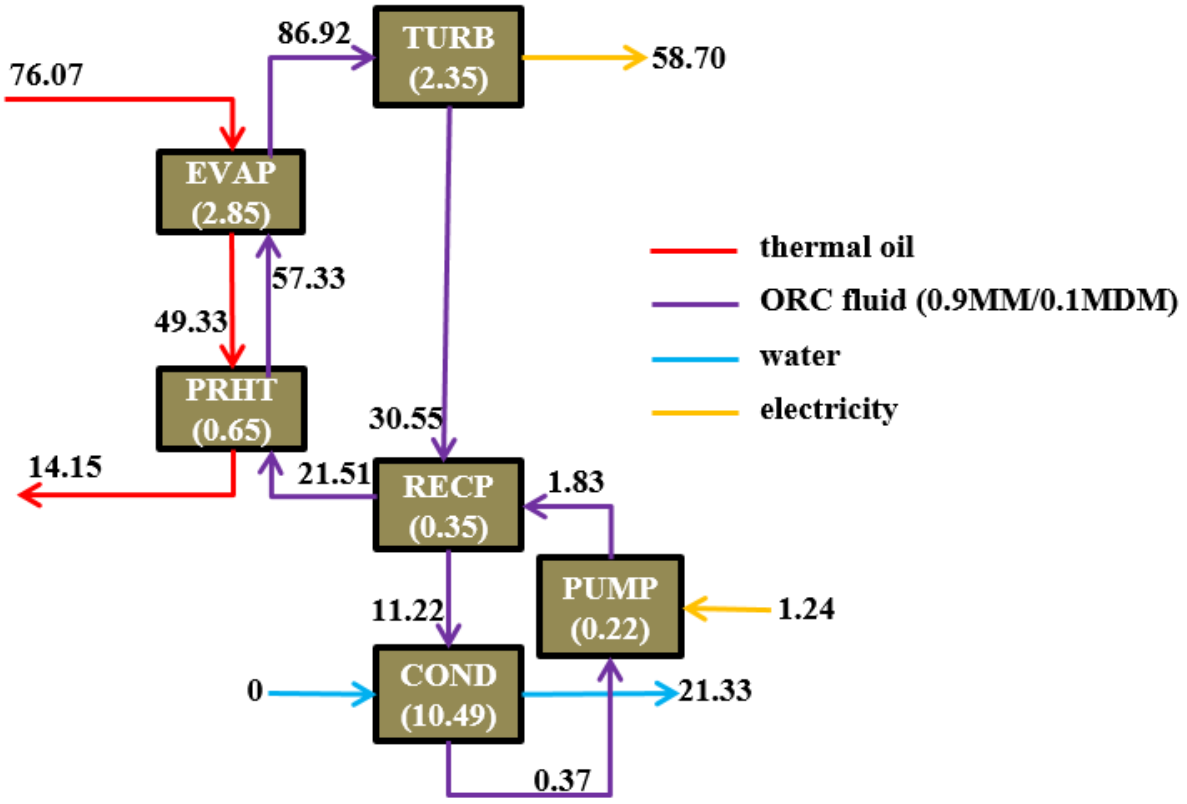

Figure 5.9: Block diagram for cost rate flow in the ORC using 0.9MM/0.1MDM (€/h).

Table 5.4: Specific investment cost and exergoeconomic results.

Parameter	MM	0.1MM/0.9MDM	0.8MM/0.2MDM	0.9MM/0.1MDM
SIC_{ORC} (€/kWh)	1621.90	1865.90	1788.60	1739.90
c_P (c€/kWh)	8.87	9.20	9.04	8.97
c_{net} (c€/kWh)	12.52	12.88	12.58	12.50
f_{PRHT} (%)	15.74	18.39	16.67	16.00
f_{EVAP} (%)	50.92	47.29	48.12	49.36
f_{RECP} (%)	5.12	4.41	4.53	4.70
f_{COND} (%)	49.38	53.56	57.72	56.82
f_{PUMP} (%)	40.85	64.32	45.41	43.00
f_{TURB} (%)	18.80	18.35	18.49	18.57
f_{ORC} (%)	32.24	34.13	34.87	34.55

By charging all the cost rates due to exergy losses at condenser exit to turbine fuel stream, results show that net specific exergy costs of ORC production are about the same for pure fluid and the most efficient mixture (0.9MM/0.1MDM). In this regard, economic comparison that captures the operational life of the plant would be valuable to examine the fluid with most prospective economic performance at off-design conditions. With respect to the parts of investment costs that lead to useful products in each component, reported exergoeconomic factors imply that mixtures better utilize investment costs in preheater and condenser. For other components, reverse is the case. Overall for the ORC unit, results show that higher percentage of investment costs leads to useful product by using mixtures, relative to pure fluid.

5.3.5 Off-design comparative analysis

5.3.5.1 Variation of thermal source mass flow rate

In this section, the variation of mass flow rate of heat transfer fluid feeding the ORC is compared, for pure MM and selected mixture compositions. Figure 5.10 shows the effects of heat source mass flow rate on ORC net power and exergetic efficiency.

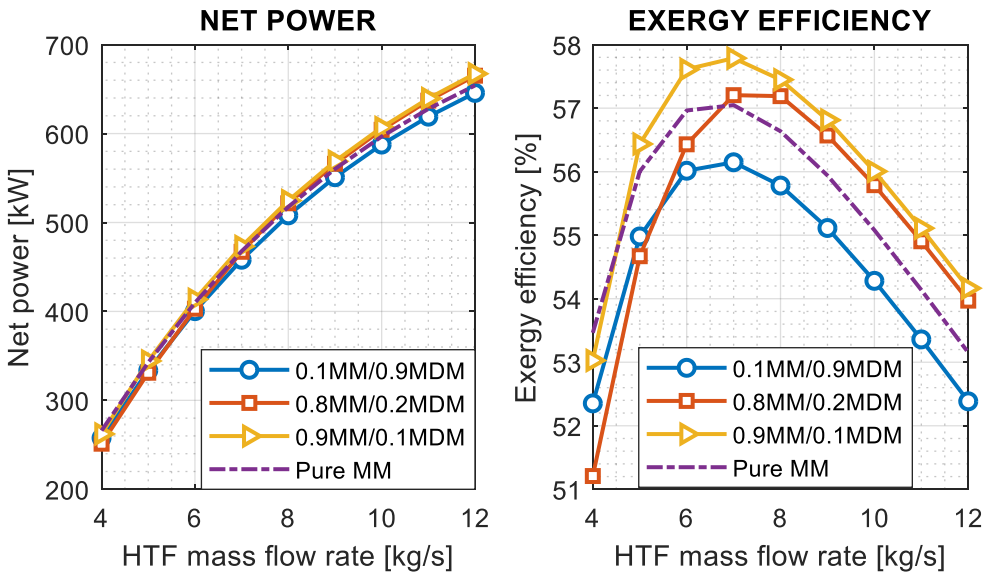

Figure 5.10: Effects of source HTF mass flow rate on ORC net power production and exergetic efficiency.

As shown, the rise of net power with increase in heat source mass flow rate is moderate and similar for all fluids. It can be observed that increase in net power of mixtures (0.8MM/0.2MDM and 0.9MM/0.1MDM) relative to pure fluid is only significant at high mass flow rate of HTF, say beyond 8 kg/s. In fact, net power obtainable for pure MM is marginally higher for mass flow rate lower than 5 kg/s. In this regard, it is essential to compare annual off-design ORC electrical energy production for pure fluid and selected mixtures. This is to verify the assertion of thermodynamic benefits of the working-fluid mixtures identified under design operating conditions. Furthermore, it can be seen also from Figure 5.10 that similar trends are obtained for variation of exergetic efficiency with HTF mass flow rate, for all fluids. In particular, exergetic efficiency grows steadily from low HTF mass flow rate and reaches an optimum point, where it takes a downward turn with

further increase in HTF mass flow rate. This behavior is understood to be a consequence of the irregular variation of destroyed exergy in ORC components, especially in the evaporator, turbine and condenser. Specifically, increasing HTF mass flow rate leads to increase in irreversibility in the evaporator, while irreversibilities decrease in turbine and condenser at the same time. For all fluids, the optimum exergetic efficiency point is at about the same mass flow rate, around 7 kg/s. As with net power, it is also observed here that exergy efficiency of pure fluid is higher at lower HTF mass flow rate. Actually, exergetic efficiency of 0.8MM/0.2MDM only exceeds that of pure fluid from the optimum point at 7 kg/s. This underscores the importance of incorporating off-design economic analysis into study of working fluid mixtures in ORC applications. This is even more important for solar-related applications, since high mass flow rate of HTF used for design is only obtainable at high solar irradiation conditions, which fluctuates with time in reality.

5.3.5.2 Variation of thermal source temperature

Here, off-design behaviours of the ORC unit with varying heat source temperature are examined, for all the fluid cases. As depicted in Figure 5.11, increasing heat source temperature leads to increase in ORC net power, for all fluids. It can be observed that the fluid with highest net power is not the same for all the inlet temperature range considered. For instance, from 230 ^{o}C to about 250 ^{o}C, 0.1MM/0.9MDM performs better than other fluids studied. Beyond 270 ^{o}C, it turns out with worst performance in terms of net power produced, and 0.9MM/0.1MDM becomes a better option. Similarly, for exergetic efficiency, the growth is inconsistent for different fluid at temperature below 250 ^{o}C, beyond which 0.9MM/0.1MDM shows better performance than other mixtures and pure MM. Thus, for heat sources with varying temperature, off-design analysis is essential for true assessment of working fluid performance.

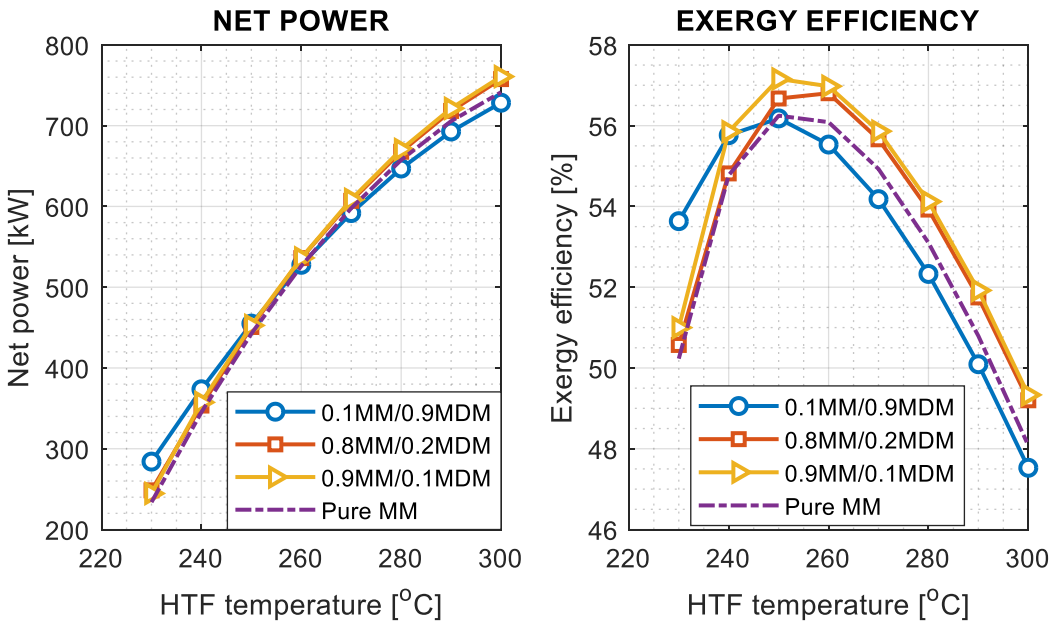

Figure 5.11: Effects of source HTF temperature on ORC net power production and exergetic efficiency.

5.3.5.3 Variation of cooling water inlet temperature

Here, effects of cooling water inlet temperature on net power and exergetic efficiency are presented, as shown in Figure 5.12. As it can be seen, responses of both net power and exergetic efficiency to increase in cooling water inlet temperature are the same for all fluid. In particular, increasing cooling water inlet temperature decreases both net power and exergetic efficiency almost linearly, as it would be expected. Having the same trend in net power and exergetic efficiency is because the available energy input into the ORC from heat source does not vary with cooling water inlet temperature.

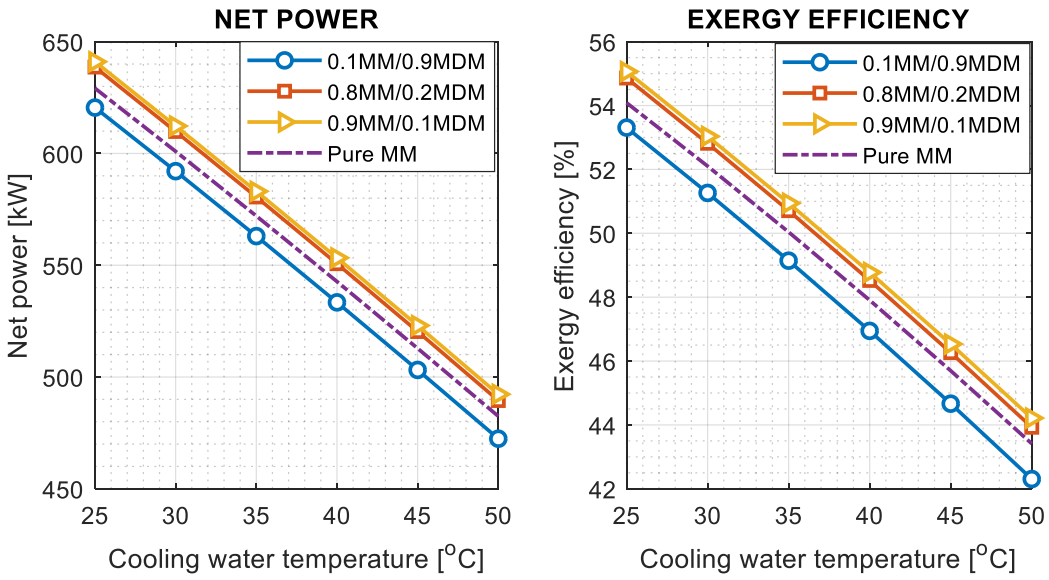

Figure 5.12: Effects of cooling water inlet temperature on ORC net power production and exergetic efficiency.

5.3.6 Yearly performance evaluation

Results of comparative annual performance evaluation of pure MM and selected working-fluid mixtures are presented in Table 5.5. As shown, total annual ORC electrical energy obtained with all considered fluid mixtures are higher than that of pure MM. In particular, increase in annual net energy of 2.3 %, 3.2 % and 5.2 % were obtained for 0.1MM/0.9MDM, 0.8MM/0.2MDM and 0.9MM/0.1MDM respectively, relative to pure MM. For 0.8MM/0.2MDM and 0.9MM/0.1MDM, this trend is the same as obtained under design condition. However, for 0.1MM/0.9MDM, off-design analysis shows that its thermodynamic performance is also better than that of pure MM, contrary to what was insinuated under design comparative analysis.

What's more, results showed that the thermodynamic advantages that could be obtained by adopting fluid mixtures as ORC working fluid do not translate to better economic performance of the plant. In fact, all economic metrics adopted for comparative evaluation in this study show that pure MM is more prospective than all the studied mixture compositions. Exemplarily for the most thermodynamically efficient fluid mixture (0.9MM/0.1MDM), LCOE and SPB increase by 8 % and 13 % respectively, while NPV reduces by 15.7 %, relative to pure MM. Economic performances of

the other working-fluid mixtures considered are even worst, in comparison with pure fluid. Suffice it to mention that of the selected mixtures in this study, the one with highest thermodynamic benefits is also the most economically prospective choice. This is true both at design and off-design conditions, for different exergy and energy costing methodologies implemented in this study.

Table 5.5: Yearly performance of studied fluids at off-design conditions.

Parameter	**MM**	**0.1MM/0.9MDM**	**0.8MM/0.2MDM**	**0.9MM/0.1MDM**
Electrical energy (GWh/y)	3.48	3.56	3.59	3.66
LCOE (€/MWh)	161	180	178	174
NPV (M€)	2.314	1.628	1.721	1.950
SPB (years)	7.0	8.4	8.3	7.9

5.4Summary

Techno-economic performance of some selected siloxane mixtures as ORC working fluids in hybrid solar-biomass applications have been evaluated in this chapter. Potential working fluid mixtures were initially identified based on thermo-physical and transport properties obtained directly from REFPROP database. Then, the thermodynamic and economic implications of using the selected mixtures were quantified and compared with those of pure fluid, at both design and off-design operating conditions. Although a number of studies have investigated thermo-economic implications of applying mixtures in ORCs before now, none of them considered a whole range of yearly performance at off-design conditions. Moreover, consideration has not been given to mixtures as ORC working fluids for hybrid solar-biomass applications, even though it has been affirmed that mixture performance is sensitive to heat source characteristics. Both energy and exergy approaches were used for comparative thermo-economic analyses of mixtures and pure fluid. For comprehensive economic analysis, ORC heat exchangers were sized based on process conditions that are different for pure fluid and mixtures.

Some main findings derived from the study presented in this chapter are highlighted as follows:

- Out of several combinations of siloxanes considered, the mixtures 0.1MM/0.9MDM, 0.8MM/0.2MDM and 0.9MM/0.1MDM were actively selected for detailed thermo-economic analysis. This is based on close proximity of condensation temperature glide of mixtures to temperature difference of cooling fluid, as well as temperature match of heat source with critical properties of mixtures.
- At design conditions, the use of 0.9MM/0.1MDM and 0.8MM/0.2MDM increase net ORC power by 2 % and 1.4 % respectively, while 0.1MM/0.9MDM reduces net power by 1.3 %, relative to pure MM. Similarly, for exergetic efficiency, increase of 1 and 0.8 percent points were recorded for 0.9MM/0.1MDM and 0.8MM/0.2MDM respectively, while decrease of 0.8 percent point was obtained for 0.1MM/0.9MDM, relative to pure fluid. The potential of efficiency increase by zeotropic mixtures regarding the selected application with heat source temperature higher than 200 °C is limited due to the few suitable pure siloxane components. In consequence, relatively high condensation temperature glides result which are unfavorable for the proposed ORC system. The obtained trend of efficiency is observed to be a consequence of reduction and/or increase of total irreversibility obtained in ORC system for different fluids. The fluid with lowest total irreversibility recorded highest net power and exergy efficiency, and vice-versa, as it would be expected.
- Total ORC heat transfer area was found to increase by 18.5 %, 21.3 % and 17.3 % for 0.1MM/0.9MDM, 0.8MM/0.2MDM and 0.9MM/0.1MDM respectively, relative to pure MM. Consequently, energy-based specific investment cost of ORC unit increases by 15 %, 10.3 % and 7.3 % for 0.1MM/0.9MDM, 0.8MM/0.2MDM and 0.9MM/0.1MDM respectively, relative to pure MM. Similarly, specific exergy costs of power production increases by 3.7 %, 1.9 % and 1 % for 0.1MM/0.9MDM, 0.8MM/0.2MDM and 0.9MM/0.1MDM respectively, relative to pure MM. However, reported exergoeconomic

factors imply that higher percentage of investment costs leads to useful product by using mixtures, relative to pure fluid.

- Effects of varying heat source transfer fluid mass flow rate and temperature, as well as cooling fluid inlet temperature on ORC off-design performance were obtained to be similar for mixtures and pure fluid. Also, it was obtained that thermodynamic advantages of mixtures are obtained at somewhat high mass flow rate and temperature of heat source fluid, below which pure fluid would be more advantageous.
- With the implementation of off-design models, increase in annual net energy of 2.3 %, 3.2 % and 5.2 % were obtained for 0.1MM/0.9MDM, 0.8MM/0.2MDM and 0.9MM/0.1MDM respectively, relative to pure MM. However, results showed that these thermodynamic advantages do not translate to better economic performance of the plant by adopting mixtures. In fact, all economic metrics adopted for comparative evaluation in this study showed that pure MM is more prospective than all the studied working-fluid mixtures, at off-design conditions.

In sum, researchers and designers of ORC plants should exercise caution when considering the use of siloxane mixtures as ORC working-fluids in real applications with heat source temperature higher than 225 ^{o}C. These could badly impact economic performance over the range of plant life. For investors looking for ways to improve profit, this is not a favourable point.

Page left blank intentionally

Chapter 6
Multi-objective Thermo-economic Optimization of Biomass Retrofit for the Existing CSP-ORC Plant

6.1Preamble

The study directed at obtaining design parameters of biomass furnace that would simultaneously optimize thermo-economic performance of the CSP-ORC plant post biomass retrofit is presented in this chapter. This is sequel to the importance of incorporating design optimization to development of energy systems, as underscored by a literature review presented earlier in Chapter 2. The specific objectives of this chapter are:

- Obtainment of the Pareto frontier for maximum exergetic efficiency and minimum investment cost rate of the existing plant sequel to biomass hybridization;
- Determination of optimal design parameters of the biomass retrofit system that would satisfy the aforementioned dual objectives for the hybrid plant;
- Investigation of the sensitivity of optimal design solutions to selected thermo-economic parameters.

6.2Methodology

Reference is made to the proposed CSP-biomass hybridization scheme, as presented earlier in Chapter 2. All the design and analyses models presented earlier are preserved here as well. However, modelling of the adopted biomass unit has been extended in this chapter, for clearer formulation of the optimization problems.

6.2.1 Retrofitted biomass furnace modelling

6.2.1.1 Combustion zone

The simulation of the biomass furnace requires estimation of the hot combustion gas temperature (T_{GAS}). The furnace mass and energy balance are given as follows:

$$\dot{m}_B + \dot{m}_{AIR} = \dot{m}_{GAS} + \dot{m}_{ASH} \tag{6.1}$$

$$LHV\eta_{FUR} = (\alpha + 1)(1 - y_{ASH})c_{P,GAS}(T_{GAS} - T_0) + y_{ASH}c_{ASH}(T_{GAS} - T_0) + y_{H20}\lambda_{H20} \tag{6.2}$$

where η_{FUR} is the combustion zone efficiency (related to convection and radiation losses), LHV is the lower heating value of biomass fuel, α is the ratio of air mass flow rate to ash-free biomass mass flow rate, y_{H20} is the water produced during the biomass combustion (without considering the biomass moisture), λ_{H20} is the water evaporation heat (2.273 kJ/kg at ambient pressure), y_{ASH} is the ash content in the biomass (%weight), c_P represents specific heat capacity at constant pressure and T_0 is the ambient temperature. Thus, with known furnace efficiency and air-fuel ratio, it was possible to estimate gas temperature from the energy balance. The overall combustion reaction had been expressed as:

$$C_m H_n O_x N_y S_z + x_W H_2O + \alpha_{St}(1 + e)(wO_2 + yN_2 + zH_2O) \rightarrow mCO_2 + (n/2 + x_W + \alpha_{St}(1 + ex)z) H_2O + (y/2 + \alpha_{St}(1 + ex)y) N_2 + zSO_2 + (\alpha_{St}(1 + e)w + x - m - n/4 - z) O_2 \tag{6.3}$$

where α_{St} is the stoichiometric air-fuel ratio and ex is the excess air, which is a decision variable in this study.

6.2.1.2 Boiler heat exchangers

Counter-flow heat exchanger type was assumed for modelling and analysis. By assuming the heat losses toward the environment negligible, the energy balance of the heat exchanger was used for calculating the required $\dot{m}_{GAS}$ under nominal conditions:

$$\dot{m}_{HTF}\left(h_{HTF,o} - h_{HTF,i}\right) = \dot{m}_{GAS}(h_{GAS} - h_{GAS,o}) \quad (6.4)$$

where $\dot{m}_{HTF}$ is the HTF mass flow rate, h is enthalpy, and subscripts i and o represent inlet and outlet, respectively. The HTF inlet and outlet temperatures were taken to coincide with exit and entry temperatures of the ORC at design conditions, and based on the thermal power required from biomass furnace, HTF mass flow rate was thus obtainable. The gas outlet temperature from furnace heater ($T_{GAS,o}$) relates with inlet HTF temperature ($T_{HTF,i}$) through furnace heater pinch point temperature difference ($\Delta T_{min,FHTR}$), which is a design variable in this study, as follows:

$$T_{GAS,o} = T_{HTF,i} + \Delta T_{min,FHTR} \quad (6.5)$$

Moreover, the required heat exchange area in the furnace heater (A_{FHTR}) was obtained from:

$$\dot{m}_{HTF}\left(h_{HTF,o} - h_{HTF,i}\right) = U_{FHTR} A_{FHTR} \Delta T_{ml,FHTR} \quad (6.6)$$

where U_{FHTR} is the overall heat transfer coefficient and $\Delta T_{ml,FHTR}$ is the mean logarithmic temperature difference. By assuming the conductive thermal resistance negligible, the overall heat transfer coefficient was obtained as:

$$U_{FHTR} = \frac{1}{\frac{1}{h_{HTF,D}} + \frac{1}{h_{GAS,D}}} \quad (6.7)$$

where $h_{HTF,D}$ and $h_{GAS,D}$ are the convective heat transfer coefficients under design conditions for the HTF and hot combustion gases, taken as 900 W/m^{2}K and 150 W/m^{2}K, respectively [269]. Similarly, temperature of pre-heated air ($T_{air,o}$) relates with $T_{GAS,o}$ through the air pre-heater pinch point temperature difference ($\Delta T_{min,AP}$), which is also a design variable, as follows:

$$T_{air,o} = T_{GAS,o} - \Delta T_{min,AP} \quad (6.8)$$

Consequently, the exchange area in the air pre-heater (A_{AP}) was calculated from the correlation:

$$\dot{m}_{air} c_{P,air}\left(T_{air,o} - T_0\right) = U_{AP} A_{AP} \Delta T_{ml,AP} \quad (6.9)$$

where U_{AP} is the overall heat transfer coefficient of the air pre-heater, calculated according to eq. (6.7) and by assuming convective heat transfer coefficient for air to be 150 W/m^{2}K.

6.2.2 Optimization approach

The non-dominated sorting genetic algorithm (NSGA-II) multi-objective optimization approach proposed originally by Deb et al. [270] was implemented in this study. The evolutionary algorithm possesses a number of highly desirable features, such as fast methodology for estimating crowding distance, relatively simple comparison operator for crowding, as well as speedy non-dominated sorting technique. Consequently, it is common to find this approach implemented in many detailed and recent optimization studies in literature [271–273].

In order to optimize thermo-economic performance of biomass retrofit for the existing CSP-ORC plant intended in this chapter, maximization of exergetic efficiency (ε) and minimization of investment cost rate ($\dot{C}$) were set as objective functions, defined as follows:

$$\varepsilon = \frac{\dot{W}_{net}}{\dot{E}_{sf} + (\dot{m}_B \cdot e_b)} \tag{6.10}$$

$$\dot{C} = \sum_k \mathrm{Z}_k \cdot \frac{1}{\mathrm{H}} \cdot \frac{i(1+i)^N}{(1+i)^N - 1} \cdot (1 + MF) \tag{6.11}$$

where $\dot{W}_{net}$ is the net electrical power produced by the power plant, $\dot{m}_B$ is the mass flow rate of biomass fuel, Z_k is the purchase and maintenance cost of component k, H is the annual operating hours of the plant (taken as 6000 hours), MF is the maintenance factor (imposed equal to 6%), N is the lifetime of plant operation (assumed equal to 25 years) and i is the interest rate (taken as 7%). The exergy of solar irradiation entering the system ($\dot{E}_{sf}$) and specific exergy of biomass fuel (e_b) were obtained based on the classical models earlier presented in Chapter 4.

Given that this scheme concerns a retrofit to a real and operational plant, design specifications of the existing units were preserved in the study being reported, as aforementioned, thereby

introducing equality optimization constraints for $\dot{W}_{net}$, $\dot{E}_{sf}$ as well as investment cost functions of the existing units. In essence, the main optimization variables lie with the newly introduced biomass furnace. Moreover, by imposing the aforementioned equality constraints, exergetic efficiency maximization would be satisfied by minimizing biomass consumption rate, based on eq. (6.10). Therefore, the optimization problem is reduced to seeking design variables of main components of the biomass furnace that would minimize biomass mass flow rate and investment cost rate simultaneously, when retrofitted to the existing units. In more specific terms, and for the sake of emphasis, combustion excess air supplied to the biomass furnace (*ex*), pinch point temperature difference in the air preheater ($\Delta T_{min,AP}$) and pinch point temperature difference in the furnace heater ($\Delta T_{min,FHTR}$) were investigated for the multi-objective optimization problem studied in this chapter, based on the relations expressed in section 6.2.1 above. The lower and upper boundaries imposed for the optimized design variables were selected empirically, as highlighted in Table 6.1. Cost relations used here are as presented in previous chapters. By optimizing $\Delta T_{min,FHTR}$ and $\Delta T_{min,AP}$, heat transfer processes in furnace heater and air preheater are improved, thereby reducing required surface areas and consequently purchase costs of the heat exchangers. Population size of 50 was implemented in the NSGA-II algorithm, with termination criterion set as 60 generations. The main optimization output is the Pareto frontier, which comprises optimal design variables for each population.

Table 6.1: Imposed values for optimization decision variables.

Parameter	Unit	Lower bound	Upper bound
Excess air	(%)	50	200
$\Delta T_{min,FHTR}$	^{o}C	25	100
$\Delta T_{min,AP}$	^{o}C	20	200

6.3Results and Discussion

6.3.1 Pareto frontier and optimized design variables

The solutions obtained for the studied optimization problem are presented as a Pareto frontier, shown in Figure 6.1. As aforementioned, the optimization scheme sought to minimize mass flow rate of biomass consumed by the hybrid plant (with the original intention of maximizing exergy efficiency of the overall hybrid plant), while also minimizing investment cost rate of the hybrid plant. It should first be pointed out that each solution point shown in Figure 6.1 could give optimal biomass retrofit to the existing solar-ORC plant. Any of the solution points could be selected by the designer, based on empirical and/or technical criteria. As it can be confirmed from Figure 6.1, the solution points that minimize biomass mass flow rate also maximize investment cost rate, and vice versa, giving conflicting effects to the set objectives. Exemplarily for the conflicting effects, increasing pinch point temperature differences of heat exchangers lower required heat exchange surface areas, in favour of cost objective function, but it also lowers exergetic efficiency, against thermodynamic objective function. However, reduction in biomass mass flow rate from 0.150 kg/s to about 0.135 kg/s increases investment cost rate of the hybrid plant only marginally, while further reduction in biomass mass flow rate leads to more significant increase in investment cost rate. This signals the fact that the optimum solution lies around biomass flow rate of 0.135 kg/s. More specifically, this assertion was confirmed by another decision-making analysis. The minimum mass flow rate represented in Figure 6.1 corresponds to point PX, and it is the best solution that satisfies the single objective of minimizing biomass mass flow rate. Conversely, the minimum investment cost rate corresponds to point PY in Figure 6.1, and it is also the best solution that satisfies single objective of minimizing investment cost rate of the hybrid solar-biomass power plant. By drawing a straight line towards horizontal axis from PX and a straight line towards vertical axis from PY, an intersection point of the straight lines is obtained, termed here as imaginary optimal point (IOP). At IOP, the two optimization objectives are well satisfied, and it would ordinarily provide the best design. However, this point is out of the Pareto frontier, and it cannot provide real solution to the

multi-objective optimization problem. In this regard, the next best solution is to be selected, which is the point on the Pareto frontier that is closest to IOP. The selected optimal design point is boxed in Figure 6.1, with biomass mass flow rate and investment cost rate of about 0.133 kg/s and 57 €/h, respectively. The design variables at the selected optimal point, as well as those satisfying individual single objectives (points PX and PY), are highlighted in Table 6.2. In addition, positions of $\Delta T_{min,FHTR}$ and $\Delta T_{min,AP}$ are illustrated by heat-exchange-characteristic diagram, for the three optimization solution points, as shown in Figure 6.2. Furthermore, design variables that produced each optimized solution on the Pareto frontier are represented in form of scatter distribution, as shown in Figure 6.3. Specifically, distribution of excess air, pinch point temperature difference of furnace heater as well as pinch point temperature difference of air pre-heater on the Pareto frontier are illustrated in the first, second and third layers of Figure 6.3, respectively.

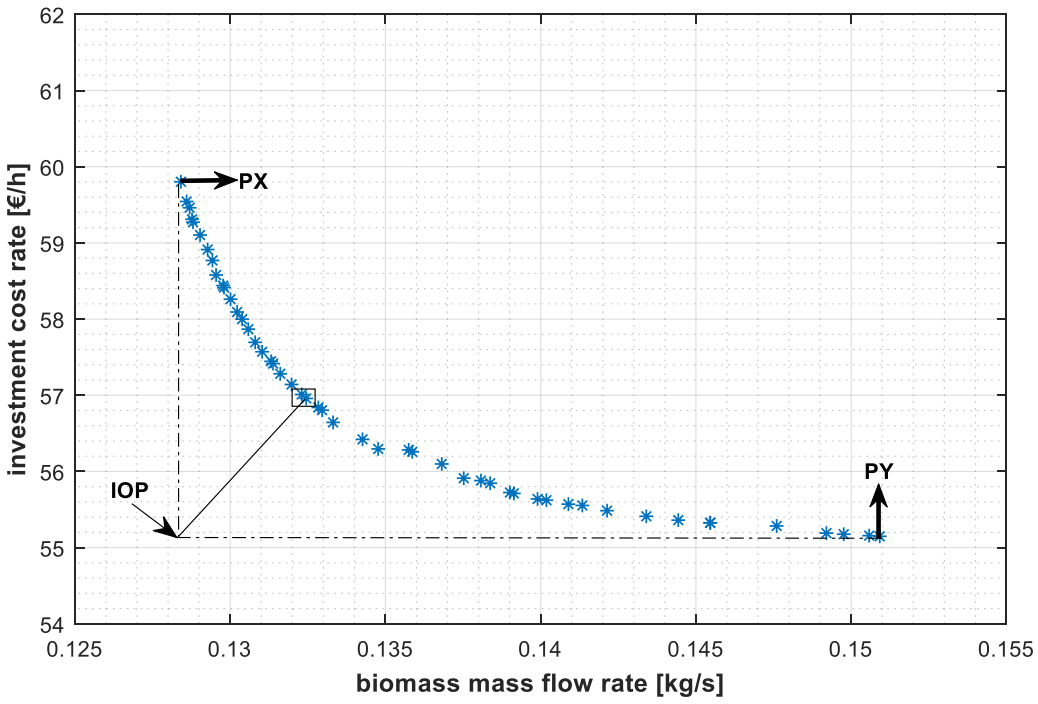

Figure 6.1: Pareto frontier of the optimized biomass retrofit.

Table 6.2: Design variables at single and selected multi-objective optimal points.

Point	Excess air (%)	$\Delta T_{min,FHTR}$ (^oC)	$\Delta T_{min,AP}$ (^oC)
PX	153	25.9	20
PY	50	77.3	123.5
Multi-objective choice	56	28.8	38.5

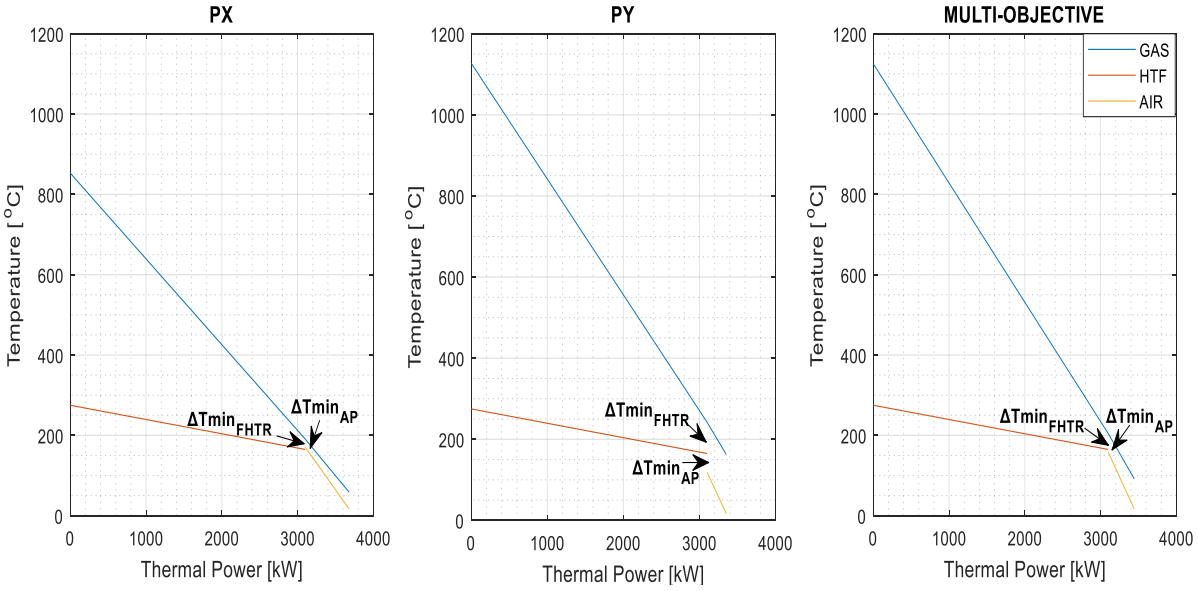

Figure 6.2: Heat exchange characteristics in the biomass boiler for different optimization solution points.

As it can be seen, about 80% of solution points on the Pareto frontier have their excess air value between 50% and 100%. The implication of this is that the desired excess air value that satisfies the dual-objective optimization problem investigated in this study is less than 100%. This contradicts the insinuation that high excess air of 153% best optimizes the thermodynamic performance of the biomass retrofit, as obtained in point PX and

Table 6.2 for single objective optimization. The importance of such multi-objective optimization as studied in this chapter is thus underscored. Also, it is observed in the second layer of Figure 6.3 that values of pinch point temperature difference of furnace heater on Pareto frontier are evenly distributed, with highest density observed between 20 and 80 ^{o}C, making it the preferred range. Similarly, third layer of Figure 6.3 shows that about 60% of values of pinch point temperature difference for air pre-heater on the Pareto frontier are between 20 and 80 ^{o}C, which makes the desired value for the dual-objective optimization to fall within this range.

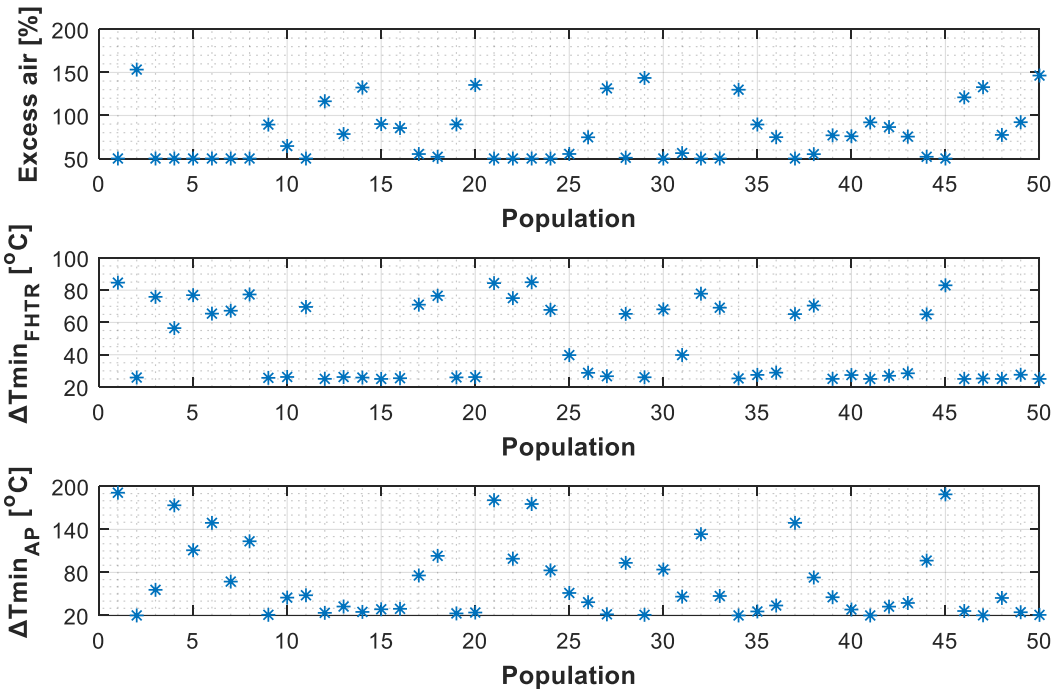

Figure 6.3: Scatter distribution of design variables at Pareto frontier.

6.3.2 Sensitivity analyses

Either due to imperfect design or inevitable variation of adopted design parameters during actual operation, real-time workings of energy systems often deviate from predictions at design conditions. It is thus a good practice to evaluate performance of system designs with changes in selected design parameters. In this chapter, sensitivity of the obtained optimal solutions to both thermodynamic and economic parameters have been investigated. In particular, Figure 6.4 shows the behavior of Pareto frontier with change in overall heat transfer coefficient of furnace heater (U_{FHTR}) and air pre-heater

(U_{AP}). As it would be expected, increasing U_{FHTR} shifts the Pareto frontier downwards, thereby reducing investment cost rate at optimal points, albeit with marginal increase in biomass mass flow rate. It is however worthwhile to note that the downward shift in the optimal solutions is less significant with U_{FHTR} of more than 125 W/m^{2}K, relative to a lower value. A similar effect is obtained for air pre-heater, however with less absolute significance. The reason for this is obvious; enhancing heat transfer performance of a heat exchanger reduces required surface area, and consequently the investment cost. In addition, Figure 6.5 shows the sensitivity of the optimal solutions to interest rate value (*i*) and annual operating hour of the plant (*H*). Similar patterns are observed for the Pareto frontier for all interest rates implemented, with optimal solutions shifting upwards as interest rate increases, as expected. More so, increase in annual operating hours of the hybrid plant shifts the Pareto frontier downwards, due to consequent reduction in investment cost rates. In essence, the clamour for hybridization of transient renewable energy sources such as solar and wind to enhance dispatchability and annual operating hours is justified.

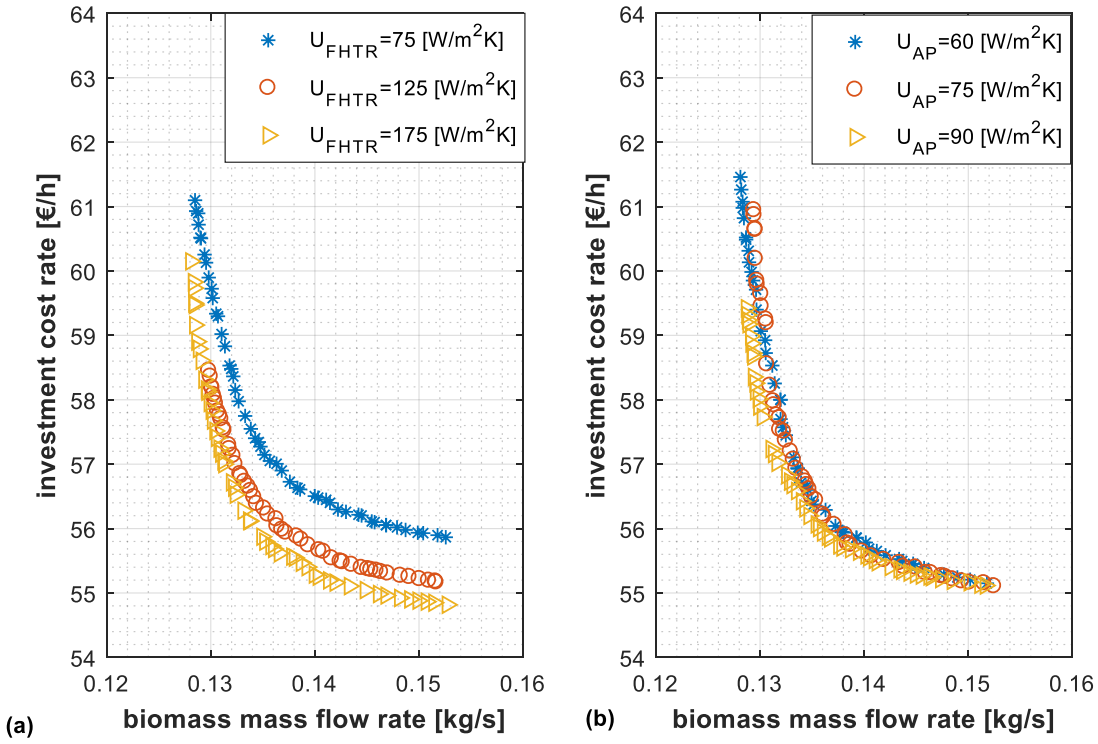

Figure 6.4: Sensitivity of optimal solutions to heat exchanger overall heat transfer coefficient.

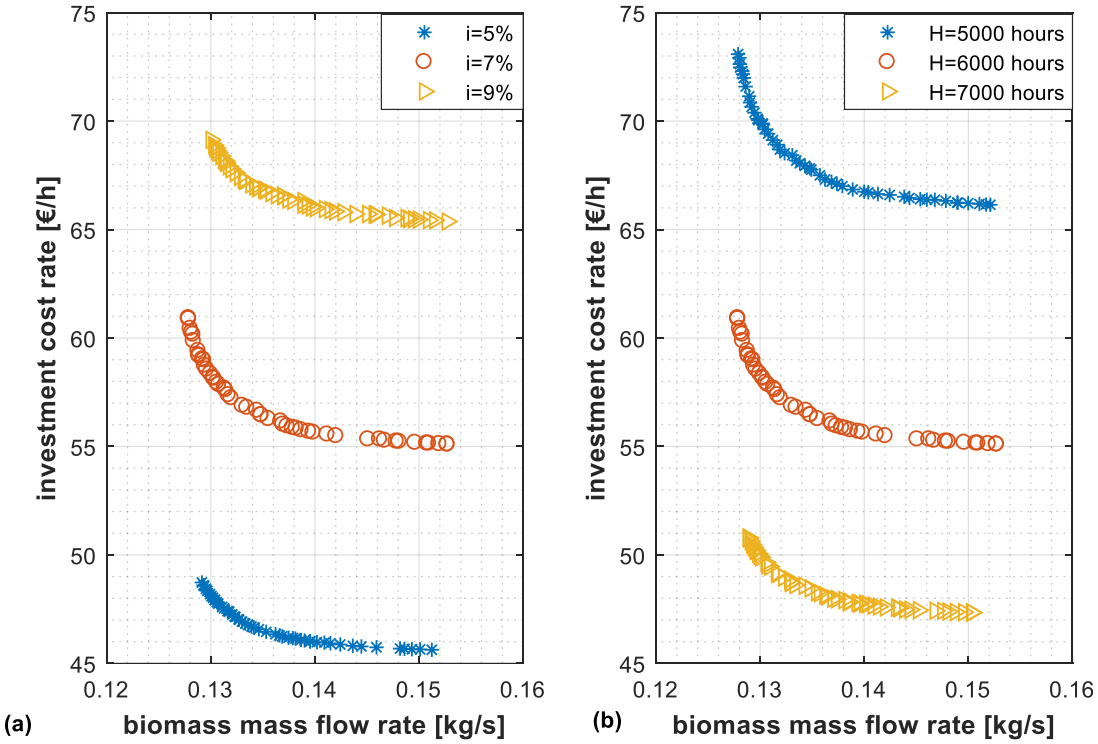

Figure 6.5: Sensitivity of optimal solutions to interest rate (*i*) and annual operating hours (*H*).

6.4Summary

NSGA-II evolutionary algorithm had been employed to obtain design parameters of biomass furnace that would optimize thermo-economic performance of the existing CSP-ORC plant upon which this study is based, post biomass retrofit. Design parameters of the currently operating units were adopted as equality constraints in the optimization problem, leaving the possible decision variables to biomass furnace parameters. In particular, the combustion excess air value, as well as pinch point temperature difference of the air pre-heater and furnace heater were set as decision variables. The actual objective was to simultaneously minimize biomass consumption rate (equivalent to maximizing exergetic efficiency of the retrofitted hybrid plant at nominal conditions) as well as investment cost rate of the hybrid plant post retrofit. The main findings are highlighted below:

- Amongst several possible optimal solutions represented at the Pareto frontier, the design point with biomass mass flow rate of 0.133 kg/s and investment cost rate of about 57 €/h was adjudged the most adequate for the studied biomass retrofit. At this point, excess air was obtained as 56%, furnace heater pinch point temperature difference as 28.8 ^{o}C and air pre-heater pinch point temperature difference as 38.5 ^{o}C.
- For the optimization of biomass retrofit studied, excess air value of less than 100 %, furnace heater pinch point temperature difference of less than 80 ^{o}C, and air pre-heater pinch point temperature difference of less than 80 ^{o}C were found to satisfy the set objectives the most.
- Lower investment cost rate would be achieved for the hybrid plant post biomass retrofit, with lower interest rate and peradventure the hybrid plant operates for longer hours annually. Also, the optimal design solutions for the biomass retrofit scheme reported in this study are less sensitive to overall heat transfer coefficient of furnace heater higher than 125 W/m^{2}K, as well as the range implemented for the air pre-heater (75 W/m^{2}K).

Page left blank intentionally

Chapter 7
Conclusions, Thesis Contributions and Recommendations for Further Studies

7.1 Conclusions

Conceptual design and thermo-economic optimization of hybrid solar-biomass ORC power plants have been carried out in this study. The main aim was to propose and analyse biomass hybridization scheme that could improve dispatchability and thermo-economic performance of CSP-ORC plants. In pursuit of this aim, four tangential objectives were defined, as contained in Chapter 1. For clarity and completeness of this chapter, the tangential objectives are highlighted here again, as follows:

- Conceptual design and techno-economic assessment of a novel biomass hybridization scheme, which could be applied both as retrofit to upgrade existing CSP-ORC plants as well as in newly-designed hybrid CSP-biomass ORC plants;
- Investigation of sources of thermo-economic losses in the proposed hybrid CSP-biomass ORC plant through second-law analysis;
- Assessment of thermo-economic effects of using siloxane mixtures as working fluid in the ORC unit of the proposed hybrid CSP-biomass plant;
- Determination of selected design parameters of the biomass system that would simultaneously optimize thermodynamic and economic performance of the hybrid plant for a retrofit case study.

The applied methodologies are in four distinct phases, as contained in Chapters 3, 4, 5 and 6 of the thesis, respectively. Each of these methodologies/chapters addressed each of the highlighted tangential study objectives, as summarized in the following.

Firstly, in consonance with the first tangential objective, a real CSP-ORC plant that had been built and is currently running at Ottana (NU), Italy was used as study reference in Chapter 3, to evaluate

potential thermo-economic benefits of retrofitting biomass systems to plants of such kind around the world. Specifically, the design and operational features of this existing ORC plant were adopted for analyses, and the simulated ORC off-design behaviour was validated using operational data of the real plant. However, as aforementioned, the scope had been expanded to give room for new designs of such fully-renewable plants, thereby introducing novel strategies for sizing heat source systems in a different study scenario. The main results obtained with respect to this objective are summarized as follows:

- Supposed biomass retrofit can lead to an increase in electrical efficiency in the order of 5 percent points compared to CSP-ORC plant;
- Retrofit can increase annualized plant operating duration by about 3,500 hours, with marginal LCOE and NPV of 109 €/MWh and 1.83 M€, respectively. Additional investment cost incurred due to retrofit can be offset in 1.4 years of plant operation;
- Validity of the applied ORC off-design methods is satisfied. This is based on the obtained relative deviation of ORC gross efficiency between simulation results and real power plant data, which is below 3 %;
- In comparison with retrofit case study, newly integrated design leads to a more economically-prospective hybrid plant, with LCOE, SPB and NPV obtained at 130 €/MWh, 4.3 years and 3.99 M€, respectively. Also, relative to stand-alone solar ORC power plants of equivalent ratings, these economic values portend market competitiveness [250],[251].

Secondly, detailed conventional and enhanced exergy and exergoeconomic analyses were employed to investigate the sources of thermo-economic losses in the proposed hybrid plant, and to propose necessary schemes for improvement, as contained in Chapter 4. This is in agreement with the second tangential objective highlighted above. The main results obtained with respect to this objective are summarized as follows:

- Exergy flow rates were quantified for all thermodynamic states, and irreversibilities in different components were obtained and illustrated, using Sankey flow diagram. Exergetic efficiency of about 7 % was obtained for the overall hybrid plant;
- Similarly, flows of exergy cost rates were obtained and illustrated for all thermodynamic states, including investment cost rates for the components and cost rates due to irreversibility. Overall, results showed that the fully-renewable hybrid energy system being studied is capable of producing electrical energy at the rate of between 10.50 to 12.10 euro cents per kWh, depending on the adopted exergoeconomic approach;
- The cost of producing electricity increases in integrated exergoeconomic approach by about 15 %, relative to the conventional approach. Conversely, the cost of producing warm water decreases by about 56 % in integrated approach, which portends a more reasonable analysis, if the plant would be operated in co-generation mode. Overall, loss of total investment cost of the hybrid plant is marginally lower by adopting integrated approach, relative to the conventional approach;
- The studied enhanced exergy and exergoeconomic analyses facilitated the decision on the best approach to apply thermodynamic and cost improvement measures to each component of the hybrid plant, and thus to the system as a whole. Results showed that relative avoidable cost rates of between 2 % and 69 % of total cost rates could be theoretically avoided. Also, it was obtained that investment costs of solar field, thermal energy storage tanks, furnace heater, recuperator and ORC preheater should be reduced, for acceptable economic performance of the hybrid plant. Efforts should be made to improve thermodynamic performance of all other components, for optimized hybrid power plant. This type of information is highly essential for improved design and quicker market penetration of fully-renewable energy plants.

Thirdly, sequel to the information obtained from exergy analysis that thermodynamic performance of ORC components should be improved, the impacts of adopting siloxane mixtures as working

fluid in the ORC plant were assessed for the hybrid solar-biomass heat source. This is also in agreement with the third tangential objective highlighted above. The main results obtained with respect to this objective are summarized as follows:

- Out of several combinations of siloxanes considered, the mixtures 0.1MM/0.9MDM, 0.8MM/0.2MDM and 0.9MM/0.1MDM were actively selected for detailed thermo-economic analysis;
- At design conditions, the use of 0.9MM/0.1MDM and 0.8MM/0.2MDM increase net ORC power by 2 % and 1.4 % respectively, while 0.1MM/0.9MDM reduces net power by 1.3 %, relative to pure MM. A similar trend was obtained for exergetic efficiency, obviously in direct response to reduction and/or increase of total irreversibility obtained in the ORC system for different fluid;
- Total ORC heat transfer areas were found to increase by 18.5 %, 21.3 % and 17.3 % for 0.1MM/0.9MDM, 0.8MM/0.2MDM and 0.9MM/0.1MDM respectively, relative to pure MM;
- Effects of varying heat source transfer fluid mass flow rate and temperature, as well as cooling fluid inlet temperature on ORC off-design performance were obtained to be similar for mixtures and pure fluid;
- With the implementation of off-design models, increase in annual net energy of 2.3 %, 3.2 % and 5.2 % were obtained for 0.1MM/0.9MDM, 0.8MM/0.2MDM and 0.9MM/0.1MDM respectively, relative to pure MM. However, results showed that these thermodynamic advantages would not translate to better economic performance of the plant by adopting mixtures.

Lastly, based on the need to reduce exergoeconomic losses in the biomass system as obtained under the second tangential objective, some design parameters of the biomass furnace that would simultaneously optimize thermodynamic and economic performance of the hybrid plant were

investigated for the retrofit case study. This is also in agreement with the fourth tangential objective highlighted above. The main results obtained with respect to this objective are summarized as follows:

- Amongst several possible optimal solutions represented at the Pareto frontier, the design point with biomass mass flow rate of 0.133 kg/s and investment cost rate of about 57 €/h was adjudged the most adequate for the studied biomass retrofit. At this point, excess air was obtained as 56 %, furnace heater pinch point temperature difference as 28.8 ^{o}C and air pre-heater pinch point temperature difference as 38.5 ^{o}C;
- For optimization of the biomass retrofit system studied, excess air value of less than 100 %, furnace heater pinch point temperature difference of less than 80 ^{o}C, and air pre-heater pinch point temperature difference of less than 80 ^{o}C were found to satisfy the set optimization objectives the most;
- Lower investment cost rate would be achieved for the hybrid plant post biomass retrofit, with lower interest rate and peradventure the hybrid plant operates for longer hours annually. Also, the optimal design solutions for the biomass retrofit scheme reported in this study are less sensitive to overall heat transfer coefficient of furnace heater higher than 125 W/m^{2}K, as well as the range implemented for the air pre-heater (75 W/m^{2}K).

It is clear from the foregoing that the tangential objectives set for this study were succinctly achieved, and thus the overall aim. The main contributions of the thesis to the body of knowledge are highlighted separately in the following section.

7.2 Thesis Contributions

The main points of research novelties contributed by this thesis are highlighted as follows:

- It is the first to propose parallel biomass hybridization scheme that can be applied in reality to upgrade existing CSP-ORC plants, for improved dispatchability and thermo-economic

performance. Also, the proposed scheme can be adapted to design new hybrid CSP-biomass ORC power plants;

- It is the first to incorporate off-design analysis into thermo-economic evaluation of working fluid mixtures in ORC plants, irrespective of nature of heat source;
- It is the first to study working fluid mixtures for ORC application in hybrid solar-biomass plants;
- It underscores the importance of integrating energy quality level of thermodynamic states into exergy cost formulation process, for improved exergoeconomic assessments.

7.3Recommendations for Further Studies

The following topics, related to the focus of this thesis, are recommended for further studies:

- Dynamic models of the complete hybrid CSP-biomass ORC plant should be incorporated into thermo-economic analysis, for improved assessment and better control strategy of the hybrid plant operation. Software such as Dymola or TRNSYS would be adequate for this task;
- Exergy and exergoeconomic analyses of the hybrid plant should be extended to include the effects of varying availability of solar irradiation and other transient parameters;
- Also, the suggested steps that could improve exergy and exergy cost performance of the plant should be implemented, and the effects on overall exergy and exergoeconomic performance of the hybrid plant should be re-examined;
- A resource-assessment and comparative analyses should be carried out for the existing CSP-ORC plant at Ottana, to investigate the biomass technology and available biomass fuels that would optimize the practical implementation of the proposed hybridization scheme for this plant in particular;

- The multi-objective optimization study should be expanded to include determination of optimal design parameters for all the units of the hybrid plant, assuming that a newly-designed hybrid power plant is planned;
- Environmental analysis should be incorporated into multi-objective optimization of the hybrid plant, for further minimization of life cycle cost and carbon emissions.

References

[1] World Energy Outlook 2018. OECD; 2018. doi:10.1787/weo-2018-en.

[2] About the Sustainable Development Goals - United Nations Sustainable Development n.d. https://www.un.org/sustainabledevelopment/sustainable-development-goals/ (accessed September 13, 2018).

[3] Sansaniwal SK, Sharma V, Mathur J. Energy and exergy analyses of various typical solar energy applications: A comprehensive review. Renew Sustain Energy Rev 2018;82:1576–601. doi:10.1016/J.RSER.2017.07.003.

[4] Powell KM, Rashid K, Ellingwood K, Tuttle J, Iverson BD. Hybrid concentrated solar thermal power systems: A review. Renew Sustain Energy Rev 2017;80:215–37. doi:10.1016/j.rser.2017.05.067.

[5] Heydari A, Askarzadeh A. Optimization of a biomass-based photovoltaic power plant for an off-grid application subject to loss of power supply probability concept. Appl Energy 2016;165:601–11. doi:10.1016/J.APENERGY.2015.12.095.

[6] Storm K, Storm K. Solar thermal power plant. Ind Process Plant Constr Estim Man-Hour Anal 2019:187–215. doi:10.1016/B978-0-12-818648-0.00009-0.

[7] Ennio M, Astolfi M. Organic Rankine Cycle (ORC) Power Systems: Technologies and Applications. 2016.

[8] Quoilin S, Broek M Van Den, Declaye S, Dewallef P, Lemort V. Techno-economic survey of organic rankine cycle (ORC) systems. Renew Sustain Energy Rev 2013;22:168–86. doi:10.1016/j.rser.2013.01.028.

[9] Petrollese M, Cau G, Cocco D. The Ottana solar facility: dispatchable power from small-scale CSP plants based on ORC systems. Renew Energy 2018. doi:10.1016/j.renene.2018.07.013.

[10] Gibb D, Johnson M, Romaní J, Gasia J, Cabeza LF, Seitz A. Process integration of thermal energy storage systems – Evaluation methodology and case studies. Appl Energy 2018;230:750–60. doi:10.1016/J.APENERGY.2018.09.001.

[11] Shivarama Krishna K, Sathish Kumar K. A review on hybrid renewable energy systems. Renew Sustain Energy Rev 2015;52:907–16. doi:10.1016/J.RSER.2015.07.187.

[12] Lovegrove K, Csiro WS. Introduction to concentrating solar power (CSP) technology. Conc Sol Power Technol 2012:3–15. doi:10.1533/9780857096173.1.3.

[13] Lovegrove K, Pye J. Fundamental principles of concentrating solar power (CSP) systems. Conc Sol Power Technol 2012:16–67. doi:10.1533/9780857096173.1.16.

[14] Weinstein LA, Loomis J, Bhatia B, Bierman DM, Wang EN, Chen G. Concentrating Solar Power. Chem Rev 2015;115:12797–838. doi:10.1021/acs.chemrev.5b00397.

[15] Chang C. Tracking solar collection technologies for solar heating and cooling systems. Adv Sol Heat Cool 2016:81–93. doi:10.1016/B978-0-08-100301-5.00005-9.

[16] Barlev D, Vidu R, Stroeve P. Innovation in concentrated solar power. Sol Energy Mater Sol Cells 2011;95:2703–25. doi:10.1016/J.SOLMAT.2011.05.020.

[17] Hafez AZ, Yousef AM, Harag NM. Solar tracking systems: Technologies and trackers drive types – A review. Renew Sustain Energy Rev 2018;91:754–82. doi:10.1016/J.RSER.2018.03.094.

[18] Imtiaz Hussain M, Ménézo C, Kim JT. Advances in solar thermal harvesting technology based on surface solar absorption collectors: A review. Sol Energy Mater Sol Cells 2018;187:123–39. doi:10.1016/j.solmat.2018.07.027.

[19] Arancibia-Bulnes CA, Peña-Cruz MI, Mutuberría A, Díaz-Uribe R, Sánchez-González M. A survey of methods for the evaluation of reflective solar concentrator optics. Renew Sustain Energy Rev 2017;69:673–84. doi:10.1016/J.RSER.2016.11.048.

[20] Cavallaro F, Zavadskas EK, Streimikiene D, Mardani A. Assessment of concentrated solar power (CSP) technologies based on a modified intuitionistic fuzzy topsis and trigonometric

entropy weights. Technol Forecast Soc Change 2019;140:258–70. doi:10.1016/J.TECHFORE.2018.12.009.

[21] CSP Projects Around the World - SolarPACES n.d.

[22] Rovira A, Barbero R, Montes MJ, Abbas R, Varela F. Analysis and comparison of Integrated Solar Combined Cycles using parabolic troughs and linear Fresnel reflectors as concentrating systems. Appl Energy 2016;162:990–1000. doi:10.1016/J.APENERGY.2015.11.001.

[23] Cau G, Cocco D. Comparison of medium-size concentrating solar power plants based on parabolic trough and linear Fresnel collectors. Energy Procedia 2014;45:101–10. doi:10.1016/j.egypro.2014.01.012.

[24] Zhang HL, Baeyens J, Degrève J, Cacères G. Concentrated solar power plants: Review and design methodology. Renew Sustain Energy Rev 2013;22:466–81. doi:10.1016/j.rser.2013.01.032.

[25] Bellos E, Tzivanidis C, Moghimi MA. Reducing the optical end losses of a linear Fresnel reflector using novel techniques. Sol Energy 2019;186:247–56. doi:10.1016/J.SOLENER.2019.05.020.

[26] Yang M, Zhu Y, Taylor RA. End losses minimization of linear Fresnel reflectors with a simple, two-axis mechanical tracking system. Energy Convers Manag 2018;161:284–93. doi:10.1016/J.ENCONMAN.2018.01.082.

[27] Abbas R, Valdés M, Montes MJ, Martínez-Val JM. Design of an innovative linear Fresnel collector by means of optical performance optimization: A comparison with parabolic trough collectors for different latitudes. Sol Energy 2017;153:459–70. doi:10.1016/J.SOLENER.2017.05.047.

[28] Morin G, Dersch J, Platzer W, Eck M, Häberle A. Comparison of Linear Fresnel and Parabolic Trough Collector power plants. Sol Energy 2012;86:1–12. doi:10.1016/J.SOLENER.2011.06.020.

[29] Wang G, Wang F, Shen F, Chen Z, Hu P. Novel design and thermodynamic analysis of a

solar concentration PV and thermal combined system based on compact linear Fresnel reflector. Energy 2019;180:133–48. doi:10.1016/J.ENERGY.2019.05.082.

[30] Rungasamy AE, Craig KJ, Meyer JP. Comparative study of the optical and economic performance of etendue-conserving compact linear Fresnel reflector concepts. Sol Energy 2019;181:95–107. doi:10.1016/J.SOLENER.2019.01.081.

[31] Kumar V, Shrivastava RL, Untawale SP. Fresnel lens: A promising alternative of reflectors in concentrated solar power. Renew Sustain Energy Rev 2015;44:376–90. doi:10.1016/J.RSER.2014.12.006.

[32] Desai N, Pranov H, Haglind F. Techno-economic analysis of a power generation system consisting of a foil-based concentrating solar collector and an organic Rankine cycle unit. 2019.

[33] Noč L, Ruiz-Zepeda F, Merzel F, Jerman I. High-temperature “ion baseball” for enhancing concentrated solar power efficiency. Sol Energy Mater Sol Cells 2019;200:109974. doi:10.1016/J.SOLMAT.2019.109974.

[34] Seshie YM, N’Tsoukpoe KE, Neveu P, Coulibaly Y, Azoumah YK. Small scale concentrating solar plants for rural electrification. Renew Sustain Energy Rev 2018;90:195–209. doi:10.1016/J.RSER.2018.03.036.

[35] Islam MT, Huda N, Abdullah AB, Saidur R. A comprehensive review of state-of-the-art concentrating solar power (CSP) technologies: Current status and research trends. Renew Sustain Energy Rev 2018;91:987–1018. doi:10.1016/J.RSER.2018.04.097.

[36] Sarvghad M, Delkasar Maher S, Collard D, Tassan M, Will G, Steinberg TA. Materials compatibility for the next generation of Concentrated Solar Power plants. Energy Storage Mater 2018;14:179–98. doi:10.1016/J.ENSM.2018.02.023.

[37] Li P-W, Chan CL, Li P-W, Chan CL. Thermal Storage System Configurations and Basic Operation. Therm. Energy Storage Anal. Des., Academic Press; 2017, p. 7–19. doi:10.1016/B978-0-12-805344-7.00002-X.

[38] Lehtola T, Zahedi A. Solar energy and wind power supply supported by storage technology: A review. Sustain Energy Technol Assessments 2019;35:25–31. doi:10.1016/J.SETA.2019.05.013.

[39] Gauché P, Rudman J, Mabaso M, Landman WA, von Backström TW, Brent AC. System value and progress of CSP. Sol Energy 2017;152:106–39. doi:10.1016/J.SOLENER.2017.03.072.

[40] Li D, Wang J, Ding Y, Yao H, Huang Y. Dynamic thermal management for industrial waste heat recovery based on phase change material thermal storage. Appl Energy 2019;236:1168–82. doi:10.1016/J.APENERGY.2018.12.040.

[41] Merlin K, Soto J, Delaunay D, Traonvouez L. Industrial waste heat recovery using an enhanced conductivity latent heat thermal energy storage. Appl Energy 2016;183:491–503. doi:10.1016/J.APENERGY.2016.09.007.

[42] Ortega-Fernández I, Rodríguez-Aseguinolaza J. Thermal energy storage for waste heat recovery in the steelworks: The case study of the REslag project. Appl Energy 2019;237:708–19. doi:10.1016/J.APENERGY.2019.01.007.

[43] Cabeza LF, Martorell I, Miró L, Fernández AI, Barreneche C. 1 - Introduction to thermal energy storage (TES) systems. In: Cabeza LFBT-A in TESS, editor. Woodhead Publ. Ser. Energy, Woodhead Publishing; 2015, p. 1–28. doi:https://doi.org/10.1533/9781782420965.1.

[44] Navarro ME, Martínez M, Gil A, Fernández AI, Cabeza LF, Olives R, et al. Selection and characterization of recycled materials for sensible thermal energy storage. Sol Energy Mater Sol Cells 2012;107:131–5. doi:10.1016/J.SOLMAT.2012.07.032.

[45] Cingarapu S, Singh D, Timofeeva E V., Moravek MR. Use of encapsulated zinc particles in a eutectic chloride salt to enhance thermal energy storage capacity for concentrated solar power. Renew Energy 2015;80:508–16. doi:10.1016/J.RENENE.2015.02.026.

[46] Andreu-Cabedo P, Mondragon R, Hernandez L, Martinez-Cuenca R, Cabedo L, Julia JE. Increment of specific heat capacity of solar salt with SiO2 nanoparticles. Nanoscale Res Lett

2014;9:582. doi:10.1186/1556-276X-9-582.

[47] Pelay U, Luo L, Fan Y, Stitou D, Rood M. Thermal energy storage systems for concentrated solar power plants. Renew Sustain Energy Rev 2017;79:82–100. doi:10.1016/J.RSER.2017.03.139.

[48] Reddy KS, Mudgal V, Mallick TK. Review of latent heat thermal energy storage for improved material stability and effective load management. J Energy Storage 2018;15:205–27. doi:10.1016/J.EST.2017.11.005.

[49] Enhancing the thermal response of latent heat storage systems. Int J Energy Res 1997;21:759–66. doi:10.1002/(SICI)1099-114X(199707)21:9<759::AID-ER254>3.0.CO;2-7.

[50] Crespo A, Barreneche C, Ibarra M, Platzer W. Latent thermal energy storage for solar process heat applications at medium-high temperatures – A review. Sol Energy 2018. doi:10.1016/J.SOLENER.2018.06.101.

[51] Kenisarin MM. High-temperature phase change materials for thermal energy storage. Renew Sustain Energy Rev 2010;14:955–70. doi:10.1016/J.RSER.2009.11.011.

[52] Tay NHS, Liu M, Belusko M, Bruno F. Review on transportable phase change material in thermal energy storage systems. Renew Sustain Energy Rev 2017;75:264–77. doi:10.1016/J.RSER.2016.10.069.

[53] Kerskes H. Chapter 17 - Thermochemical Energy Storage. In: Letcher TMBT-SE, editor., Oxford: Elsevier; 2016, p. 345–72. doi:https://doi.org/10.1016/B978-0-12-803440-8.00017-8.

[54] Chen X, Zhang Z, Qi C, Ling X, Peng H. State of the art on the high-temperature thermochemical energy storage systems. Energy Convers Manag 2018;177:792–815. doi:10.1016/J.ENCONMAN.2018.10.011.

[55] Abedin AH. A Critical Review of Thermochemical Energy Storage Systems. Open Renew Energy J 2011;4:42–6. doi:10.2174/1876387101004010042.

[56] Michel B, Mazet N, Mauran S, Stitou D, Xu J. Thermochemical process for seasonal storage of solar energy: Characterization and modeling of a high density reactive bed. Energy 2012;47:553–63. doi:10.1016/J.ENERGY.2012.09.029.

[57] Aydin D, Casey SP, Riffat S. The latest advancements on thermochemical heat storage systems. Renew Sustain Energy Rev 2015;41:356–67. doi:10.1016/J.RSER.2014.08.054.

[58] Qin FGF, Yang X, Ding Z, Zuo Y, Shao Y, Jiang R, et al. Thermocline stability criterions in single-tanks of molten salt thermal energy storage. Appl Energy 2012;97:816–21. doi:10.1016/J.APENERGY.2012.02.048.

[59] Reddy KS, Jawahar V, Sivakumar S, Mallick TK. Performance investigation of single-tank thermocline storage systems for CSP plants. Sol Energy 2017;144:740–9. doi:10.1016/J.SOLENER.2017.02.012.

[60] Muñoz-Sánchez B, Iparraguirre-Torres I, Madina-Arrese V, Izagirre-Etxeberria U, Unzurrunzaga-Iturbe A, García-Romero A. Encapsulated High Temperature PCM as Active Filler Material in a Thermocline-based Thermal Storage System. Energy Procedia 2015;69:937–46. doi:10.1016/J.EGYPRO.2015.03.177.

[61] Bastien D, Athienitis AK. Passive thermal energy storage, part 1: Design concepts and metrics. Renew Energy 2018;115:1319–27. doi:10.1016/J.RENENE.2016.04.011.

[62] Nazir H, Batool M, Bolivar Osorio FJ, Isaza-Ruiz M, Xu X, Vignarooban K, et al. Recent developments in phase change materials for energy storage applications: A review. Int J Heat Mass Transf 2019;129:491–523. doi:10.1016/J.IJHEATMASSTRANSFER.2018.09.126.

[63] Yu D-H, He Z-Z. Shape-remodeled macrocapsule of phase change materials for thermal energy storage and thermal management. Appl Energy 2019;247:503–16. doi:10.1016/J.APENERGY.2019.04.072.

[64] Jacob R, Liu M, Sun Y, Belusko M, Bruno F. Characterisation of promising phase change materials for high temperature thermal energy storage. J Energy Storage 2019;24:100801. doi:10.1016/J.EST.2019.100801.

[65] Becattini V, Haselbacher A. Toward a new method for the design of combined sensible/latent thermal-energy storage using non-dimensional analysis. Appl Energy 2019;247:322–34. doi:10.1016/J.APENERGY.2019.03.022.

[66] Ahmed N, Elfeky KE, Lu L, Wang QW. Thermal and economic evaluation of thermocline combined sensible-latent heat thermal energy storage system for medium temperature applications. Energy Convers Manag 2019;189:14–23. doi:10.1016/J.ENCONMAN.2019.03.040.

[67] Becattini V, Geissbühler L, Zanganeh G, Haselbacher A, Steinfeld A. Pilot-scale demonstration of advanced adiabatic compressed air energy storage, Part 2: Tests with combined sensible/latent thermal-energy storage. J Energy Storage 2018;17:140–52. doi:10.1016/J.EST.2018.02.003.

[68] An GL, Wang LW, Gao J. Two-stage cascading desorption cycle for sorption thermal energy storage. Energy 2019;174:1091–9. doi:10.1016/J.ENERGY.2019.03.069.

[69] Chirino H, Xu B, Xu X. Parametric study of cascade latent heat thermal energy storage (CLHTES) system in Concentrated Solar Power (CSP) plants. J Energy Inst 2019;92:653–64. doi:10.1016/J.JOEI.2018.03.007.

[70] Zayed ME, Zhao J, Elsheikh AH, Hammad FA, Ma L, Du Y, et al. Applications of cascaded phase change materials in solar water collector storage tanks: A review. Sol Energy Mater Sol Cells 2019;199:24–49. doi:10.1016/J.SOLMAT.2019.04.018.

[71] Cheng X, Zhai X. Thermal performance analysis and optimization of a cascaded packed bed cool thermal energy storage unit using multiple phase change materials. Appl Energy 2018;215:566–76. doi:10.1016/J.APENERGY.2018.02.053.

[72] Mostafavi Tehrani SS, Shoraka Y, Nithyanandam K, Taylor RA. Cyclic performance of cascaded and multi-layered solid-PCM shell-and-tube thermal energy storage systems: A case study of the 19.9 MWe Gemasolar CSP plant. Appl Energy 2018;228:240–53. doi:10.1016/J.APENERGY.2018.06.084.

[73] Iniesta AC, Diago M, Delclos T, Falcoz Q, Shamim T, Calvet N. Gravity-fed Combined Solar Receiver/Storage System Using Sand Particles as Heat Collector, Heat Transfer and Thermal Energy Storage Media. Energy Procedia 2015;69:802–11. doi:10.1016/J.EGYPRO.2015.03.089.

[74] Ma Z, Mehos M, Glatzmaier G, Sakadjian BB. Development of a Concentrating Solar Power System Using Fluidized-bed Technology for Thermal Energy Conversion and Solid Particles for Thermal Energy Storage. Energy Procedia 2015;69:1349–59. doi:10.1016/J.EGYPRO.2015.03.136.

[75] Basu P, Basu P. Introduction. Biomass Gasification, Pyrolysis and Torrefaction 2018:1–27. doi:10.1016/B978-0-12-812992-0.00001-7.

[76] Ashter SA, Ashter SA. Biomass and its sources. Technol Appl Polym Deriv from Biomass 2018:11–36. doi:10.1016/B978-0-323-51115-5.00002-5.

[77] García R, Pizarro C, Lavín AG, Bueno JL. Biomass sources for thermal conversion. Techno-economical overview. Fuel 2017;195:182–9. doi:10.1016/J.FUEL.2017.01.063.

[78] Bajwa DS, Peterson T, Sharma N, Shojaeiarani J, Bajwa SG. A review of densified solid biomass for energy production. Renew Sustain Energy Rev 2018;96:296–305. doi:10.1016/J.RSER.2018.07.040.

[79] Wang A, Austin D, Song H. Investigations of thermochemical upgrading of biomass and its model compounds: Opportunities for methane utilization. Fuel 2019;246:443–53. doi:10.1016/J.FUEL.2019.03.015.

[80] Mousa E, Wang C, Riesbeck J, Larsson M. Biomass applications in iron and steel industry: An overview of challenges and opportunities. Renew Sustain Energy Rev 2016;65:1247–66. doi:10.1016/J.RSER.2016.07.061.

[81] Li P, Sakuragi K, Makino H. Extraction techniques in sustainable biofuel production: A concise review. Fuel Process Technol 2019;193:295–303. doi:10.1016/J.FUPROC.2019.05.009.

[82] Hassan SS, Williams GA, Jaiswal AK. Moving towards the second generation of lignocellulosic biorefineries in the EU: Drivers, challenges, and opportunities. Renew Sustain Energy Rev 2019;101:590–9. doi:10.1016/J.RSER.2018.11.041.

[83] Cesário MT, da Fonseca MMR, Marques MM, de Almeida MCMD. Marine algal carbohydrates as carbon sources for the production of biochemicals and biomaterials. Biotechnol Adv 2018;36:798–817. doi:10.1016/J.BIOTECHADV.2018.02.006.

[84] Chen H, Wang L, Chen H, Wang L. Pandect of Practice Unit and Process Engineering of Biomass Biochemical Conversion. Technol Biochem Convers Biomass 2017:11–9. doi:10.1016/B978-0-12-802417-1.00002-8.

[85] Xu F, Li Y. Biomass Digestion. Encycl Sustain Technol 2017:197–204. doi:10.1016/B978-0-12-409548-9.10108-3.

[86] Advances in thermochemical conversion of woody biomass to energy, fuels and chemicals. Biotechnol Adv 2019;37:589–97. doi:10.1016/J.BIOTECHADV.2018.11.004.

[87] Malico I, Nepomuceno Pereira R, Gonçalves AC, Sousa AMO. Current status and future perspectives for energy production from solid biomass in the European industry. Renew Sustain Energy Rev 2019;112:960–77. doi:10.1016/J.RSER.2019.06.022.

[88] Wikberg H, Grönqvist S, Niemi P, Mikkelson A, Siika-aho M, Kanerva H, et al. Hydrothermal treatment followed by enzymatic hydrolysis and hydrothermal carbonization as means to valorise agro- and forest-based biomass residues. Bioresour Technol 2017;235:70–8. doi:10.1016/J.BIORTECH.2017.03.095.

[89] Mandø M. Direct combustion of biomass. Biomass Combust Sci Technol Eng 2013:61–83. doi:10.1533/9780857097439.2.61.

[90] Sansaniwal SK, Pal K, Rosen MA, Tyagi SK. Recent advances in the development of biomass gasification technology: A comprehensive review. Renew Sustain Energy Rev 2017;72:363–84. doi:10.1016/J.RSER.2017.01.038.

[91] Mansfield AB, Wooldridge MS. The effect of impurities on syngas combustion. Combust

Flame 2015;162:2286–95. doi:10.1016/J.COMBUSTFLAME.2015.01.026.

[92] Yasin M, Cha M, Chang IS, Atiyeh HK, Munasinghe P. Syngas Fermentation Into Biofuels and Biochemicals. Biofuels Altern Feed Convers Process Prod Liq Gaseous Biofuels 2019:301–27. doi:10.1016/B978-0-12-816856-1.00013-0.

[93] Samiran NA, Jaafar MNM, Ng J-H, Lam SS, Chong CT. Progress in biomass gasification technique – With focus on Malaysian palm biomass for syngas production. Renew Sustain Energy Rev 2016;62:1047–62. doi:10.1016/J.RSER.2016.04.049.

[94] Watson J, Zhang Y, Si B, Chen W-T, de Souza R. Gasification of biowaste: A critical review and outlooks. Renew Sustain Energy Rev 2018;83:1–17. doi:10.1016/J.RSER.2017.10.003.

[95] Hu X, Gholizadeh M. Biomass pyrolysis: A review of the process development and challenges from initial researches up to the commercialisation stage. J Energy Chem 2019;39:109–43. doi:10.1016/J.JECHEM.2019.01.024.

[96] Hawash SI, Farah JY, El-Diwani G. Pyrolysis of agriculture wastes for bio-oil and char production. J Anal Appl Pyrolysis 2017;124:369–72. doi:10.1016/J.JAAP.2016.12.021.

[97] Liu J, Huang L, Xie W, Kuo J, Buyukada M, Evrendilek F. Characterizing and optimizing (co-)pyrolysis as a function of different feedstocks, atmospheres, blend ratios, and heating rates. Bioresour Technol 2019;277:104–16. doi:10.1016/J.BIORTECH.2019.01.003.

[98] Wang C, Li L, Zeng Z, Xu X, Ma X, Chen R, et al. Catalytic performance of potassium in lignocellulosic biomass pyrolysis based on an optimized three-parallel distributed activation energy model. Bioresour Technol 2019;281:412–20. doi:10.1016/J.BIORTECH.2019.02.118.

[99] Quesada L, Pérez A, Godoy V, Peula FJ, Calero M, Blázquez G. Optimization of the pyrolysis process of a plastic waste to obtain a liquid fuel using different mathematical models. Energy Convers Manag 2019;188:19–26. doi:10.1016/J.ENCONMAN.2019.03.054.

[100] Macchi E. Theoretical basis of the Organic Rankine Cycle. Org Rank Cycle Power Syst 2017:3–24. doi:10.1016/B978-0-08-100510-1.00001-6.

[101] Tartière T, Astolfi M. A World Overview of the Organic Rankine Cycle Market. Energy

Procedia 2017;129:2–9. doi:10.1016/j.egypro.2017.09.159.

[102] F. Tchanche B, Pétrissans M, Papadakis G. Heat resources and organic Rankine cycle machines. Renew Sustain Energy Rev 2014;39:1185–99. doi:10.1016/J.RSER.2014.07.139.

[103] Mahmoudi A, Fazli M, Morad MR. A recent review of waste heat recovery by Organic Rankine Cycle. Appl Therm Eng 2018;143:660–75. doi:10.1016/J.APPLTHERMALENG.2018.07.136.

[104] Rahbar K, Mahmoud S, Al-Dadah RK, Moazami N, Mirhadizadeh SA. Review of organic Rankine cycle for small-scale applications. Energy Convers Manag 2017;134:135–55. doi:10.1016/J.ENCONMAN.2016.12.023.

[105] Anvari S, Taghavifar H, Parvishi A. Thermo- economical consideration of Regenerative organic Rankine cycle coupling with the absorption chiller systems incorporated in the trigeneration system. Energy Convers Manag 2017;148:317–29. doi:10.1016/J.ENCONMAN.2017.05.077.

[106] Jang Y, Lee J. Influence of superheat and expansion ratio on performance of organic Rankine cycle-based combined heat and power (CHP) system. Energy Convers Manag 2018;171:82–97. doi:10.1016/J.ENCONMAN.2018.05.053.

[107] Zhang H-H, Xi H, He Y-L, Zhang Y-W, Ning B. Experimental study of the organic rankine cycle under different heat and cooling conditions. Energy 2019;180:678–88. doi:10.1016/J.ENERGY.2019.05.072.

[108] Liu P, Shu G, Tian H. How to approach optimal practical Organic Rankine cycle (OP-ORC) by configuration modification for diesel engine waste heat recovery. Energy 2019;174:543–52. doi:10.1016/J.ENERGY.2019.03.016.

[109] Wang X, Levy EK, Pan C, Romero CE, Banerjee A, Rubio-Maya C, et al. Working fluid selection for organic Rankine cycle power generation using hot produced supercritical CO2 from a geothermal reservoir. Appl Therm Eng 2019;149:1287–304. doi:10.1016/J.APPLTHERMALENG.2018.12.112.

[110] Mondejar ME, Andreasen JG, Pierobon L, Larsen U, Thern M, Haglind F. A review of the use of organic Rankine cycle power systems for maritime applications. Renew Sustain Energy Rev 2018;91:126–51. doi:10.1016/J.RSER.2018.03.074.

[111] Reis MML, Guillen JA V., Gallo WLR. Off-design performance analysis and optimization of the power production by an organic Rankine cycle coupled with a gas turbine in an offshore oil platform. Energy Convers Manag 2019;196:1037–50. doi:10.1016/J.ENCONMAN.2019.06.051.

[112] Ahmed A, Esmaeil KK, Irfan MA, Al-Mufadi FA. Design methodology of organic Rankine cycle for waste heat recovery in cement plants. Appl Therm Eng 2018;129:421–30. doi:10.1016/J.APPLTHERMALENG.2017.10.019.

[113] Peris B, Navarro-Esbrí J, Molés F, Mota-Babiloni A. Experimental study of an ORC (organic Rankine cycle) for low grade waste heat recovery in a ceramic industry. Energy 2015;85:534–42. doi:10.1016/J.ENERGY.2015.03.065.

[114] Campana F, Bianchi M, Branchini L, De Pascale A, Peretto A, Baresi M, et al. ORC waste heat recovery in European energy intensive industries: Energy and GHG savings. Energy Convers Manag 2013;76:244–52. doi:10.1016/J.ENCONMAN.2013.07.041.

[115] Ramirez M, Epelde M, de Arteche MG, Panizza A, Hammerschmid A, Baresi M, et al. Performance evaluation of an ORC unit integrated to a waste heat recovery system in a steel mill. Energy Procedia 2017;129:535–42. doi:10.1016/J.EGYPRO.2017.09.183.

[116] Zanellato L, Astolfi M, Serafino A, Rizzi D, Macchi E. Field performance evaluation of geothermal ORC power plants with a focus on radial outflow turbines. Renew Energy 2018. doi:10.1016/J.RENENE.2018.08.068.

[117] Pereira JS, Ribeiro JB, Mendes R, Vaz GC, André JC. ORC based micro-cogeneration systems for residential application – A state of the art review and current challenges. Renew Sustain Energy Rev 2018;92:728–43. doi:10.1016/J.RSER.2018.04.039.

[118] Briola S, Gabbrielli R, Bischi A. Off-design performance analysis of a novel hybrid binary

geothermal-biomass power plant in extreme environmental conditions. Energy Convers Manag 2019;195:210–25. doi:10.1016/J.ENCONMAN.2019.05.008.

[119] Manfrida G, Pacini L, Talluri L. An upgraded Tesla turbine concept for ORC applications. Energy 2018;158:33–40. doi:10.1016/J.ENERGY.2018.05.181.

[120] Talluri L, Fiaschi D, Neri G, Ciappi L. Design and optimization of a Tesla turbine for ORC applications. Appl Energy 2018;226:300–19. doi:10.1016/J.APENERGY.2018.05.057.

[121] Pereira JS, Ribeiro JB, Mendes R, André JC. Analysis of a hybrid (topping/bottoming) ORC based CHP configuration integrating a new evaporator design concept for residential applications. Appl Therm Eng 2019;160:113984. doi:10.1016/J.APPLTHERMALENG.2019.113984.

[122] Miao Z, Zhang K, Wang M, Xu J. Thermodynamic selection criteria of zeotropic mixtures for subcritical organic Rankine cycle. Energy 2019;167:484–97. doi:10.1016/J.ENERGY.2018.11.002.

[123] Aboelwafa O, Fateen SEK, Soliman A, Ismail IM. A review on solar Rankine cycles: Working fluids, applications, and cycle modifications. Renew Sustain Energy Rev 2018;82:868–85. doi:10.1016/j.rser.2017.09.097.

[124] Heberle F, Hofer M, Ürlings N, Schröder H, Anderlohr T, Brüggemann D. Techno-economic analysis of a solar thermal retrofit for an air-cooled geothermal Organic Rankine Cycle power plant. Renew Energy 2017;113:494–502. doi:10.1016/j.renene.2017.06.031.

[125] Dimarzio G, Angelini L, Price W, Chin C, Harris S. The Stillwater Triple Hybrid Power Plant: Integrating Geothermal , Solar Photovoltaic and Solar Thermal Power Generation. World Geotherm. Congr. 2015, 2015, p. 5.

[126] Hussain CMI, Norton B, Duffy A. Technological assessment of different solar-biomass systems for hybrid power generation in Europe. Renew Sustain Energy Rev 2017;68:1115–29. doi:10.1016/j.rser.2016.08.016.

[127] Peterseim JH, Hellwig U, Tadros A, White S. Hybridisation optimization of concentrating

solar thermal and biomass power generation facilities. Sol Energy 2014;99:203–14. doi:10.1016/j.solener.2013.10.041.

[128] Saidur R, Abdelaziz EA, Demirbas A, Hossain MS, Mekhilef S. A review on biomass as a fuel for boilers. Renew Sustain Energy Rev 2011;15:2262–89. doi:10.1016/j.rser.2011.02.015.

[129] Bajwa DS, Peterson T, Sharma N, Shojaeiarani J, Bajwa SG. A review of densified solid biomass for energy production. Renew Sustain Energy Rev 2018;96:296–305. doi:10.1016/J.RSER.2018.07.040.

[130] Anvari S, Khalilarya S, Zare V. Power generation enhancement in a biomass-based combined cycle using solar energy: Thermodynamic and environmental analysis. Appl Therm Eng 2019;153:128–41. doi:10.1016/j.applthermaleng.2019.02.112.

[131] Liu Q, Bai Z, Wang X, Lei J, Jin H. Investigation of thermodynamic performances for two solar-biomass hybrid combined cycle power generation systems. Energy Convers Manag 2016;122:252–62. doi:10.1016/j.enconman.2016.05.080.

[132] Bai Z, Liu Q, Hong H, Jin H. Thermodynamics evaluation of a solar-biomass power generation system integrated a two-stage gasifier. Energy Procedia 2016;88:368–74. doi:10.1016/j.egypro.2016.06.134.

[133] Bai Z, Liu Q, Lei J, Wang X, Sun J, Jin H. Thermodynamic evaluation of a novel solar-biomass hybrid power generation system. Energy Convers Manag 2017;142:296–306. doi:10.1016/j.enconman.2017.03.028.

[134] Sterrer R, Schidler S, Schwandt O, Franz P, Hammerschmid A. Theoretical analysis of the combination of CSP with a biomass CHP-plant using ORC-technology in Central Europe. Energy Procedia 2013;49:1218–27. doi:10.1016/j.egypro.2014.03.131.

[135] Zourellis A, Perers B, Donneborg J, Matoricz J. Optimizing Efficiency of Biomass—Fired Organic Rankine Cycle with Concentrated Solar Power in Denmark. Energy Procedia 2018;149:420–6. doi:10.1016/J.EGYPRO.2018.08.206.

[136] Soares J, Oliveira AC. Numerical simulation of a hybrid concentrated solar power/biomass mini power plant. Appl Therm Eng 2017;111:1378–86. doi:10.1016/J.APPLTHERMALENG.2016.06.180.

[137] Desideri A, Amicabile S, Alberti F, Vitali-Nari S, Quoilin S, Crema L, et al. Dynamic modeling and control strategies analysis of a novel small CSP biomass plant for cogeneration applications in building. Sol. World Congr., 2015, p. 8–12. doi:10.18086/swc.2015.04.14.

[138] Pantaleo AM, Camporeale SM, Miliozzi A, Russo V, Shah N, Markides CN. Novel hybrid CSP-biomass CHP for flexible generation: Thermo-economic analysis and profitability assessment. Appl Energy 2017;204:994–1006. doi:10.1016/j.apenergy.2017.05.019.

[139] Pantaleo AM, Camporeale SM, Sorrentino A, Miliozzi A, Shah N, Markides CN. Hybrid solar-biomass combined Brayton/organic Rankine-cycle plants integrated with thermal storage: Techno-economic feasibility in selected Mediterranean areas. Renew Energy 2018. doi:10.1016/J.RENENE.2018.08.022.

[140] Sadeghi M, Nemati A, ghavimi A, Yari M. Thermodynamic analysis and multi-objective optimization of various ORC (organic Rankine cycle) configurations using zeotropic mixtures. Energy 2016;109:791–802. doi:10.1016/j.energy.2016.05.022.

[141] Demir ME. 4.8 Steam and Organic Rankine Cycles. Compr Energy Syst 2018:264–311. doi:10.1016/B978-0-12-809597-3.00410-7.

[142] Regulation (EU) No 517/2014 of the European Parliament and of the council of 16 April 2014 on fluorinated greenhouse gases and repealing Regulation (EC) No 842/2006 n.d. https://eur-lex.europa.eu/legal-content/EN/TXT/?uri=uriserv:OJ.L_.2014.150.01.0195.01.ENG (accessed May 2, 2019).

[143] Durkee J, Durkee J. US and global environmental regulations. Manag Ind Clean Technol Process 2006:43–98. doi:10.1016/B978-008044888-6/50016-8.

[144] Aghahosseini S, Dincer I. Comparative performance analysis of low-temperature Organic Rankine Cycle (ORC) using pure and zeotropic working fluids. Appl Therm Eng

2013;54:35–42. doi:10.1016/j.applthermaleng.2013.01.028.

[145] Chen H, Goswami DY, Rahman MM, Stefanakos EK. A supercritical Rankine cycle using zeotropic mixture working fluids for the conversion of low-grade heat into power. Energy 2011;36:549–55. doi:10.1016/J.ENERGY.2010.10.006.

[146] Zhao L, Bao J. Thermodynamic analysis of organic Rankine cycle using zeotropic mixtures. Appl Energy 2014;130:748–56. doi:10.1016/J.APENERGY.2014.03.067.

[147] Su W, Hwang Y, Deng S, Zhao L, Zhao D. Thermodynamic performance comparison of Organic Rankine Cycle between zeotropic mixtures and pure fluids under open heat source. Energy Convers Manag 2018;165:720–37. doi:10.1016/J.ENCONMAN.2018.03.071.

[148] Chys M, van den Broek M, Vanslambrouck B, De Paepe M. Potential of zeotropic mixtures as working fluids in organic Rankine cycles. Energy 2012;44:623–32. doi:10.1016/J.ENERGY.2012.05.030.

[149] Heberle F, Preißinger M, Brüggemann D. Zeotropic mixtures as working fluids in Organic Rankine Cycles for low-enthalpy geothermal resources. Renew Energy 2012;37:364–70. doi:10.1016/j.renene.2011.06.044.

[150] Radulovic J, Beleno Castaneda NI. On the potential of zeotropic mixtures in supercritical ORC powered by geothermal energy source. Energy Convers Manag 2014;88:365–71. doi:10.1016/J.ENCONMAN.2014.08.048.

[151] Kang Z, Zhu J, Lu X, Li T, Wu X. Parametric optimization and performance analysis of zeotropic mixtures for an organic Rankine cycle driven by low-medium temperature geothermal fluids. Appl Therm Eng 2015;89:323–31. doi:10.1016/J.APPLTHERMALENG.2015.06.024.

[152] Liu Q, Shen A, Duan Y. Parametric optimization and performance analyses of geothermal organic Rankine cycles using R600a/R601a mixtures as working fluids. Appl Energy 2015;148:410–20. doi:10.1016/J.APENERGY.2015.03.093.

[153] Yue C, Han D, Pu W, He W. Thermal matching performance of a geothermal ORC system

using zeotropic working fluids. Renew Energy 2015;80:746–54. doi:10.1016/J.RENENE.2015.02.063.

[154] Ge Z, Li J, Liu Q, Duan Y, Yang Z. Thermodynamic analysis of dual-loop organic Rankine cycle using zeotropic mixtures for internal combustion engine waste heat recovery. Energy Convers Manag 2018;166:201–14. doi:10.1016/J.ENCONMAN.2018.04.027.

[155] Xi X, Zhou Y, Guo C, Yang L, Du X. Characteristics of Organic Rankine Cycles with Zeotropic Mixture for Heat Recovery of Exhaust Gas of Boiler. Energy Procedia 2015;75:1093–101. doi:10.1016/J.EGYPRO.2015.07.496.

[156] Song J, Gu C. Analysis of ORC (Organic Rankine Cycle) systems with pure hydrocarbons and mixtures of hydrocarbon and retardant for engine waste heat recovery. Appl Therm Eng 2015;89:693–702. doi:10.1016/J.APPLTHERMALENG.2015.06.055.

[157] Li Y-R, Du M-T, Wu C-M, Wu S-Y, Liu C. Potential of organic Rankine cycle using zeotropic mixtures as working fluids for waste heat recovery. Energy 2014;77:509–19. doi:10.1016/J.ENERGY.2014.09.035.

[158] Braimakis K, Preißinger M, Brüggemann D, Karellas S, Panopoulos K. Low grade waste heat recovery with subcritical and supercritical Organic Rankine Cycle based on natural refrigerants and their binary mixtures. Energy 2015;88:80–92. doi:10.1016/J.ENERGY.2015.03.092.

[159] Yang K, Zhang H, Wang Z, Zhang J, Yang F, Wang E, et al. Study of zeotropic mixtures of ORC (organic Rankine cycle) under engine various operating conditions. Energy 2013;58:494–510. doi:10.1016/J.ENERGY.2013.04.074.

[160] Shu G, Gao Y, Tian H, Wei H, Liang X. Study of mixtures based on hydrocarbons used in ORC (Organic Rankine Cycle) for engine waste heat recovery. Energy 2014;74:428–38. doi:10.1016/J.ENERGY.2014.07.007.

[161] Zhang J, Zhang H, Yang K, Yang F, Wang Z, Zhao G, et al. Performance analysis of regenerative organic Rankine cycle (RORC) using the pure working fluid and the zeotropic

mixture over the whole operating range of a diesel engine. Energy Convers Manag 2014;84:282–94. doi:10.1016/J.ENCONMAN.2014.04.036.

[162] Weith T, Heberle F, Preißinger M, Brüggemann D. Performance of siloxane mixtures in a high-temperature organic rankine cycle considering the heat transfer characteristics during evaporation. Energies 2014;7:5548–65. doi:10.3390/en7095548.

[163] Aboelwafa O, Fateen S-EK, Soliman A, Ismail IM. A review on solar Rankine cycles: Working fluids, applications, and cycle modifications. Renew Sustain Energy Rev 2018;82:868–85. doi:10.1016/J.RSER.2017.09.097.

[164] Zheng N, Wei J, Zhao L. Analysis of a solar Rankine cycle powered refrigerator with zeotropic mixtures. Sol Energy 2018;162:57–66. doi:10.1016/J.SOLENER.2018.01.011.

[165] Wang XD, Zhao L. Analysis of zeotropic mixtures used in low-temperature solar Rankine cycles for power generation. Sol Energy 2009;83:605–13. doi:10.1016/J.SOLENER.2008.10.006.

[166] Wang JL, Zhao L, Wang XD. A comparative study of pure and zeotropic mixtures in low-temperature solar Rankine cycle. Appl Energy 2010;87:3366–73. doi:10.1016/J.APENERGY.2010.05.016.

[167] Mavrou P, Papadopoulos AI, Stijepovic M, Seferlis P, Linke P, Voutetakis S. Assessment of working fluid mixtures for solar organic Rankine cycles. Chem Eng Trans 2014;39:283–8. doi:10.3303/CET1439048.

[168] Habka M, Ajib S. Performance estimation of mixtures in solar Organic Rankine Cycle with two mini cogeneration options for improvement purpose. Sustain Energy Technol Assessments 2016;16:174–89. doi:10.1016/J.SETA.2016.06.002.

[169] Le VL, Kheiri A, Feidt M, Pelloux-Prayer S. Thermodynamic and economic optimizations of a waste heat to power plant driven by a subcritical ORC (Organic Rankine Cycle) using pure or zeotropic working fluid. Energy 2014;78:622–38. doi:10.1016/J.ENERGY.2014.10.051.

[170] Heberle F, Brüggemann D. Thermo-economic evaluation of organic rankine cycles for

geothermal power generation using zeotropic mixtures. Energies 2015;8:2097–124. doi:10.3390/en8032097.

[171] Heberle F, Brüggemann D. Thermo-economic analysis of zeotropic mixtures and pure working fluids in Organic Rankine Cycles for waste heat recovery. Energies 2016;9. doi:10.3390/en9040226.

[172] Oyewunmi O, Markides C. Thermo-Economic and Heat Transfer Optimization of Working-Fluid Mixtures in a Low-Temperature Organic Rankine Cycle System. Energies 2016;9:448. doi:10.3390/en9060448.

[173] Feng Y, Hung T, Greg K, Zhang Y, Li B, Yang J. Thermoeconomic comparison between pure and mixture working fluids of organic Rankine cycles (ORCs) for low temperature waste heat recovery. Energy Convers Manag 2015;106:859–72. doi:10.1016/J.ENCONMAN.2015.09.042.

[174] Feng Y, Hung T, Zhang Y, Li B, Yang J, Shi Y. Performance comparison of low-grade ORCs (organic Rankine cycles) using R245fa, pentane and their mixtures based on the thermoeconomic multi-objective optimization and decision makings. Energy 2015;93:2018–29. doi:10.1016/J.ENERGY.2015.10.065.

[175] Yang M-H, Yeh R-H, Hung T-C. Thermo-economic analysis of the transcritical organic Rankine cycle using R1234yf/R32 mixtures as the working fluids for lower-grade waste heat recovery. Energy 2017;140:818–36. doi:10.1016/J.ENERGY.2017.08.059.

[176] Kolahi M, Yari M, Mahmoudi SMS, Mohammadkhani F. Thermodynamic and economic performance improvement of ORCs through using zeotropic mixtures: Case of waste heat recovery in an offshore platform. Case Stud Therm Eng 2016;8:51–70. doi:10.1016/J.CSITE.2016.05.001.

[177] Dong B, Xu G, Luo X, Zhuang L, Quan Y. Potential of Low Temperature Organic Rankine Cycle with Zeotropic Mixtures as Working Fluid. Energy Procedia 2017;105:1489–94. doi:10.1016/J.EGYPRO.2017.03.444.

[178] Li S, Dai Y. Thermo-Economic Analysis of Waste Heat Recovery ORC Using Zeotropic Mixtures. J Energy Eng 2015;141:04014050. doi:10.1061/(ASCE)EY.1943-7897.0000245.

[179] Liu C, Gao T. Off-design performance analysis of basic ORC, ORC using zeotropic mixtures and composition-adjustable ORC under optimal control strategy. Energy 2019;171:95–108. doi:10.1016/j.energy.2018.12.195.

[180] Collings P, Yu Z, Wang E. A dynamic organic Rankine cycle using a zeotropic mixture as the working fluid with composition tuning to match changing ambient conditions. Appl Energy 2016;171:581–91. doi:10.1016/j.apenergy.2016.03.014.

[181] Wang E, Yu Z, Collings P. Dynamic control strategy of a distillation system for a composition-adjustable organic Rankine cycle. Energy 2017;141:1038–51. doi:10.1016/J.ENERGY.2017.09.141.

[182] T. J. Kotas. The exergy method of thermal plant analysis. Butterworths; 1985.

[183] Dincer I, Rosen MA. Exergy. Elsevier Ltd; 2013.

[184] Tsatsaronis G, Park MH. On avoidable and unavoidable exergy destructions and investment costs in thermal systems. Energy Convers Manag 2002;43:1259–70. doi:10.1016/S0196-8904(02)00012-2.

[185] Leiva-Illanes R, Escobar R, Cardemil JM, Alarcón-Padilla D-C, Uche J, Martínez A. Exergy cost assessment of CSP driven multi-generation schemes: Integrating seawater desalination, refrigeration, and process heat plants. Energy Convers Manag 2019;179:249–69. doi:10.1016/J.ENCONMAN.2018.10.050.

[186] Ahmadi P. 1.8 Exergoeconomics. Compr Energy Syst 2018:340–76. doi:10.1016/B978-0-12-809597-3.00107-3.

[187] Lazzaretto A, Tsatsaronis G. SPECO: A systematic and general methodology for calculating efficiencies and costs in thermal systems. Energy 2006;31:1257–89. doi:10.1016/j.energy.2005.03.011.

[188] Torres C, Valero A, Serra L, Royo J. Structural theory and thermoeconomic diagnosis: Part I.

On malfunction and dysfunction analysis. Energy Convers Manag 2002;43:1503–18. doi:10.1016/S0196-8904(02)00032-8.

[189] Valero A, Usón S, Torres C, Valero A, Agudelo A, Costa J. Thermoeconomic tools for the analysis of eco-industrial parks. Energy 2013;62:62–72. doi:10.1016/J.ENERGY.2013.07.014.

[190] Yürüsoy M, Keçebaş A. Advanced exergo-environmental analyses and assessments of a real district heating system with geothermal energy. Appl Therm Eng 2017;113:449–59. doi:10.1016/J.APPLTHERMALENG.2016.11.054.

[191] Faleh N, Khila Z, Wahada Z, Pons M-N, Houas A, Hajjaji N. Exergo-environmental life cycle assessment of biodiesel production from mutton tallow transesterification. Renew Energy 2018;127:74–83. doi:10.1016/J.RENENE.2018.04.046.

[192] Abam FI, Briggs TA, Ekwe EB, Effiom SO. Investigation of intercooler-effectiveness on exergo-economic and exergo-sustainability parameters of modified Brayton cycles. Case Stud Therm Eng 2017;10:9–18. doi:10.1016/J.CSITE.2017.03.001.

[193] Balli O. Advanced exergy analyses to evaluate the performance of a military aircraft turbojet engine (TJE) with afterburner system: Splitting exergy destruction into unavoidable/avoidable and endogenous/exogenous. Appl Therm Eng 2017;111:152–69. doi:10.1016/J.APPLTHERMALENG.2016.09.036.

[194] Mortazavi A, Ameri M. Conventional and advanced exergy analysis of solar flat plate air collectors. Energy 2018;142:277–88. doi:10.1016/j.energy.2017.10.035.

[195] Ebrahimi M, Carriveau R, Ting DS-K, McGillis A. Conventional and advanced exergy analysis of a grid connected underwater compressed air energy storage facility. Appl Energy 2019;242:1198–208. doi:10.1016/J.APENERGY.2019.03.135.

[196] Liu Z, Liu B, Guo J, Xin X, Yang X. Conventional and advanced exergy analysis of a novel transcritical compressed carbon dioxide energy storage system. Energy Convers Manag 2019;198:111807. doi:10.1016/J.ENCONMAN.2019.111807.

[197] Valero A, Valero A. Exergoecology: A thermodynamic approach for accounting the Earth's mineral capital. The case of bauxite–aluminium and limestone–lime chains. Energy 2010;35:229–38. doi:10.1016/J.ENERGY.2009.09.013.

[198] Torres C, Valero A, Valero A. Exergoecology as a tool for ecological modelling. The case of the US food production chain. Ecol Modell 2013;255:21–8. doi:10.1016/J.ECOLMODEL.2013.01.021.

[199] http://www.exergoecology.com/exergoecology n.d.

[200] Mady CEK, Albuquerque C, Fernandes TL, Hernandez AJ, Saldiva PHN, Yanagihara JI, et al. Exergy performance of human body under physical activities. Energy 2013;62:370–8. doi:10.1016/J.ENERGY.2013.09.050.

[201] Mady CEK, Ferreira MS, Yanagihara JI, de Oliveira S. Human body exergy analysis and the assessment of thermal comfort conditions. Int J Heat Mass Transf 2014;77:577–84. doi:10.1016/J.IJHEATMASSTRANSFER.2014.05.039.

[202] Henriques IB, Mady CEK, de Oliveira Junior S. Exergy model of the human heart. Energy 2016;117:612–9. doi:10.1016/J.ENERGY.2016.02.150.

[203] Wang J, Lu Z, Li M, Lior N, Li W. Energy, exergy, exergoeconomic and environmental (4E) analysis of a distributed generation solar-assisted CCHP (combined cooling, heating and power) gas turbine system. Energy 2019;175:1246–58. doi:10.1016/J.ENERGY.2019.03.147.

[204] Nemati A, Nami H, Yari M. Assessment of different configurations of solar energy driven organic flash cycles (OFCs) via exergy and exergoeconomic methodologies. Renew Energy 2018;115:1231–48. doi:10.1016/J.RENENE.2017.08.096.

[205] Soltani S, Mahmoudi SMS, Yari M, Morosuk T, Rosen MA, Zare V. A comparative exergoeconomic analysis of two biomass and co-firing combined power plants. Energy Convers Manag 2013;76:83–91. doi:10.1016/J.ENCONMAN.2013.07.030.

[206] Wang J, Li M, Ren F, Li X, Liu B. Modified exergoeconomic analysis method based on

energy level with reliability consideration: Cost allocations in a biomass trigeneration system. Renew Energy 2018;123:104–16. doi:10.1016/J.RENENE.2018.02.040.

[207] Behzadi A, Gholamian E, Houshfar E, Habibollahzade A. Multi-objective optimization and exergoeconomic analysis of waste heat recovery from Tehran's waste-to-energy plant integrated with an ORC unit. Energy 2018;160:1055–68. doi:10.1016/J.ENERGY.2018.07.074.

[208] Dai B, Zhu K, Wang Y, Sun Z, Liu Z. Evaluation of organic Rankine cycle by using hydrocarbons as working fluids: Advanced exergy and advanced exergoeconomic analyses. Energy Convers Manag 2019;197:111876. doi:10.1016/J.ENCONMAN.2019.111876.

[209] Wang J, Yang Y. Energy, exergy and environmental analysis of a hybrid combined cooling heating and power system utilizing biomass and solar energy. Energy Convers Manag 2016;124:566–77. doi:10.1016/J.ENCONMAN.2016.07.059.

[210] Anvari S, Khalilarya S, Zare V. Exergoeconomic and environmental analysis of a novel configuration of solar-biomass hybrid power generation system. Energy 2018;165:776–89. doi:10.1016/J.ENERGY.2018.10.018.

[211] Eren Y, Küçükdemiral İB, Üstoğlu İ. Introduction to Optimization. Optim Renew Energy Syst 2017:27–74. doi:10.1016/B978-0-08-101041-9.00002-8.

[212] Nguyen TT. A high performance social spider optimization algorithm for optimal power flow solution with single objective optimization. Energy 2019;171:218–40. doi:10.1016/J.ENERGY.2019.01.021.

[213] Lu Y, Wang S, Zhao Y, Yan C. Renewable energy system optimization of low/zero energy buildings using single-objective and multi-objective optimization methods. Energy Build 2015;89:61–75. doi:10.1016/J.ENBUILD.2014.12.032.

[214] Bejan A, Mamut E, editors. Thermodynamic Optimization of Complex Energy Systems. Kluwer Academic Publishers; 1999.

[215] Larsson C, Larsson C. Optimization Techniques. 5G Networks 2018:103–22.

doi:10.1016/B978-0-12-812707-0.00010-3.

[216] Bejan A. Method of entropy generation minimization, or modeling and optimization based on combined heat transfer and thermodynamics. Rev Générale Therm 1996;35:637–46. doi:10.1016/S0035-3159(96)80059-6.

[217] Bejan A. Constructal theory: from thermodynamic and geometric optimization to predicting shape in nature. Energy Convers Manag 1998;39:1705–18. doi:10.1016/S0196-8904(98)00054-5.

[218] Vaccari M, Mancuso GM, Riccardi J, Cantù M, Pannocchia G. A Sequential Linear Programming algorithm for economic optimization of Hybrid Renewable Energy Systems. J Process Control 2019;74:189–201. doi:10.1016/J.JPROCONT.2017.08.015.

[219] Bahlawan H, Morini M, Pinelli M, Spina PR. Dynamic programming based methodology for the optimization of the sizing and operation of hybrid energy plants. Appl Therm Eng 2019;160:113967. doi:10.1016/J.APPLTHERMALENG.2019.113967.

[220] Agamah SU, Ekonomou L. Energy storage system scheduling for peak demand reduction using evolutionary combinatorial optimisation. Sustain Energy Technol Assessments 2017;23:73–82. doi:10.1016/J.SETA.2017.08.003.

[221] Nasruddin, Sholahudin, Satrio P, Mahlia TMI, Giannetti N, Saito K. Optimization of HVAC system energy consumption in a building using artificial neural network and multi-objective genetic algorithm. Sustain Energy Technol Assessments 2019;35:48–57. doi:10.1016/J.SETA.2019.06.002.

[222] Sarma U, Ganguly S. Determination of the component sizing for the PEM fuel cell-battery hybrid energy system for locomotive application using particle swarm optimization. J Energy Storage 2018;19:247–59. doi:10.1016/J.EST.2018.08.008.

[223] Keshtkar A, Arzanpour S. An adaptive fuzzy logic system for residential energy management in smart grid environments. Appl Energy 2017;186:68–81. doi:10.1016/J.APENERGY.2016.11.028.

[224] Elsheikh AH, Sharshir SW, Abd Elaziz M, Kabeel AE, Guilan W, Haiou Z. Modeling of solar energy systems using artificial neural network: A comprehensive review. Sol Energy 2019;180:622–39. doi:10.1016/J.SOLENER.2019.01.037.

[225] Zhang W, Maleki A, Rosen MA, Liu J. Sizing a stand-alone solar-wind-hydrogen energy system using weather forecasting and a hybrid search optimization algorithm. Energy Convers Manag 2019;180:609–21. doi:10.1016/J.ENCONMAN.2018.08.102.

[226] Bravo R, Friedrich D. Two-stage optimisation of hybrid solar power plants. Sol Energy 2018;164:187–99. doi:10.1016/J.SOLENER.2018.01.078.

[227] Akbari Vakilabadi M, Bidi M, Najafi AF. Energy, Exergy analysis and optimization of solar thermal power plant with adding heat and water recovery system. Energy Convers Manag 2018;171:1639–50. doi:10.1016/J.ENCONMAN.2018.06.094.

[228] Costa M, Rocco V, Caputo C, Cirillo D, Di Blasio G, La Villetta M, et al. Model based optimization of the control strategy of a gasifier coupled with a spark ignition engine in a biomass powered cogeneration system. Appl Therm Eng 2019;160:114083. doi:10.1016/J.APPLTHERMALENG.2019.114083.

[229] Han J, Kim J. Process Simulation and Optimization of 10-MW EFB Power Plant. Comput Aided Chem Eng 2018;43:723–9. doi:10.1016/B978-0-444-64235-6.50128-5.

[230] Sahoo U, Kumar R, Singh SK, Tripathi AK. Energy, exergy, economic analysis and optimization of polygeneration hybrid solar-biomass system. Appl Therm Eng 2018;145:685–92. doi:10.1016/J.APPLTHERMALENG.2018.09.093.

[231] Lee Y, Kim J, Ahmed U, Kim C, Lee Y-W. Multi-objective optimization of Organic Rankine Cycle (ORC) design considering exergy efficiency and inherent safety for LNG cold energy utilization. J Loss Prev Process Ind 2019;58:90–101. doi:10.1016/J.JLP.2019.01.006.

[232] Özahi E, Tozlu A, Abuşoğlu A. Thermoeconomic multi-objective optimization of an organic Rankine cycle (ORC) adapted to an existing solid waste power plant. Energy Convers Manag 2018;168:308–19. doi:10.1016/J.ENCONMAN.2018.04.103.

[233] MathWorks stellt mit dem Release 2017b für MATLAB und Simulink neue Funktionen für Deep Learning vor - MATLAB & Simulink n.d. https://de.mathworks.com/company/newsroom/mathworks-announces-release-2017b-of-the-matlab-and-simulink-product-families.html (accessed September 21, 2018).

[234] Aspen Technology n.d. https://www.aspentech.com/en/products/pages/aspen-simulation-workbook (accessed September 21, 2018).

[235] Gölles M, Reiter S, Brunner T, Dourdoumas N, Obernberger I. Model based control of a small-scale biomass boiler. Control Eng Pract 2014;22:94–102. doi:10.1016/j.conengprac.2013.09.012.

[236] Mureddu M, Dessì F, Orsini A, Ferrara F, Pettinau A. Air- and oxygen-blown characterization of coal and biomass by thermogravimetric analysis. Fuel 2018;212:626–37. doi:10.1016/j.fuel.2017.10.005.

[237] Manente G, Toffolo A, Lazzaretto A, Paci M. An Organic Rankine Cycle off-design model for the search of the optimal control strategy. Energy 2013;58:97–106. doi:10.1016/j.energy.2012.12.035.

[238] TEMA. Standards of the Tubular Exchanger, 8th Edition 1999.

[239] Ghasemi H, Sheu E, Tizzanini A, Paci M, Mitsos A. Hybrid solar–geothermal power generation: Optimal retrofitting. Appl Energy 2014;131:158–70. doi:10.1016/J.APENERGY.2014.06.010.

[240] Meteonorm: Meteonorm Software n.d. https://www.meteonorm.com/en/product/productpage/meteonorm-software (accessed October 24, 2018).

[241] Petrollese M, Cocco D. Optimal design of a hybrid CSP-PV plant for achieving the full dispatchability of solar energy power plants. Sol Energy 2016;137:477–89. doi:10.1016/j.solener.2016.08.027.

[242] GmbH eclareon. single 2017.

[243] GmbH E. single 2017.

[244] Askari IB, Ameri M, Calise F. Energy, exergy and exergo-economic analysis of different water desalination technologies powered by Linear Fresnel solar field. Desalination 2018;425:37–67. doi:10.1016/j.desal.2017.10.008.

[245] Rovira A, Barbero R, Montes MJ, Abbas R, Varela F. Analysis and comparison of Integrated Solar Combined Cycles using parabolic troughs and linear Fresnel reflectors as concentrating systems. Appl Energy 2016;162:990–1000. doi:10.1016/j.apenergy.2015.11.001.

[246] Petrollese M, Cocco D, Migliari L, Cau G. Techno-economic analysis of a hybrid CSP-CPV power plant. Proc. ECOS 2016 - 29th Int. Conf. Effic. Cost, Optim. Simul. Environ. Impact Energy Syst. June 19-23, PortoroŽ, Slovenia: 2016.

[247] Hottel HC. A simple model for estimating the transmittance of direct solar radiation through clear atmospheres. Sol Energy 1976;18:129–34. doi:10.1016/0038-092X(76)90045-1.

[248] Weiß AP, Popp T, Müller J, Hauer J, Brüggemann D, Preißinger M. Experimental characterization and comparison of an axial and a cantilever micro-turbine for small-scale Organic Rankine Cycle. Appl Therm Eng 2018;140:235–44. doi:10.1016/j.applthermaleng.2018.05.033.

[249] Ueckerdt F, Hirth L, Luderer G, Edenhofer O. System LCOE: What are the costs of variable renewables? Energy 2013;63:61–75. doi:10.1016/j.energy.2013.10.072.

[250] Patil VR, Biradar VI, Shreyas R, Garg P, Orosz MS, Thirumalai NC. Techno-economic comparison of solar organic Rankine cycle (ORC) and photovoltaic (PV) systems with energy storage. Renew Energy 2017;113:1250–60. doi:10.1016/J.RENENE.2017.06.107.

[251] Desai NB, Bandyopadhyay S. Thermo-economic analysis and selection of working fluid for solar organic Rankine cycle. Appl Therm Eng 2016;95:471–81. doi:10.1016/j.applthermaleng.2015.11.018.

[252] Petela R. Exergy of Heat Radiation. J Heat Transfer 2012;86:187. doi:10.1115/1.3687092.

[253] Nag PK. Power plant engineering. Tata McGraw-Hill Publishing Company Ltd; 2008.

[254] Demir ME, Dincer I. Development and analysis of a new integrated solar energy system with thermal storage for fresh water and power production. Int J Energy Res 2018;42:2864–74. doi:10.1002/er.3846.

[255] Bell IH, Wronski J, Quoilin S, Lemort V. Pure and pseudo-pure fluid thermophysical property evaluation and the open-source thermophysical property library coolprop. Ind Eng Chem Res 2014;53:2498–508. doi:10.1021/ie4033999.

[256] Turton R, Bailie RC, Whiting WB, Shaeiwitz JA, Bhattacharyya D. Analysis , Synthesis , and Design of Chemical Processes. vol. 106. fourth ed. Upper Saddle River, NJ (USA): Prentice Hall; 2012.

[257] Zhang X, Li H, Liu L, Bai C, Wang S, Song Q, et al. Exergetic and exergoeconomic assessment of a novel CHP system integrating biomass partial gasification with ground source heat pump. Energy Convers Manag 2018;156:666–79. doi:10.1016/j.enconman.2017.11.075.

[258] Jiang XZ, Wang X, Feng L, Zheng D, Shi L. Adapted computational method of energy level and energy quality evolution for combined cooling, heating and power systems with energy storage units. Energy 2017;120:209–16. doi:10.1016/j.energy.2016.12.124.

[259] Wang Z, Han W, Zhang N, Liu M, Jin H. Exergy cost allocation method based on energy level (ECAEL) for a CCHP system. Energy 2017;134:240–7. doi:10.1016/j.energy.2017.06.015.

[260] Miao Z, Zhang K, Wang M, Xu J. Thermodynamic selection criteria of zeotropic mixtures for subcritical organic Rankine cycle. Energy 2019;167:484–97. doi:10.1016/j.energy.2018.11.002.

[261] Zhai H, An Q, Shi L. Zeotropic mixture active design method for organic Rankine cycle. Appl Therm Eng 2018;129:1171–80. doi:10.1016/j.applthermaleng.2017.10.027.

[262] Lemmon EW, Bell IH, Huber ML, McLinden MO. NIST Standard Reference Database 23: Reference Fluid Thermodynamic and Transport Properties-REFPROP, Version 10.0,

National Institute of Standards and Technology 2018. doi:http://dx.doi.org/10.18434/T4JS3C.

[263] Steiner D. Wärmeübertragung beim Sieden gesättigter Flüssigkeiten (Abschnitt Hbb). VDI-Wärmeatlas, Berlin, Germany: Springer Verlag; 2006.

[264] Schlunder EU. Heat transfer in nucleate boiling of mixtures. Int Chem Eng; (United States) 1983;23:4.

[265] Shah MM. A general correlation for heat transfer during film condensation inside pipes. Int J Heat Mass Transf 1979;22:547–56. doi:10.1016/0017-9310(79)90058-9.

[266] Silver RS. An Approach to a General Theory of Surface Condensers. Proc. Inst. Mech. Eng., 1964, p. 339–57. doi:https://doi.org/10.1177/002034836317800155.

[267] Bell K, Ghaly M. An approximate generalized design method for multicomponent/partial condenser. AIChE Symp. Ser. 69, 1973, p. 72–9.

[268] Seider WD, Seader JD, Lewin DR. Product & Process Design Principles: Synthesis, Analysis and Evaluation. John Wiley & Sons: Hoboken, NJ, USA; 2009.

[269] Shah RK, Sekulić DP. Fundamentals of Heat Exchanger Design - Shah - Wiley Online Library. 2007. doi:10.1002/9780470172605.

[270] Deb K. NSGA II paper by Kalyanmoy Deb. 182 Ieee Trans Evol Comput 2002;6:182–97. doi:10.1109/4235.996017.

[271] Yan F, Wei L, Hu J, Zeng J, Zheng S, Wang J. Simultaneous optimization of urea dosing and ammonia coverage ratio of selective catalytic reduction system in diesel engine by using physico-chemical model based NSGA-II algorithm. Appl Therm Eng 2019;154:46–62. doi:10.1016/J.APPLTHERMALENG.2019.03.031.

[272] Wang S, Zhao D, Yuan J, Li H, Gao Y. Application of NSGA-II Algorithm for fault diagnosis in power system. Electr Power Syst Res 2019;175:105893. doi:10.1016/J.EPSR.2019.105893.

[273] Niu X, Wang H, Hu S, Yang C, Wang Y. Multi-objective online optimization of a marine

diesel engine using NSGA-II coupled with enhancing trained support vector machine. Appl Therm Eng 2018;137:218–27. doi:10.1016/J.APPLTHERMALENG.2018.03.080.